MODELING AND EVALUATION OF EROSION WEAR SUSPENSION SYSTEM

Thesis submitted in the partial fulfillment of the requirements for the award of

the Degree of

MASTER OF ENGINEERING

IN

(PRODUCTION AND INDUSTRIAL ENGINEERING)

Submitted By:

Lalit Upadhayay

Registration No: 800882004

Under the supervision of:

Mr. Satish Kumar
Assistant Professor, MED

Dr. S.K. Mohapatra
Professor & Head, MED

MECHANICAL ENGINEERING DEPARTMENT

THAPAR UNIVERSITY, PATIALA

JULY 2010

DECLARATION

I hereby declare that the work which is being presented in the dissertation work entitled, **"MODELING AND EVALUATION OF EROSION WEAR SUSPENSION SYSTEM"**, in partial fulfillment of the requirements for the award of degree of Master of Engineering in Mechanical Engineering with specialization in **PRODUCTION & INDUSTRIAL ENGINEERING** submitted in Mechanical Engineering Department of Thapar University, Patiala, is an authentic record of my own work carried out under the supervision of **Dr. S.K Mohapatra and Mr. Satish Kumar** refers other researcher's works which are duly listed in the reference section.

The matter presented in this thesis has not been submitted for the award of any other degree of this or any other university.

Date: - July'2010
Place: - Patiala

(LALIT UPADHAYAY)

.....

This is to certify that the above statement made by the candidate is correct and true to the best of my knowledge.

Supervisors:

Dr .S.K Mohapatra
Professor & Head
Mechanical Engineering Department
Thapar University, Patiala

Mr. Satish Kumar
Assistant Professor
Mechanical Engineering Department
Thapar University, Patiala

Dr. S.K Mohapatra
Professor & Head
Mechanical Engineering Department
Thapar University, Patiala

Dr. R.K. Sharma
Dean of Academic Affairs
Thapar University, Patiala

ACKNOWLDGEMENT

ieve succes in any work, guidance plays an important role. It makes us put right t of energy in the right direction and at right time to obtain the desired result. I express cere gratitude to my guides, **Dr. S.K. Mohapatra**, Professor, and **Mr. Satish Kumar**, ant Professor, Mechanical Engineering Department, Thapar University, Patiala, for valuable guidance during the course of this investgation, for their ever encouraging nely moral support. Their enormous knowledge always helped me unconditionally to various problems.

greatly thankful to **Dr. S.K. Mohapatra**, Professor and Head, Mechanical Engineering tment, Thapar University, for his encouragement and inspiration for execution of the work. I express my feelings of thanks to the entire faculty and staff, Department of anical Engineering, Thapar University, Patiala for their help, inspiration and moral rt, which went a long way in the successful completion of my Thesis.

Lalit Upadhayay

(Reg. No. 800882004)

ABSTRACT

A proper understanding of the phenomenon of wear in slurry pipelines is essential for any designer of a slurry transportation system. In view of this, many investigators have developed erosion wear test rigs, among which the slurry pot tester is common. Suspension system of a slurry pot tester plays a vital role in accurate evaluation of wear rate. Therefore, the need for the study and optimization of solid-liquid suspension, specifically in the pot tester has arisen. The primary objectives of solid-liquid mixing are to avoid solid accumulation in the agitated vessel, to maximize the contacting area between the solids and liquid, and to ensure the system is homogeneous or solids particles are uniformly distributed throughout the vessel. A lot of work has been reported in the literature regarding solid-liquid suspension in large stir tanks and reactors used in chemical mixing and dispersion. In the present investigation, solid concentrations at various cylinderical heights are determined experimentally and then compared with simulation results obtained by using Eulerian-granular model. Four different types of PBT propellers are used in the experiments. Experimental results are taken at 3 different impeller speeds and solid concentrations and compared with the corresponding simulation results. Effect of the provision of baffle clearance on solid-liquid suspension in the slurry pot tester has also been studied in the present investigation. Commercial CFD code FLUENT has been used to generate the simulation results. A multiple reference frame approach was adopted to simulate the impeller rotation in the baffled cylinderical tank of the pot tester. Solid-liquid suspension in the pot tester has been examined quantitatively by calculating relative standard deviations of both the experimental and simulation results.

CONTENTS

LIST OF FIGURES AND TABLES

NOMENCLATURE

D	Diamter of propeller, mm
ρ	Density of liquid, Kg/m^3
W	Blade width, mm
t	Blade thickness, mm
H	Height of liquid in slurry pot, mm
T	Diameter of cylinderical tank, mm
S	Diameter of propeller shaft, mm
b	Baffle width, mm
n	Frequency of the impeller revolution, rpm
P_o	Power Number
Ep	Efficiency of the impeller
NQp	Flow rate number
C	Impeller clearance, mm
η	Viscosity, Pa-s
R_e	Reynolds number
σ_k	Turbulent Prandtl number for k
σ_ε	Turbulent Prandtl number for ε
σ	Relative standard deviation

CHAPTER 1

INTRODUCTION

Slurries contain abrasive and erosive solid particles, which eventually cause wear of wetted components. Wear of slurry pump impellers and other wetted components is a main cause that makes pumps out of work. A number of bench scale test rigs have been used to evaluate slurry erosion rate. Slurry pot tester has been commonly used by various investigators. In a slurry pot tester, two wear specimens have been generally rotated with or without a propeller. The propeller is needed for suspension of solid particles. But rotation of the propeller with wear specimen at different test speeds generates different turbulence and flow field inside the pot, and the particles may not remain uniformly distributed in the pot. Therefore, solid-liquid suspension in the slurry pot tester plays a vital role in the evaluation of erosion wear rate.

1.1 WEAR

Wear is defined as *'progressive volume loss of material from a solid surface due to corrosion, abrasion and erosion' [6]*. Wear is one of the most common problems encountered in industrial applications.

Wear, along with other aging processes such as fatigue, creep and fracture toughness, causes progressive degradation of materials with time leading to failure of material at an advanced stage. Under normal circumstances, the property changes during usage normally occur in three different stages. Primary or early stage or run-in period, where rate of changes can be high, Secondary or mid-age process where a steady rate of aging process is maintained. Tertiary or old-age stage, where rapid rate of aging leads to early failure. With increasing severity of environmental conditions, such as, higher temperatures, strain rates, stress and sliding velocities, the secondary stage is shortened and the primary stage tends to merge with the tertiary stage, thus drastically reducing the working life.

1.1.1 Erosion wear

Erosion wear is the dominant process and can be defined as the removal of material from a solid surface due to mechanical interaction between the surface and the impinging particles in a liquid stream. Erosion involves the transfer of kinetic energy to the surface. This means that

in erosion, material removal is a function of particle velocity squared to the higher power. Erosive wear depends on the predominant impact angle of particle impingement with the material surface. The material loss due to erosion increases with the increase in kinetic energy of the particles impacting at the target surface. The material removal due to erosion is caused by two dominant mechanisms namely brittle fractures and platelet deformations. In brittle type material, the solid particles impacting on the target surface forms cracks in longitudinal and lateral directions. These cracks propagate due to impact of succeeding particles and broken materials pieces will be carried out by flowing fluid. In Platelet mechanism, the impact of solid particles deforms the target surface to form hills and valleys. The repeated impacts of particles remove the material and forms crater at the surface.

1.1.1.1 Types of erosion wear

The major type of erosion wear in a slurry pump impeller is due to the *particle impingement*. This is where the particles impact at angles substantially normal to the surface (15°– 90°). The predominant type of wear in centrifugal pump discharge casing is *sliding-bed erosion*. Particles impacting directly onto a surface can generate very high specific contact pressures. The actual value of the contact stress depends on the particle velocity, the mass, and the particle shape. Particles with sharp edges wear the surface faster because of their smaller contact area (and thus higher stresses). Material is removed by a process of cutting and/or ploughing.

Ploughing erosion

Ploughing Erosion is a two stage process involving localized plastic deformation of the surface from rounded particle impacts. Initial particle impacts form surface craters with plastic flow of the surface occuring around the particle edges during impact. An extruded shear lip is formed as a result of the particle collision. The second stage involves repeated particle impacts causing fatigue of the extruded shear lip regions. The shear lips fail and are broken off.

Cutting Erosion

Cutting Erosion occurs when the particles are very sharp and interaction with the material surface causes a micromachining action. Minimal plastic deformation of the surface region

occurs at the point of particle impact. The angle of particle impact is a critical factor in controlling the rate of cutting wear due to sharp particles. Lower impact angles tend to increase cutting wear.

1.1.2 Parameters affecting erosion wear:

The prominent parameters and their effect on erosion wear are as under :

Impact angle:

Impact angle is defined as the angle between the target surface and the direction striking velocity of the solid particle. The variation of erosion wear with the impact angle depends on the characteristics of the target surface material namely brittle or ductile type.

Velocity of solid particles:

Velocity of solid particle strongly affects the erosion wear. As particle velocity increases there is a significant increase in erosion rate. The erosion rate is generally related to the particle velocity using power law relationship in which the power index for velocity varies in the range of 2-4.

Hardness:

Hardness is the characteristic of a solid material expressing its resistance to permanent deformation. Surface hardness as well as hardness of solid particles has profound effect on the erosion wear mechanism. Hardness ratio has been defined as the ratio of hardness of target material to the hardness of solid particles [43].

Particle size and shape:

Particle size and shape is also one of the prominent parameter, which affect the erosion wear. Many investigators have considered solid particle size important to erosion. The erosion wear increases with increase in particle size according to the power law relationship. The effect of particle shape on the erosion is not very well established due to the difficulties in defining the different shape features. Generally roundness factor is taken into consideration. If roundness factor is one then the particles are perfectly spheres and a lower values show the particle angularity [43].

Effect of particle size:

Larger particles (greater than 500 microns) remove material by a combination of cutting and ploughing on a relatively macro scale. The sharp corners of these particles may either chip individual carbide or gouge a portion of matrix, but are not generally able to cut right across carbide. Very fine particles (less than 100 microns) generally do not have sufficient energy to inflict significant damage to the hard carbide phase. They remove portions of the softer matrix however, leaving carbides exposed and prone to impact from the larger particles. Commercial slurries are generally a broad mix of particle sizes, and all 3 modes of wear will occur simultaneously. The wear caused by the larger particle sizes will always predominate.

Effect of particle shape on wear:

Particle shape is one of the most important variables in the erosion wear process. Sharp particles erode at a much faster rate than rounded particles because of the high contact stresses at the point of impact. Rounded particles are not able to erode between the carbides (if they are significantly larger than the intercarbide spacing) and the resulting wear rate is influenced much more by the volume of carbides present than for sharp particles [43].

Solid concentration:

Concentration is the amount of solid particles by weight or by volume in the fluid. As concentration of particle increases, more particles strike the surface of the impeller which increase the erosion rate, the concentration of slurries can vary from 2% to 50% depending upon the type of slurry. However, at very high concentrations particle-particle interaction increases and this decreases the striking velocity of particle on the surface [43].

1.2 SLURRY

Slurry is a mixture of solids and liquids. Its physical characteristics are dependent on many factors such as size and distribution of particles, concentration of solids in the liquid phase, size of the conduit, level of turbulence, temperature, and absolute (or dynamic) viscosity of the carrier. Nature offers examples of slurry flows such as seasonal floods that carry silt and gravel. A slurry mixture is a mixture of a carrying fluid and solid particles held in suspension. The most commonly used fluid is water, however in some cases air is also used such as in pneumatic conveying. Theoretically, a single-phase liquid of low absolute (or dynamic)

viscosity can be allowed to flow at slow speeds from a laminar flow to a turbulent flow. However, a two-phase mixture, such as slurry, must overcome a deposition critical velocity or a viscous transition critical velocity. If the slurry's speed of flow is not sufficiently high, the particles will not be maintained in suspension. On the other hand, in the case of highly viscous mixtures, if the shear rate in the pipeline is excessively low, the mixture will be too viscous and will resist flow.

1.2.1 Types of slurry flows

There are generally two types of flows:

i) Homogeneous Flows:

In homogeneous flows solids are uniformly distributed throughout the liquid carrier. For example, copper concentrate slurry after undergoing a process of grinding and thickening. Drilling mud,sewage, sludge and fine limestone behave as homogeneous flows.

ii) Heterogeneous flows

In heterogeneous flows, solids are not uniformly mixed in the horizontal plane. Heavier particles tend to settle down and lighter particles tend to float. Sliding bed may form in the

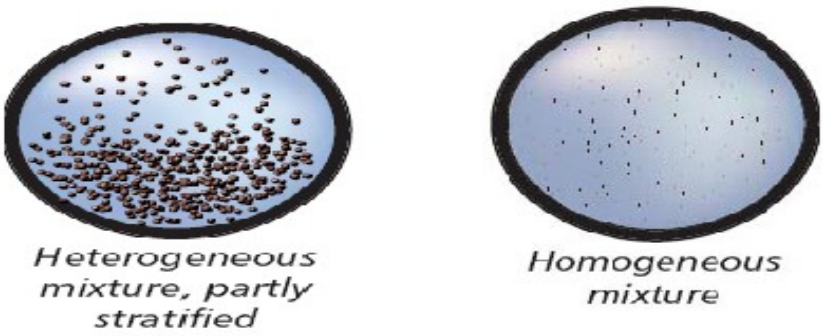

Figure 1.1 Heterogeneous and Homogenous mixtures [22]

pipe, with the heavier particles at the bottom and the lighter ones in suspension. Heterogeneous slurries are encountered in many places mining, phosphate rock mining, and dredging applications. Heterogeneous flows require a minimum carrier velocity.

1.3 SOLID-LIQUID SUSPENSION SYSTEM

Particles may float on a liquid surface due to a low solid density, due to low solid wettability combined with a large contact area, or due to low bulk density of the solid powder. When a single particle is placed at the surface of a stationary denser and/or non-wetting liquid, as shown in Figure 1.3, the particle stays at the surface if the combined buoyancy and surface tension forces are greater than the gravitational force. Once the impeller is turned on and the fluid is in motion, two additional forces emerge in the system; the mean drag force and the dynamic forces due to the turbulent velocity fluctuations and coherent meso-scale eddies. These forces and the gravitational force have to overcome the buoyancy and surface tension forces to draw the floating particles down from the surface, allowing them to be distributed throughout the tank. Suspension follows three basic mechanisms as shown in the figure 1.2 below. Solid particles get suspended in the liquid by drag, lift, turbulence and vortices and ejection by collision.

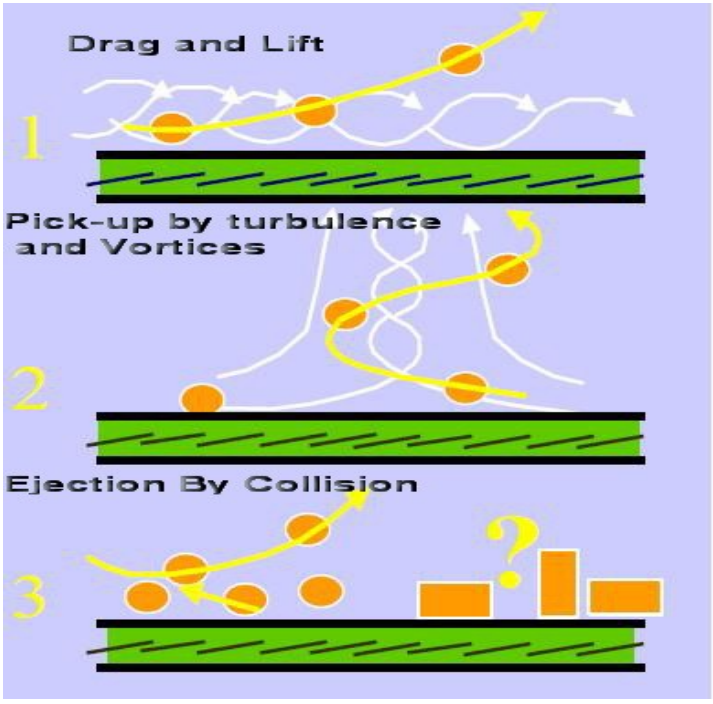

Figure 1.2: Mechanism of solid-liquid suspension [22]

Mixing occurs when a material is moved from one region to another region. In the past it may have been of interest to achieve a required degree of homogeneity but now it is also being used to enhance heat and mass transfer, often with a system undergoing chemical reactions.

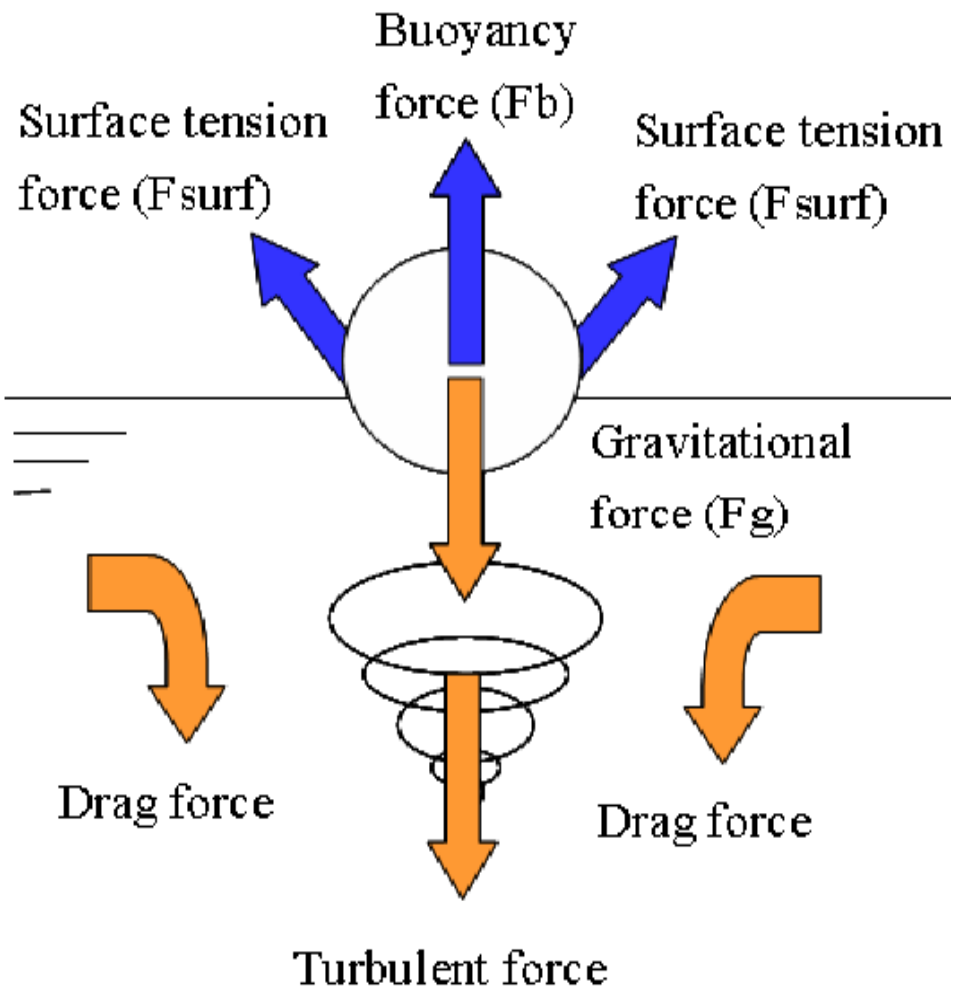

Figure 1.3: Forces interacting on a particle in solid-liquid suspension system [39]

In order to produce a uniform mixture by mixing, two things need to occur. First, there must be a bulk or convective flow to avoid any low velocity zones usually referred to as dead/stagnant zones. Secondly, there must be an intensive or high-shear mixing zone, in which the homogeneities are broken down. Laminar and turbulent flow types occur simultaneously in the different part of the mixer with a substantial transitional zone in between them depending upon the fluid properties, primarily viscosity. Processing with mechanical mixers occurs under either laminar or turbulent flow conditions, depending on the impeller Reynolds number, defined as $Re = \rho ND^2/\eta$. For Reynolds numbers below 10, the process is laminar, also called creeping flow. Fully turbulent conditions are achieved at Reynolds numbers higher than about 10^4 and the flow is considered transitional between these two regimes.

The suspension speed is the optimum speed of the propeller and appears to be a function of particle size, concentration and terminal settling velocity of solid particles. Published results show that the increase in particle size results in increase in suspension speed for nearly uniform distribution. *Desale et al* [27] have given a best fit equation, determined using least square method, to calculate the minimum suspension speed. The following correlation is obtained,

$$Ns=276.303\times d^{0.0372}\times Cw^{0.1886}\times Vt^{0.1889} \quad (1)$$

where, d is the mean daimeter of the solid particles, Cw is concentration by weight, Vt is the mean settling velocity of the particles in the solid-liquid suspension system.

1.3.1 Design parameters of a stir tank

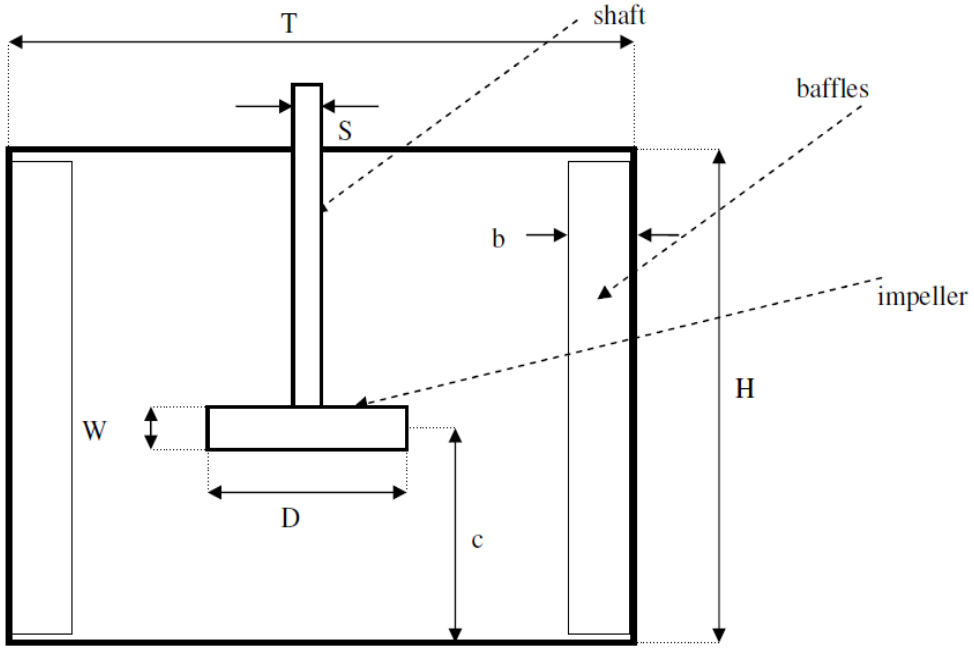

Figure 1.4 : Design parameters for a stir tank [39]

A conventional stir tank consists of a vessel equipped with a rotating mixer. The vessel is generally a vertical cylindrical tank. The rotating mixer has several components: an impeller, shaft, shaft seal, gearbox and a motor drive. Wall baffles are generally installed for transitional and turbulent mixing to prevent solid body rotation (sometimes called fluid swirl) and cause axial mixing between the top and bottom of the tank. A conventional vertical

cylindrical stirred tank with a top-entering mixer is shown in Figure 1.4, where a Newtonian liquid of density, m, and viscosity, n, is agitated by an impeller of diameter, D, and its clearance from the tank bottom is c. The vessel diameter is T, the liquid depth is H, the height of impeller blade is W, the baffle width is b, and the shaft diameter is S.

The pumping capacity of a pitched blade impeller (PBT) is defined as the amount of liquid leaving the rotor region of the impeller, i.e., the cylindrical volume circumscribed by the rotating impeller blades, per unit time.This quantity is an important process characteristic of the pitched blade turbine (PBT) and plays an important role in calculating the process characteristics of solid-liquid suspensions, i.e. The impeller frequency for just off bottom suspension.The pumping capacity of the PBT, NQp, can be expressed in dimensionless form as the impeller flow rate number [15],

$$NQp = Qp / nD^3 \tag{2}$$

where, n is the frequency of the impeller revolution and D is its diameter. For impeller power input P the Power Number is given by [15],

$$Po = \rho * n^3 * D^5 \tag{3}$$

where ρ is the density of the agitated liquid. A combination of the dimensionless quantities NQp and Po gives the so called hydraulic efficiency of the impeller defined as [15],

$$Ep = NQp^3 * (D/T)^4 \tag{4}$$

where, T is the diameter of the vessel.The higher the quantity Ep, the greater the ability to convert impeller energy consumption into its pumping effect. The flow rate criterion N_{Qp} and the Power number P_0 were correlated in the literature on the basis of many experiments carried out for pitched blade impellers in a baffled flat bottomed cylindrical pilot plant agitated system under a turbulent regime of an agitated liquid. Medek [15] published a correlation,

$$P0 = 1.507 * nB^{0.701} * (C/D)^{-0.165} * (T/D)^{-0.365} * (H/T)^{0.14} * (Sin\alpha)^{2.077} \tag{5}$$

While, Medek and Fort [15] published,

$$NQp = 0.745 * nB^{0.233} * (T/D)^{0.023} * (H/T)^{0.251} * (Sin\alpha)^{0.468} \tag{6}$$

From equation 4,5 and 6 the following relationship can be deduced,

$$Ep = 0.413 * nB^{0.013} * (D/T)^{3.98} * (H/T)^{0.016} * (Sin\alpha)^{0.103} \quad (7)$$

Studies by Pullum et al [35] show that by increasing the orientation angle(α) of the PBT impeller blade from 0° to 45°, the just-off bottom suspension speed Ns decreases. The Ns also decreases when the no of blades (nB) of a PBT impeller are increased.

Impeller:

The typical impellers used in transitional and turbulent mixing are listed in Table 1.1 These have been divided into different general classes, based on flow patterns, applications, and special geometries. The classifications also define application types for which these impellers are used. The pitched blade turbine, although classified as an axial flow impeller, is sometimes referred to as a mixed flow impeller, due to the flow generated in both axial and radial directions. Above a D/T ratio of 0.55, pitched blade turbines become radial flow impellers.

Table 1.1: Impeller classes and specific types

Impeller Classes	**Specific Types**
Axial Flow	Propellers, Pitched Blade Turbine, Hydrofoil
Radial Flow	Flat Blade Impeller, Disk Turbine(Rushton), Hollow Blade Turbine(Smith)
High Shear	Cowles, Disk, Pointed Blade impeller
Speciality	Swept Back Impeller, Spring Impeller, Glass Lined Turbines
Up/Down	Disk, Plates, Circles

Axial flow Impellers:

Axial flow impellers (Figure 1.5) are used for blending, solids suspension, and heat transfer. Since the present study is related to Solid-Liquid suspension, pitched blade turbine impellers with blade angle 45° have been used in the investigation. The flow discharge from a pitched blade impeller has components of both axial and radial flow velocity in low to medium viscosity liquids, and is considered to be a mixed-flow impeller.

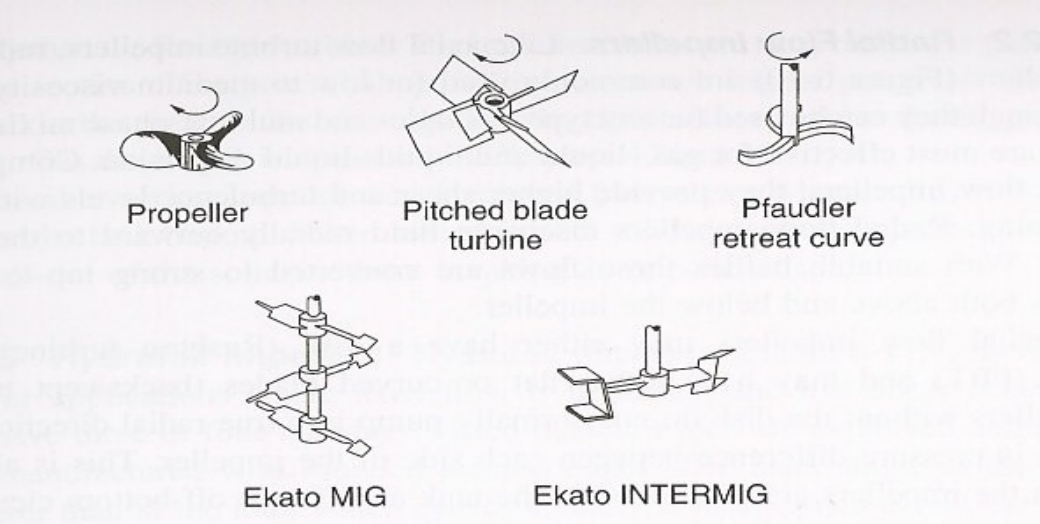

Figure 1.5 : Axial flow impellers [39]

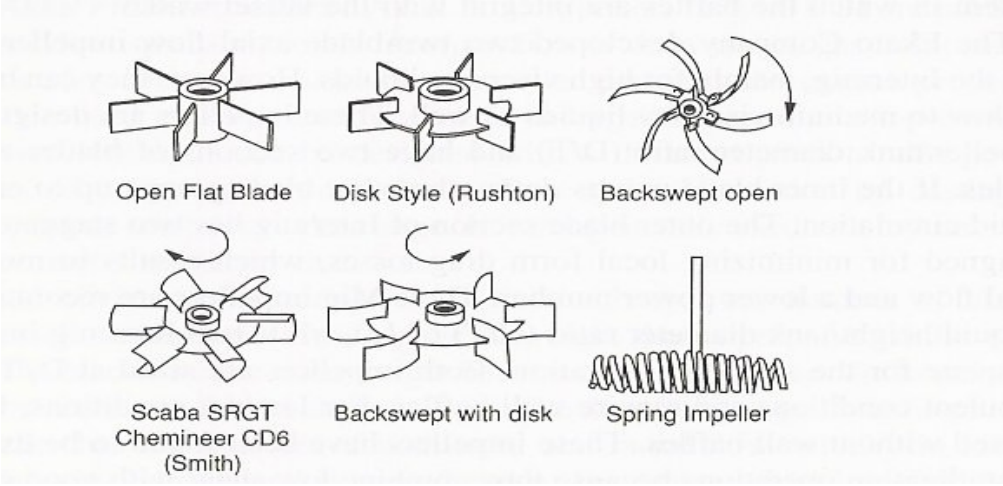

Figure 1.6: Radial flow impellers [39]

Radial Flow Impellers:

Like axial flow turbine impellers, radial flow impellers (Figure 1.6) are commonly used for low to medium viscosity fluids. Radial flow impellers discharge fluid radially outward to the vessel wall. With suitable baffles these flows are converted to strong top-to-bottom flows both above and below the impeller. Radial flow impellers may either have a disk (Rushton turbine) or be open flat blade turbine (FBT) and may have either flat or curved blades (backswept turbine).

Baffles:

When a center-mounted impeller is used in an unbaffled vessel, the impeller imparts a high velocity swirl and vortexing motion to the fluid, but very little mixing takes place. Baffles are used to convert this swirling motion to a more 3-dimensional flow accompanied by turbulent dissipation, thereby promoting top-to-bottom turnover and mixing. Placing a baffle in an agitated vessel increases the transfer of power from the impeller to the fluid. A visual indication of this transfer of power is a reduction in size of the free surface vortex, the magnitude of which is a function of the following:

Shape:

The less streamlined the baffle, the more effective it will be (i.e., a flat plate is a more effective baffle than a round pipe of equal cross section).

Placement:

The closer the baffle is to the sidewall of the vessel, the more effective it will be in converting swirl to top-to-bottom turnover.

Size:

The larger the projected area of the baffle, the greater the baffle effect. The project area of the baffle is given by the product of width b and length H of the baffle.

A fully baffled condition (complete vortex elimination, defined as 100% baffle effectiveness) is produced by four flat plates (*shape*) located at the sidewall of the vessel (*placement*), of width equal to 1/12 of the vessel's diameter (*size*). They typically extend the length of the vessel's straight side and are spaced at 90 degree intervals.

CHAPTER 2

LITERATURE REVIEW

Moving particulate materials in liquid slurry form can seriously erode their containers. Turbo machines are increasingly being applied to extensive industrial fields and tend to be operated at higher rotational speed. Therefore, to maintain high performance over a long time, it is desirable to pay attention to the wear. Erosive wear in centrifugal slurry pumps has motivated many researchers, due to its application in areas such as dredging, hydraulic transport etc. Experimental results concerning the wear of slurry pump impellers are not abundant. A variety of bench scale test rigs have been used by the investigators to predict the erosion wear. Most of them have used Slurry Pot Tester which comprises of a cylinderical tank in which wear specimens are tested against wear. These test rigs require the solid-liquid suspension to be uniform and vortex free. Therefore, detalied study of solid-liquid suspension system in an erosion wear test rig is required. This has initiated researchers to conduct research on wear as well as on the solid-liquid suspension system of wear test rigs. A review of literature available in this area has been presented in the following paragraphs to discuss the present state of knowledge.

Shawky M. et al[1] [1989] presents some experimental results of erosive wear in a centrifugal slurry pump. The objective of their investigation was to study the relation between erosive wear in a centrifugal pump impeller and solid particle concentration. The erosion rate of a centrifugal pump impeller is measured by the weighing method. They have used two different concentration of coarse sand and have investigated the effect of speed of rotation. The experimental results obtained by them show the correlation between the erosive wear development and solid particle concentration.

Desai P.V[2] [1990] has studied the erosion wear of centrifugal slurry pumps which is primarily governed by the particulate motion and concentration as well as their physical properties. The analysis and the finite element computations yield the solid velocity and concentration fields in an arbitrary radial cross-section of a centrifugal slurry pump casing. The solutions were examined in light of their applicability to the pump wear problem. Axis symmetric finite elements have to be used to analyze the flow in the volume of revolution.

The shape factor of the particles is introduced into the drag and pressure force calculations to account for the angularity of the particles.

Hector McI. Clark[3] [1991] has pointed out the importance of knowledge of flow field surrounding impinging particles and target is emphasized for an understanding of slurry erosion. He has reviewed the work on the effect of liquid viscosity and density, particle size and size range, density and concentration, target shape and suspension free stream velocity in slurry erosion. His studies show that the experimental data on the material erosion rates can only be understood if particle impact velocities and trajectories and the number of particles impacting the target surface are known. He has pointed out that the actual impact velocities of the particles on an eroding target may differ widely from the free stream velocity of the suspension and that under some circumstances most, or even all, particles directed at a target may fail to collide with it.

Steward N.R. et al[4] [1992] have emphasized on the pipeline wear which continues to be an area of specific concern, since it constitutes a major cost during the life of a pipeline installation. Wear data from an accelerated wear test and actual pipeline tests have been presented by them. Trends in the performance of the pipeline materials tested are discussed, and possible solutions to the problem of pipeline wear are presented.

Neseic.S. et al[5] [1993] have evaluated erosion rates along the length of a tubular flow cell of type 304 (UNS S30400) stainless steel (SS) carrying dilute slurries of silica sand (0.43 mm diam) and smooth glass beads of a similar size. The segmented test cell contained a sudden constriction, a sudden expansion, and a groove to produce disturbed flow conditions. Erosion rates were reduced by changes in the cell wall geometry that resulted from erosion at positions of high local metal loss and from erosion further downstream because of the reduction in turbulence and particle dispersion.

Gupta Rajat et al[6] [1994] have conducted a systematic study on a pot tester to establish the effect of velocity, concentration and particle size on erosion wear. Two correlations have been proposed, based on the data generated for equisized particulate slurries in the pot tester, to predict the expected erosion wear for two pipe materials, namely brass and mild steel. The weighted mean diameter has been established as the best representative diameter for the

multisized particulate slurries. The proposed correlations have been used to predict the extent of uneven erosion wear in a slurry pipeline using local concentration, local effective particle size and average velocity. The comparison between predicted and experimental results shows agreement within 13.5% for brass and + 14% for mild steel.

Zhong Yuan et al[7] [1995] have followed Lagrangian approach to predict the erosion wear on a pump casing wall due to impingement of solid particles and calculated the impinging velocities on the casing wall under the assumption that the water flow field remains unchanged due to the presence of the particles. They have also investigated the effect of mutual collision among the particles. Their result showed that the impinging velocities of the particles in the tongue area have remarkably a large normal component with no tangential one. Distribution of the volumetric particle concentration is hardly affected by the spinning and mutual collisions of the particles.

Zhong Yuan et al[8] [1996] have measured erosion damage of wear resistant materials due to sand particle impingement and correlated based on Bitter's erosion model to clarify the effects of particle impinging velocity and angle, particle size and concentration on the wear. Using the empirical formula for the correlation and calculating impinging velocities of sand particles on a casing wall of a pump, successive erosion of the wall is numerically calculated to demonstrate the viability of the prediction method. The erosion data of cast iron and stainless steel eroded by sand particles confirm Bitter's erosion model.

Stokes et al[9] [1999] have used axis-symmetric model to simulate two-phase flows in stirred mixing tank.The impeller used is Rushton turbine.They have studied the gas-water two phase flow and have used RNG based k-ε turbulent model in their computational study. The numerical solution of the radial, tangential and axial velocities of the air was compared with the experimental results.

Brown Gary et al[10] [1999] have studied tee junctions in a slurry pipeline system. The commercial code ANSYS-CFX has been used to predict the motion of caustic liquor and bauxite particle through a tee-junction using an Eulerian-Eulerian continuum approach in conjunction with k-ε turbulence model. The predicted wear location was found to be insensitive to the assumed level of inlet swirl and the numerical scheme employed.

Lee S. Y. et al[11] [2001] have discussed the application of computational fluid dynamics (CFD) methods to simulate the flow of slurry and predict the erosion rates so that an effective maintenance schedule can be developed for the filtration system of the waste treatment process. The location of the maximum erosion for the selected components is also identified. Solids content of the working fluid, the regions of high wall shear, and particle impingement with the walls were considered as major mechanisms associated with the erosion. All these tests were performed using sand water slurry.

Hawthorne H.M. et al[12] [2001] has conducted Coriolis tests for the evaluation of slurry erosion on different materials. Slurries consisting of glass beads of size 90- 200 micron size with 10% slurry concentration were taken and tests were performed on 1020 steel and copper at different impingement angles of 90-20 degrees. It was also observed that in slurry jet testing, most particles impact the specimen above its critical velocity resulting severe plastic deformation. In contrast, in the Coriolis test most particle impacts result in only elastic deformation or mild plastic deformation. Hence, elastic as well as plastic properties of specimen materials affect their performance in a Coriolis slurry erosion evaluation, thus the results obtained from Coriolis tests were more accurate.

Gandhi B. K. et al[13] [2001] have studied that the performance of pumps decreases for increase in solid concentration, particle size and specific gravity. The head and efficiency of the pump decrease with increase in solid concentration, particle size, and slurry viscosity, the decrease in the head being 2–10 percent higher than that of the efficiency. The presence of finer particles (less then 18micron) in coarser slurries substantially attenuates the loss of performance of the pump in terms of head and efficiency. At low solid concentrations less than 30 percent by weight, the increase in the pump input power is directly proportional to the specific gravity of slurry whereas the same relationship is not applicable at higher concentrations. The study on the pumps has confirmed that the additional head loss for slurries decrease with increase in the pump size.

L.M. oshinowo et al[14] [2002] have studied the effect of computational fluid dynamics approach to evaluate solid suspension in stirred tanks. The distribution of solids in stirred tanks under a range of solids loadings (0.5 to 50 vol%) was predicted using CFD and

validated against experimental data obtained from the literature. The multiphase flow is modeled using the Eulerian Granular Multiphase model.They have studied the performance of hydrofoil impellers and a 45° pitched-blade turbine at suspending solids under different agitation speeds.The standard deviation of solids volume fraction was shown to be useful measure of the quality of suspension.

D. Chapple et al[15] [2002] have studied the effect of impeller and tank geometry on power number for a pitched blade turbine. The changes done in the position of the impeller in the tank can have a significant impact on the power number (15%) due to changes in the flow patterns. They have shown that there is no effect of the blade thickness on the power number for a four blade PBT 45 degrees impeller.

Litian et al[16] [2003] have conducted Computational Fluid Dynamics study of Rushton turbine in stirred tanks. The commercial code used by them was ANSYS-CFX. To account for the relative movement between impeller and baffles sliding mesh method has been used by them. Fluid flow is calculated with a turbulent k-ε and RNG k-ε model using finite volume method. Their result show that mixing time highly relies on the flow field, the feeding and detection position.

Feng Wang et al[17] [2003] studied CFD simulation of solid-liquid two phase flow in baffled stirred vessel with Rushton Impellers. They have simulated three dimensional flow field and solid concentration distribution in solid liquid baffled stirred vessels using inner-outer iterative procedure. The procedure used by them can be applied to the system with high solid concentration upto 20%.

J. J. Derksen et al[18] [2003] have numerically simulated the solid suspension in the strirred tank. Large-eddy simulations of the turbulent flow driven by a Rushton turbine have been coupled to a Lagrangian description of spherical, solid particles immersed in the flow.The working fluid was water, whereas the solid particles had the properties of glass beads. It has been investigated to what level of detail the particle motion needs to be modeled in order to meet Zwietering's just suspended criterion.Their result show that it is essential to take particle-particle collisions into account, mainly because of their exclusion effect that prevents unrealistic buildup of particle concentrations closely above the bottom.

Gandhi B. K. et al[19] [2004] have developed a methodology to determine the nominal particle

size of multi-sized particulate slurry for estimation of mass loss due to the erosion wear. The effect of presence of finer particles (less than 75 micron) in relatively coarse particulate slurry has also been studied. They have observed that addition of particles finer than 75 micron in narrow-size or multi-sized slurries reduce the erosion wear. In addition, the effective particle size for narrow-size particulate slurries can be taken as the mean size whereas the weighted mass particle size seems to be a better choice for multi-sized particulate slurries. The reductions in erosion wear due to addition of fine particles decreases with increase in the concentration of coarse size particles.

Wood R.J.K. et al[20] [2004] has covered research that has been aimed at determining the distribution of erosion rates and the erosion mechanisms that occur over wetted surfaces within pilot scale pipe systems handling water-sand mixtures at 10% by volume concentrations and at a mean fluid velocity of approximately 3 m/s. The wall wear rates, obtained by gravimetric measurements, as a function of time are discussed. The erosion rates, expressed as volume loss per impact (determined gravimetrically and via computer models) in bends are found to agree well with simple laboratory scale water-sand jet impingement tests on planar stainless steel samples.

G. Montante et al[21] [2005] have studied the solid liquid multiphase flow in tall stirred vessels with multiple impeller systems. Good results were obtained using eddy viscosity turbulence models for fully baffled vessels. Their results recommend the use of Magelli drag correction for prediction of solid concentration in stirred vessels.

R. Thorpe et al[22] [2005] have conducted studies on the suspension of particles from the bottom of pipes and stirred tanks by gassed and ungassed flows. They have concluded that pick-up in pipes involves viscous sublayers where turbulent forces are not dominat force. They have compared the correlations and theoretical predictions for hydraulic conveying of solids in pipelines with the literature on the suspension of particles in stirred tanks.

Dolman K.F. et al[23] [2005] have studied the ameliorative influence on scouring erosion behavior of high carbon content, hardness and carbide volume fraction and particularly of fine carbide size. They have drawn a correlation between test data and service performance. Low impact angle erosion resistance is a critical requirement of materials used in pumps,

piping, valves, nozzles, cyclones and other components which transport and process most mineral slurries. The specific method used in their study involves high velocity erosion with aqueous slurry containing 10 wt. % of AFS 50-70 silica test sand. The test is considered to be a suitable method for evaluating the scouring erosion resistance of metallic, ceramic and cermet materials for various slurry transport components.

Sellgren A. et al[24] [2005] have modeled a selection of pump designs producing general relationships for the different pump casing, impeller and liner components for different duties. They then take these and show which offer the lowest cost of ownership for different services. Correlations against pump design specific speed show higher specific speed pump casings wear better, while lower specific speed, slower running, larger diameter impeller pumps have better impeller and liner wear. The calculated values show total cost of ownership is affected significantly by changes in operating conditions (due to wear) and is a minimum, in most cases, at around a design specific speed of NS=38 (2000 USNS).

T. Kumaresan et al[25] [2005] have studied the effect of inernals on the flow pattern and mixing in the stirred tanks. Measurements of power consumption, mixing time, and flow pattern have been carried out in a stirred vessel of 0.5 m diameter for a standard 45° pitched-blade turbine and for a hydrofoil impeller with a variety of baffle and draft tube configurations. The comparison of the flow pattern (average velocity, turbulent kinetic energy, maximum energy dissipation rate, average shear rate, and turbulent normal stress) has been presented on the basis of equal power consumption to illustrate the extent of interaction between the rotating impeller and the internals. Comparisons of laser Doppler anemometer (LDA) measurements and computational fluid dynamics (CFD) predictions have been presented.

Tian Harry H. et al[26] [2005] have observed the erosive wear of some metallic materials such as high chromium white iron and aluminium alloy using Coriolis wear testing approach. In the present study, the correlation between wear rate and particle size on the tested materials is discussed. Factors, which should be considered in wear modeling and prediction, have also been addressed. They have studied that larger solids particles resulted in higher mass loss in all test materials. Although the wear rates at smaller particle sizes were relatively close within

each material group, the wear rate difference was significantly widened with larger particle sizes.

G. Desale et al[27] [2005] have studied the improvement in the design of pot tester to simulate erosion wear due to solid-liquid mixute. The have minimized the effect of relative velocity between the wear specimens and solid particles by rotating a PBT propeller in down pumping mode. They also have made provisions in the test fixtures to evaluate the effect of impact angles, concentration, velocity etc. on the wear rate.

Feng Jianjun et al[28] [2007] have conducted numerical simulations on impeller diffuser interactions in radial diffuser pumps to investigate the unsteady flow, and more attention is paid to pressure fluctuations on the blade and vane surfaces Computational results show that a jet-wake flow structure is observed at the impeller outlet. The biggest pressure fluctuation on the blade is found to occur at the impeller trailing edge, on the pressure side near the impeller trailing edge, and at the diffuser vane leading edge, independent of the flow rate, radial gap, and blade number configuration. All of the flow rate, blade number configuration, and radial gap influence significantly the pressure fluctuation and associated unsteady effects in the diffuser pump.

Gandhi B.K. et al[29] [2007] observed that the wear at normal impact condition is a strong function of hardness hardness ratio of erodent and target materials. He carried out experiment for different solid concentrations, particle sizes and velocities. Based on experimental data, he has proposed a correlation to predict the erosion wear at normal impact conditions. Experiments have been carried out using a slurry pot tester by orienting the wear specimen normal to their rotational direction. Erosion wear due to normal impact has strong dependence on velocity and particle size but relatively weak dependence on solid concentration. SEM micrographs and surface roughness measurement of worn out surface reveals that the penetration by solid particles at the target material surface is a function of hardness ratio.

Williams A. John et al[30] [2007] proposed that when material is lost from loaded surface either entirely or principally through some form of mechanical interaction the concentration, size and shape of the debris particles carry important information about the state of the

surfaces from which they were generated and thus, by implication, the potential life of the contact and of the equipment of which this forms part. To use debris examination as a diagnostic aid in assessing health of the operating plant, which may contain many tribological contacts, requires not only careful and standardized procedures for debris extraction and observation but also an appreciation of the mechanism by which wear occurs and the regimes in which each of the contacts of interests operates when displayed on an appropriate operational map.

Ridgway N.et al[31] [2009] emphasizes that non uniform packing compression is not the sole contributor to gland seal life cycle cost and reliability, an improved scientific understanding of tribological wear process is required for existing designs. In slurry service particle size distribution, shape and relative hardness with the shaft sleeve are expected to influence the useful life of shaft sleeve and packing. They identified the key variables in the development of wear equation within the framework of contact mechanism and inorganic structural chemistry. Particle properties including size, relative hardness and fracture toughness were found to be of vital importance. The specific wear rate was found to be dependent on particle size.

Wang Yao et al[32] [2009] has proposed design of an experimental system for assessing wear conditions of slurry pumps. This experimental system is intended to provide data for both simple and advanced data analysis of the correlation between the wear status of wetted components and a number of parameters. This experimental system is a test loop which contains a slurry pump and data acquisition system among other components. Test runs at different rotating speeds with controlled particle proportion and slurry temperatures. It is designed primarily to provide good scalability with regards to field conditions and satisfactory accuracy for subsequent analysis.

Wu Yulin et al[33] [2009] have measured the internal flow field in a centrifugal pump working at the several flow conditions using the particle image velocimetry (PIV) technique with the laser induced fluorescence (LIF) particles and the refractive index matched (RIM) facilities. The impeller of the centrifugal pump has an outlet diameter in 100mm, and consists of six two-dimensional curvature backward swept blades of constant thickness. Measured results

give reliable flow patterns in the pump. It is obvious that application of LIF particle and RIM are the key methods to obtain the right PIV measured results in pump internal flow.

Suzuki Masaya et al[34] [2009] Erosion phenomenon, including the temporal change of the flow field and the wall shape. They have simulated sand erosion of a 90 degrees bend with a square cross-section. The numerical results are compared with experimental data and it is confirmed that the developed code can capture the sand erosion phenomenon reasonably.

L. Pullum et al[35] [2009] have studied the effect of varying impeller geometrical parameters on the turbulent velocity fields in mixing tanks. They have used pitched blade turbines and disc turbines and measurements have been taken through laser doppler velocimetry (LDV) technique. They have evaluated the flow number correlations based on power number in their investigation.

Achebo I. Joseph[36] [2009] have used drift flux models based on Eulerian continuum equations in predicting erosion wear rate in a transmission pipeline. In this case, a pipeline with a diameter of 0.5m was investigated. It was found that there was a large sand particle concentration on the welded parts of the pipe which has affected the internal geometry of the pipe. From physical examination, the reduction in the nominal thickness of the pipe was related to erosion wear.

Sanna Haavisto et al[37] [2009] have studied the particle velocity and concentration profiles of sand-water slurry in a stir tank. Three dimensional velocity profiles were measured utilizing ultrasound Doppler velocimetry along lines located circumferentially between two baffles of the tank. The volume fraction of the solid phase investigated by them were 5% and 10%. They have conducted CFD studies of slurry flow with algebric slip mixture model and full Eulerian multiphase model. Standard k-ε model was applied in turbulence modelling.The agreement between the simulated and the measured particle velocities was found to be relatively good in the central region of the vessel. Near the wall, deviation of the results was observed with increasing solid concentration. Eulerian multiphase model was tested with parameters corresponding closely to those used with algebraic slip mixture model. Results obtained with it deviated from measurements more than mixture model predictions.

K. Mohanarangam et al[38] [2009] have studied CFD modelling of floating and settling phases in settling tanks. A Computational Fluid Dynamics (CFD) model for modelling a floating phase has been developed and tested on a settling tank. The model used by them for settling tanks was able to predict the settling of solids and the formation of a higher density layer of solids at the bottom of the vessel.The simulations were performed by customizing the software ANSYS-CFX .

O. Khazam et al[39] [2009] have conducted study on the drawndown of the floating solids in stirred tanks. In this study they have reported the effect of the type of impeller, impeller submergence, and baffle configuration on the minimum draw down speed (Njs) are reported. They have compared the drawdown of floating solids for a range of baffle geometries in order to determine the most efficient design strategy.

CHAPTER 3

COMPUTATIONAL FLUID DYNAMICS

3.1 INTRODUCTION

Computational Fluid Dynamics is the branch of fluid dynamics providing a cost effective means of simulating real flows by the numerical solution of the governing equations. The governing equation for the Newtonian fluid dynamics, namely the Navier-Stokes equation s, have been known for over 150 years. Computational Techniques replace the governing partial differential equations with system of algebraic equation that are much easier to solve using computers. CFD techniques have been adopted by a whole range of industries, including chemical, petrochemical, oil, automotive, built environment (architecture, industrial design, building construction management, town planning), food processing and many others enabling the process engineer to begin to understand in greater detail the internal operation of individual units by relating an analysis of the flow field and other transfer processes with observed phenomena and thereby identify the cause of a problem and evaluate solutions. Moreover, it has steadily spread from research groups into the design and development departments. In short, CFD is being used as an engineering tool to aid in the understanding and design of process operations.

3.2 MODEL EQUATIONS

The governing equations for a general mixing problem are the mass and momentum balances. These govern the flow in agitated tanks. These equations are written below in cylindrical coordinates. These equations are solved in three dimensions under steady state and incompressible flow conditions.

3.2.1 Conservation Equations

If a small volume, or element of fluid in motion is considered, two changes to the element will probably take place: (1) the fluid element will translate and possibly rotate in space, and (2) it will become distorted, either by a simple stretching along one or more axes or by an angular distortion that causes it to change shape. The process of translation is often referred to as convection, and the process of distortion is related to the presence of gradients in the

velocity field and a process called diffusion. In the simplest case, these processes govern the evolution of the fluid from one state to another.

In more complicated systems, sources can also be present that give rise to additional changes in the fluid. Many more phenomena can also contribute to the way a fluid element changes with time. Many of the processes such as those that are involved in the description of generalized fluid motion are described by a set of conservation or transport equations. These equations track, over time, changes in the fluid that result from convection, diffusion, and sources or sinks of the conserved or transported quantity. Furthermore, these equations are coupled, meaning that changes in one variable (say, the velocity) can give rise to changes in other variables (say, the pressure). The equations discussed below describe many of these coupled phenomena that are typical in mixing applications.

3.2.2 Continuity Equation

The continuity equation is a statement of conservation of mass. The equation of continuity in three-dimensional cylindrical coordinates is:

$$\frac{1}{r}\frac{\delta}{\delta r}(r u_r)+\frac{1}{r}\frac{\delta}{\delta \theta}(u_\theta)+\frac{\delta}{\delta z}(u_z)=0 \tag{3.1}$$

3.2.3 Momentum Equation

The momentum equation is a statement of conservation of momentum in each of the three component directions. The three momentum equations are collectively called the Navier-Stokes equations. In addition to momentum transport by convection and diffusion, several momentum sources are also involved:

The r component,

$$\begin{aligned}&[u_r\frac{\delta u_r}{\delta r}+\frac{u_\theta}{r}\frac{\delta u_r}{\delta \theta}-\frac{u^2{}_\theta}{r}+u_z\frac{\delta u_r}{\delta z}] \\ &=\frac{-1}{\rho}\frac{\delta p}{\delta r}+\nu[\frac{\delta}{\delta r}[\frac{1}{r}\frac{\delta}{\delta r}(ru_r)]+\frac{1}{r^2}\frac{\delta^2 u_r}{\delta \theta^2}-\frac{2}{r^2}\frac{\delta^2 u_\theta}{\delta \theta}+\frac{\delta^2 u_r}{\delta z^2}]+g_r\end{aligned} \tag{3.2}$$

The θ-component,

$$[u_r\frac{\delta u_\theta}{\delta r}+\frac{u_\theta}{r}\frac{\delta u_\theta}{\delta \theta}+\frac{u_r u_\theta}{r}+u_z\frac{\delta u_\theta}{\delta z}]$$
$$=[\frac{-1}{r\rho}\frac{\delta p}{\delta \theta}+\nu[\frac{\delta}{\delta r}(\frac{1}{r}\frac{\delta}{\delta r}(r u_\theta))+\frac{1}{r^2}\frac{\delta^2 u_\theta}{\delta \theta^2}+\frac{2}{r^2}\frac{\delta u_r}{\delta \theta}+\frac{\delta^2 u_\theta}{\delta z^2}]+g_\theta] \quad (3.3)$$

and the Z component,

$$[u_r\frac{\delta u_z}{\delta r}+\frac{u_\theta}{r}\frac{\delta u_z}{\delta \theta}+u_z\frac{\delta u_z}{\delta z}]$$
$$=[\frac{-1}{r\rho}\frac{\delta p}{\delta z}+\nu[\frac{\delta}{\delta r}(r\delta\frac{u_z}{\delta r})+\frac{1}{r^2}\frac{\delta^2 u_z}{\delta \theta^2}+\frac{\delta^2 u_z}{\delta z^2}]+g_z] \quad (3.4)$$

3.3 TURBULENCE

A number of dimensionless parameters have been developed for the study of fluid dynamics that are used to categorize different flow regimes. These parameters, or numbers, are used to classify fluids as well as flow characteristics. One of the most common of these is the Reynolds number, defined as the ratio of inertial forces, or those that give rise to motion of the fluid, to frictional forces, or those that tend to slow the fluid down. In geometrically similar domains, two fluids with the same Reynolds number should behave in the same manner. For mixing tanks, the Reynolds number is defined as

$$R_e=\eta\frac{ND^2}{\rho} \quad (3.5)$$

where ρ is the fluid density, N is the impeller speed, in rev/s, and D is the impeller diameter, η is the molecular dynamic viscosity of the fluid. Based on the values if the Reynold number, flow falls either into the laminar regime, with small Reynolds numbers, or the turbulent regime, with high Reynolds numbers. The transition between laminar and turbulent regimes occurs throughout a range of Reynolds numbers rather than at a single value.

For mixing tanks, transition occurs somewhere between Re=10 and 10000, depending on the power number of the impeller. In the turbulent regime, fluctuations in the mean velocity and other variables occur, and for the model to be able to provide meaningful results, their effect needs to be incorporated into the CFD model, than at a single value. For mixing tanks, transition occurs somewhere between Re = 10 and 10000, depending on the power number of

the impeller. In the turbulent regime, fluctuations in the mean velocity and other variables occur, and for the model to be able to provide meaningful results, their effect needs to be incorporated into the CFD model. This is done through the use of a turbulence model.

Several methods are available for including turbulence in the Navier-Stokes equations. Most of these involve a process of time averaging the conservation equations that makes terms of Reynolds tensor (turbulent stresses) to appear. Among the different turbulent models developed in order to estimate the stresses, the k-ε model is largely used in process engineering, and particularly in mixing operation.

3.4 THE STANDARD *K*- *Ɛ* MODEL

The *k*-ε model is one of a family of two-equation models for which two additional transport equations must be solved to compute the Reynolds stresses. It is a robust model, meaning that it is computationally stable, even in the presence of more complex physics. It is applicable to a wide variety of turbulent flows and has served the fluid modeling community for many years. It is semi-empirical, based in large part on observations of high Reynolds-number flows. The two transport equations that need to besolved for this model are for the kinetic energy of turbulence, *k*, and the rate of dissipation of turbulence,

$$\frac{\delta}{\delta x_i}[(\eta+\frac{\eta_t}{\sigma_k})\frac{\delta k}{\delta x_i}]+G_k+G_b-\rho\varepsilon-y_M=0 \tag{3.6}$$

and,

$$\frac{\delta}{\delta x_i}[(\eta+\frac{\eta_t}{\sigma_\varepsilon})\frac{\delta k}{\delta x_i}]+C_{1\varepsilon}\frac{\varepsilon}{k}(G_k+C_{3\varepsilon}G_b)-C_{2\varepsilon}\rho\frac{\varepsilon^2}{k}=0 \tag{3.7}$$

where, G_k represents the generation of turbulent kinetic energy due to the mean velocity gradients, G_b is the generation of turbulent kinetic energy due to buoyancy, Y_M represents the contribution of the fluctuating in compressible turbulence to the overall dissipation rate. C_{1e}, C_{2e} and C_{3e} are constants, σ_k and σ_ε are the turbulent Prandtl numbers for k and ε, respectively.

In the current study, the governing equations (mass and momentum) for a general mixing problem and the transport equations are solved by using a general-purpose three dimensional commercial CFD package, FLUENT, using the standard k–ε model.

3.5 BOUNDARY CONDITIONS AND ASSUMPTIONS

The following boundary conditions have been used:

a) On the walls, no-slip conditions have been imposed.

b) The flow in the stirred tanks is fully turbulent.

c) At fully turbulent flow, the inertial forces due to the fluctuating velocity overwhelm the viscous forces, so the flow field becomes independent of the fluid viscosity (the viscous heating is negligible).

d) The surface of the liquid is always considered as flat plane, that is to say that the vortex phenomenon is considered absent.

e) The liquid surface is free, which corresponds to the following conditions:

$$u_z = 0 \; ; \frac{\delta u_r}{\delta z} = 0 \; ; \frac{\delta u_\theta}{\delta z} = 0 \qquad (3.8)$$

3.6 THE IMPELLER GEOMETRY MODEL

To model the geometry of impeller exactly, a 3D simulation must be performed. A number of solution approaches are available to incorporate the motion of the impeller, and the computational grid must be able to adapt to the solver method employed. The most commonly used geometry models will be discussed in this section.

3.6.1 The Rotating Frame (RF) Model

The rotating frame model solves the momentum equations for the entire domain in a rotating frame. In this model acceleration of the coordinate system is included in the equations of motion describing the flow.The Coriolis force is included in the process. Problems solved in rotating frame typically use the angular velocity of the primary rotating component, as the angular velocity of the frame. In stirred tanks, the impeller serves this purpose, so the frame is assumed to rotate with the impeller. Thus, the impeller is at rest in the rotating frame. Figure 4.1.a and Figure 4.1.b show the typical original and rotating reference frame taken in a cylinderical tank.

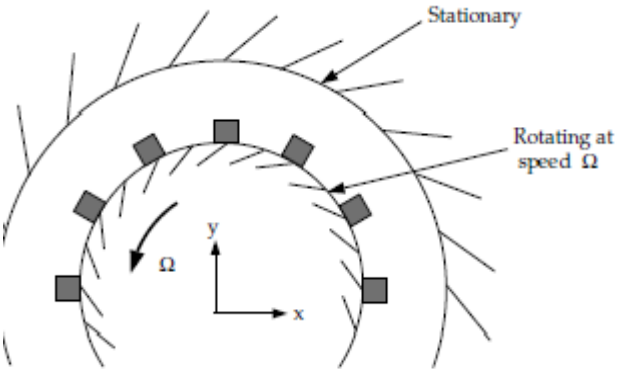

Figure : 4.1.a) Original Reference Frame [40]

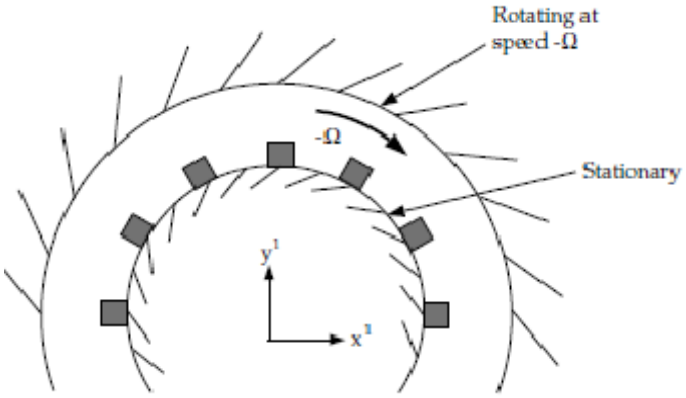

Figure : 4.1.b) Rotating Reference Frame [40]

The tank, rotates in the opposite direction, so must have a rotational boundary condition. If baffles exist, they would need to rotate into the fluid with the same angular velocity. Unfortunately, this simple steady-state model is not equipped to handle the motion of elements such as baffles into or through the fluid. The approach is therefore only useful for unbaffled tanks with smooth tank walls that are geometrically equivalent to a perfect surface of revolution. Thus an unbaffled cylindrical tank with an axisymmetric bottom shape and no angular-dependent internals could be simulated in this manner.

3.6.2 The Multiple Reference Frames (MRF) Model

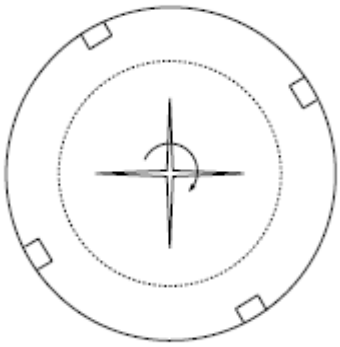

Figure : 4.2 Geometry with one rotating impeller [40]

A modification of the rotating frame model is the multiple reference frames (MRF) model . The modification is that more than one rotating (or non rotating) reference frame can be used in a simulation. This steady-state approach allows the modeling of baffled stirred tanks with other complex (rotating or stationary) internals. A rotating frame is used for the region containing the rotating components while a stationary frame is used for regions that are stationary (Figure 4.2). In the rotating frame containing an impeller, the impeller is at rest. In the stationary frame containing the tank walls and baffles, the walls and baffles are at rest.

If the interaction between the impeller and baffles is weak, the relative orientation of the impeller and baffles does not matter. If the interaction is strong, however, the solution with the impeller in one position relative to the baffles will be different from that with the impeller in a different position. The model is therefore recommended for simulations in which the impeller-baffle interaction is weak. If the interaction is high, one can perform two solutions with the impeller in two different locations and use both results (e.g., averaging them) rather than just one to get reasonable solution.

3.6.3 Sliding Mesh Model

The sliding mesh model is a time-dependent solution approach in which the grid surrounding the rotating component(s) physically moves during the solution. The velocity of the impeller and shaft relative to the moving mesh region is zero, as is the velocity of the tank, baffles, and other internals in the stationary mesh region. The motion of the impeller is realistically modeled because the grid surrounding it moves as well, giving rise to a time-accurate

simulation of the impeller-baffle interaction. The motion of the grid is not continuous. Rather, it is in small, discrete steps. After each such motion, the set of conservation equations is solved in an iterative process until convergence is reached. The grid moves again, and convergence is once again obtained from an iterative calculation.

3.7 GRID SYSTEM

The grid, also called a mesh, consists of discrete elements located throughout the computational domain and fits the contours of the vessel and its internals. After defining the model, a computational domain is generated and defined by a grid. This grid is used as the basis of the solution procedure. In mixing simulations, the computational domain is

the volume occupied by the fluid inside the vessel.

These elements, formed by surfaces in 3D, of different shape and sizes and together they constitute a grid. In a CFD analysis, conservation equations for flow are solved in each of these elements, or control volumes, throughout the domain. If the overall grid is too coarse, the resulting solution may be inaccurate. If the overall grid is too fine, the computational cost may become prohibitive.

The cost of the calculation will be directly proportional to the number of elements in the grid, so it is best to concentrate the elements where one need them, and reduce the number of elements where they are not required. Generally, the tank bottom and/or the impellers have curvature. Some dimensions may be small in one dimension (say, the thickness of a baffle) compared to other length scales of importance (the length of the baffle). Together, these factors contribute to grids that will not be orthogonal or have perfect aspect ratios, while conforming to arbitrary shapes and sizes. The best grid is usually a balance of all these factors. In 3D simulations, the impeller, baffles, and other internals are modeled using their exact geometry. The grid elements used in GAMBIT are mainly tetrahedral and hexahedral, with pyramids between differently meshed zones.

Advantages of using Tetrahedral Elements:

It produces a better grid for geometrically complicated models that include, for example, spherical or ellipsoidal geometries. It has an improved ability to vary the node spacing within the domain. It facilitates coupling among the degrees of freedom.

Disadvantage of using Tetrahedral Elements :

Using tetrahedral elements with objects that have very small dimensions (such as baffles with small thickness, or impellers with small height) can lead to very large grids.

The advantage of using hexahedral cells are:

They yield fewer cells with the same characteristics mesh sizing (element length, node distance). They are particularly accurate when the flow is oriented with the grid lines.

3.8 TYPES OF SOLVER

There are two choices of numerical methods provided by fluent segregated solver ("FLUENT/UNS") and coupled solver ("RAMPANT"). Using either method, FLUENT will solve the governing integral equations for the conservation of mass and momentum, and (when appropriate) for energy and other scalars such as turbulence and chemical species. In both cases a control-volume-based technique is used that consists of division of the domain into discrete control volumes using a computational grid, integration of the governing equations on the individual control volumes to construct algebraic equations for the discrete dependent variables ("unknowns") such as velocities, pressure, temperature, and conserved scalars, and linearization of the discretized equations and solution of the resultant linear equation system to yield updated values of the dependent variables.

3.9 DISCRETIZATION OF THE GOVERNING EQUATIONS

A control-volume method to solve the momentum and continuity equations is used by Fluent. This control volume technique consists of integrating the governing equations about each control volume, yielding discrete equations that conserve each quantity on a control-volume basis. Discretization of the governing equations can be illustrated most easily by considering the steady-state conservation equation for transport of a scalar quantity f. This is demonstrated by the following equation written in integral form for an arbitrary control volume *V* as follows:

$$\oint \rho \varphi_i v \, dA = \oint \Gamma_\varphi \nabla_{\varphi_i} dA + \int_v s_\varphi \, dV \qquad (3.9)$$

where Γ_ϕ is diffusion coefficient of ϕ in phase *i,* ϕ_i is any conserved property of phase *i,* and *V* is an arbitrary control volume. Equation 3.9 is applied to each control volume, or cell, in

the computational domain. Discretization of Equation on a given cell yields

$$\Sigma_f^{N_{faces}} f \Phi_f \nu A_f = \Sigma_f^{N_{faces}} \Gamma_\Phi (\nabla \Phi)_n A_f + S_\Phi V \tag{3.10}$$

The continuity equation can be written as :

$$\oint \rho v \, dA = 0 \tag{3.11}$$

3.10 PROBLEM SOLVING PROCEDURE

After determining the important features of the problem, the following procedure is followed to solve the problem.

1. Create the model geometry and grid using GAMBIT software.
2. Start the appropriate solver for 3D modelling.
3. Check the skewness/ smoothness.
4. Select the solver formulation.
5. Choose the basic equations to be solved: laminar or turbulent (or inviscid), chemical species or reaction, heat transfer model, etc.
6. Specify material properties (fluid or solid etc.).
7. Specify the boundary conditions.
8. Adjust the solution control parameters.
9. Initialize the flow field.
10. Calculate a solution (iteration is to be done till convergence).
11. Examine the results.
12. Save the results (case and data files to be made).
13. If necessary, refine the grid or consider revisions to be numerical or physical model

CHAPTER 4

EXPERIMENTAL SET-UP AND RESULTS

4.1 EXPERIMENTAL SET-UP FOR MEASUREMENT OF EROSION WEAR

The experimental set-up commonly used by the investigators in the measurement of erosion wear consists of a pot tester [19]. It consists of an aluminium tank of 155 mm height with inner diameter 240 mm and is covered at the top by a transparent acrylic sheet as shown in figure 4.1, Four full-length baffles are provided at the inner wall of the cylindrical tank at equal distances. A shaft is inserted from the top to rotate the wear specimens inside the pot whereas another shaft is provided from the bottom to rotate a pitched turbine blade propeller for keeping the solid–liquid mixture under suspension.

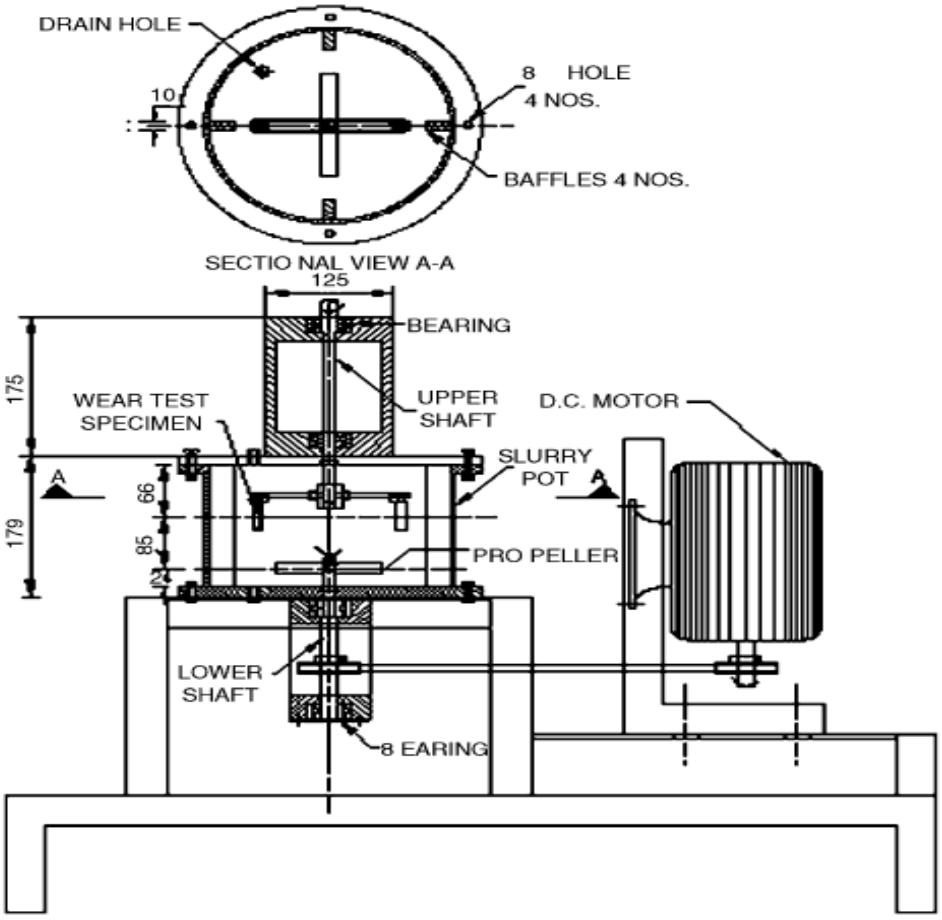

Figure 4.1: Schematic diagram of pot tester [19]

Each shaft is rotated by an independent 0.75 kW dc motor through-belt pulley drive. At the lower end of the shaft rotating the specimens, a brass sleeve of 30 mm length and 25 mm diameter is provided with provisions for fixing two horizontal arms to hold two test fixtures at 142 mm distance at diametrically opposite ends. The test fixture is hanged on the horizontal arm through its one end with the help of 4 mm screw. Two fixtures can be fitted 180° apart to balance the dynamic forces with minimum wake interference effect. A slotted angular plate is fixed on each arm to orient the test fixture at any angle in the range of 0–90° (in steps of 15°) to the tangential direction of rotation.

4.2 MEASUREMENT PROCEDURE

Figure 4.2: Slurry pot tester with speed control unit

The wear specimens of the impeller are taken and then polished before performing the test. Specimens are cleaned in tap water, rinsed in acetone and dried with hot air blower before and after each test performed on the slurry pot tester. Mass loss of each specimen is measured in an electronic balance having least count of 0.1 mg. The solid liquid mixture is prepared by mixing solid particles with water.

A predetermined mass of solid particles is poured first in the pot, which will then be closed. A known quantity of water is added through the hole at the top of the cover to completely fill the pot. To conduct the experiment propeller shaft is rotated in down pumping mode at the suspension speed, which is predetermined to achieve uniform distribution of solid particles at

different concentrations. The speed of each shaft is measured by speed control unit. For each wear test, the mass loss of each wear specimen is noted and the average value can be used for further analysis.

4.3 EXPERIMENTAL SET-UP FOR SUSPENSION OF SOLIDS

Suspension of solid particles in water is a critical parameter in accurate calculation of wear rate in the erosion pot tester. To study the suspension of solid-liquid mixtures in a cylindrical tank the experimental set-up used consists of a transparent perplex cylindrical tank fitted with four baffles, a propeller and a DC motor. To measure the concentration through cylindrical height five ports have been provided at a distance 50 mm,75 mm, 100 mm and 150 mm from the bottom of the tank respectively.

Figure 4.3: Aluminium tank replaced by a transparent tank of equal size

The cylindrical tank (as shown in the figure 4.3) is transparent for clear visualization and has flat bottom with inner diameter of 240 mm, wall thickness of 5 mm and tank height of 225 mm. The tank is fitted with four baffles; each of 25 mm x 10 mm size are placed with larger dimension along two orthogonal diametral planes inside the cylinder periphery.

At the tank wall, total 5 ports of 8 mm diameter have been provided to collect slurry samples; three at left hand side at 50 mm, 100 mm and 150 mm from the bottom, marked as L1,L2 and L3 respectively and two at its diametrically opposite side i.e., right hand side at 75 mm and

125 mm from the bottom, marked as R1 and R2 respectively. A taper cork lid has been provided at each port for quick opening and closing for sample collection.

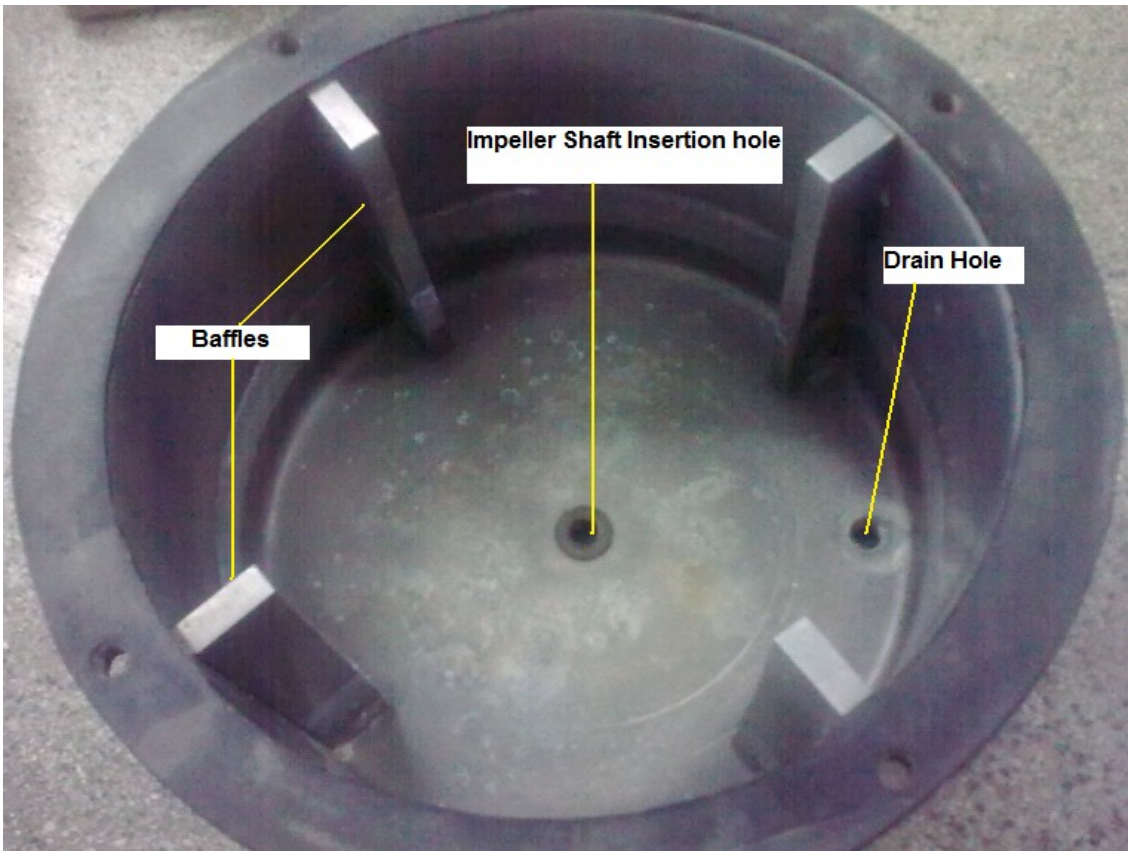

Figure 4.4: Drain hole, impeller shaft hole and baffles in the tank

A shaft of 11 mm diameter is inserted from the tank bottom to rotate a propeller inside and is sealed with oil-seal to prevent leakage of solid-liquid mixture. A drain hole of 12 mm diameter is made to drain-out the solid-liquid mixture after the experiment. The cylindrical tank is mounted on an angle-iron frame structure and fixed using nut bolts.

Experiments have been performed using 4 types of PBT propellers given in detail below.

Table : 4.1 Types of propellers used in the experiments

Name	Type	Diameter(D)	Blade Width (W)	Thickness (t)	Blade Angle
Propeller-1	PBT Impeller	105 mm	14 mm	2 mm	45 Degrees
Propeller-2	PBT Impeller	180 mm	15mm	2 mm	45 Degrees
Propeller-3	PBT Impeller	180 mm	5 mm	2 mm	45 Degrees
Propeller-4	PBT Impeller	145 mm	27mm	2 mm	45 Degrees

Figure 4.5: a) Propeller-1, b) Propeller-2, c) Propeller-3, d) Propeller-4

(i) Propeller-1 is a four blade pitched turbine (PBT) propeller with each blade having angle of 45 degrees with respect to the rotational direction. The diameter of this propeller is kept as 0.44 times of the diameter of cylindrical tank (=105 mm) and width of blade is kept as 0.13 times of the diameter of propeller (=14 mm). The propeller is operated at off bottom clearance gap of 24 mm (=0.05 times of the tank diameter) because the maximum energy from propeller to the particles is supposed to be transferred at low-off bottom clearance.

(ii) Propeller-2 is 45 degrees PBT propeller with diameter 180 mm and bade width equal to 15 mm.

iii) Propeller-3 is 45 degrees PBT propeller with diameter 180 mm and blade width 5mm.

iv) Propeller-4 used is 45 degrees PBT propeller with diameter 145 mm and width 27mm.

Table 4.2 : Impeller-Tank selection parameters

Propeller Name	No. Of Blades (nB)	C/T Ratio	D/T Ratio	H/T Ratio
Propeller-1	4	0.05	0.44	0.94
Propeller-2	4	0.03	0.75	0.94
Propeller-3	4	0.01	0.75	0.94
Propeller-4	4	0.07	0.6	0.94

The diameter of propeller shaft is taken as 10 mm. This shaft is inserted from the bottom of the tank to fix the propeller and is kept vertical with the help of two bearings fitted in an Aluminium block. The shaft can be rotated in both the directions at different speeds by a 0.75 kW DC motor through V belt-pulley drive. A magnetic sensor is fixed at the propeller motor

for measurement of the RPM of the propeller shaft. The sensor works on the principle of varying magnetic field and generates pulses at every rotation of the motor shaft. Sensors are connected with a control unit panel which displays the RPM. The RPM can be adjusted to the desired value by moving the knob on the control panel.

Figure 4.6: Speed control unit and sensor

4.4 PROPERTIES OF SOLID PARTICLES AND SOLID-LIQUID MIXTURES

Solid particles used in the experiment is Silicon Carbide (black) which forms solid-liquid mixture with tap water to conduct the experiments on erosion wear. Standard methods are used to determine physical properties of solid particles and the solid-liquid mixtures.

4.4.1 Specific gravity

Specific gravity of solids is an important parameter for the erosion wear and it plays a significant role in suspension of solids. The overall specific gravity of Silicon Carbide used was 3.22.

4.4.2 Particle size and shape

The particle size used under present investigation is of 550 microns. Silicon carbide particles are sieved through 600 microns and 500 microns size sieve respectively. The sieved particles are retained and the lot is prepared accordingly. The mean of the two sieve sizes ((500+600)/2=550) is taken as the average mean diameter of the particles retained between

the two sieve sizes. The particle size of the silicon carbide appears to be angular by visual inspection.

Figure 4.7: Silicon carbide particles retained between 500-600 micron size sieves

4.5 EXPERIMENTAL PROCEDURE AND DATA ANALYSIS

Various experiments have been performed with each propeller under varying parameters. Suspension behavior in the cylindrical tank has been studied on the following:

1. Effect of change in original concentration (Cw) on the quality of suspension.
2. Effect of 4 different types of PBT propellers on the quality of suspension.
3. Effect of change in rotational speed on the quality of suspension.
4. Effect of change in baffle design on the solid suspension quality.

The volume of cylindrical tank is 7 liters and a known amount of solid is added to the tank and water is poured up-to the top position. The weight percentage is calculated using the following formula:

Weight percent of Solid in Water = (Weight of solid in gm)/ (Weight of solid in gm +

Weight of water in gm) x 100 (1)

The sample taken was weighed first and dried to extract water. The dried sample was again weighed to get the weight of solid. Weight percentage was then calculated using equation 1. PBT propeller was rotated in down pumping mode to suspend the sand particles in water. For

collection of the samples of sand-water mixture the topmost opening port ‘L3’ was opened by pulling-off the cork lid and the sand-water mixture was collected in a beaker of 100 ml. After collecting sufficient quantity of sample, the port was closed by pushing the cork lid.

Precaution was taken while collecting the sample so as to avoid overflow and wastage of mixture while opening and closing the port. Similarly, samples from ports R2, L2, R1 and L1 were collected in sequential order in 100 ml beakers. It is assumed that the withdrawal of small quantity of the mixture in the beaker will not significantly affect the flow conditions in the tank.

The volume of solid-liquid mixture was noted and its weight was measured in an electronic weighing balance having least count of 0.1 mg. The excess water from the beaker was drained out with the help of filter paper and care was taken to ensure that no sand particle move out with water. Then it was kept in an electric oven for 1-2 hours at 100 °C. The weight of dry solid particles was then determined by weighing on an electronic balance of 0.1mg.

Solid concentration was calculated by dividing the weight of solid SiC by the total weight of solid-liquid mixture. The same procedure was repeated for all the samples collected. The weight percent of solids in the sample is determined and compared with the overall solid concentration in the tank.

The experiments are conducted on or within 10 percent variation of the suspension speed of the silicon-carbide particles. Suspension speed of the solid particles is defined as the minimum rotational speed of the impeller which bring out the uniform suspension in the stirred tank. Desale-et-al introduced the correlation of minimum suspension speed for silicon-carbide particles in water [19].

$$Ns = 276.303 \times d^{0.0372} \times Cw^{0.1886} \times Vt^{0.1889} \quad (2)$$

Where d= mean diameter of the silicon-carbide particles, Cw= Solid concentration by weight and Vt= Settling velocity of the silicon-carbide particles in water.

4.5.1 Effect of change in original concentration (Cw) on solid suspension

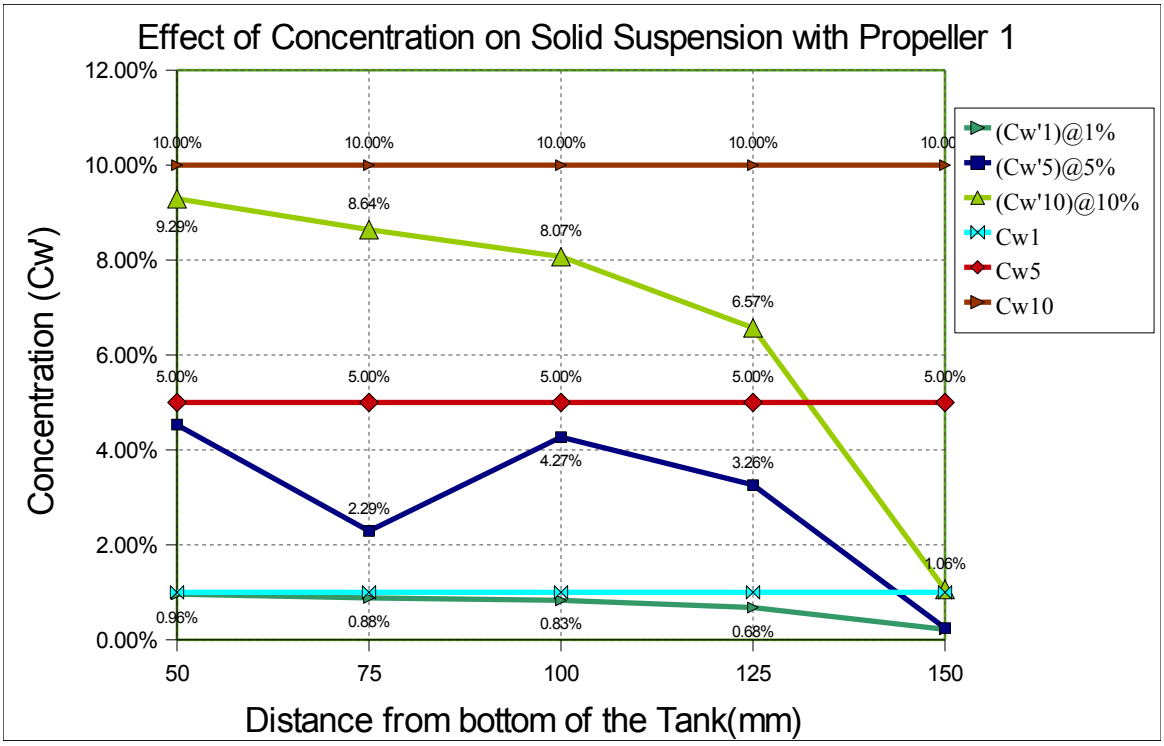

Figure 4.8: Effect of solid concentration (Cw) on propeller-1

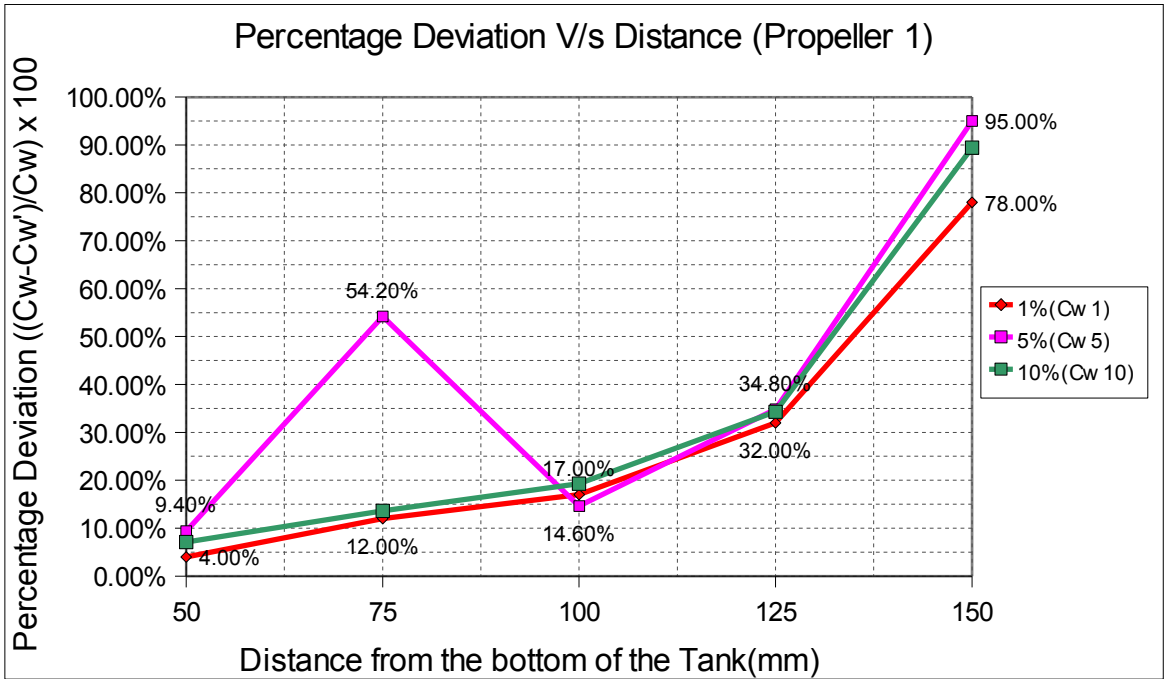

Figure 4.9: Percentage deviations from Cw, propeller-1

With Propeller 2 :

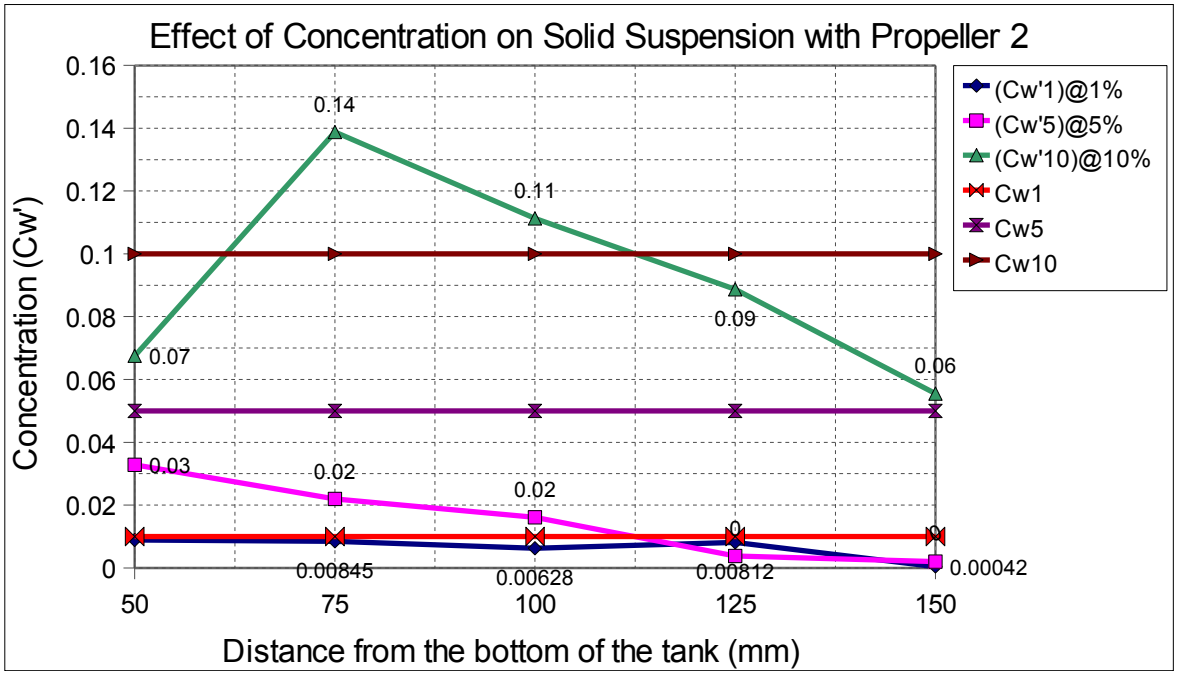

Figure 4.10: Effect of solid concentration (Cw) on propeller-2

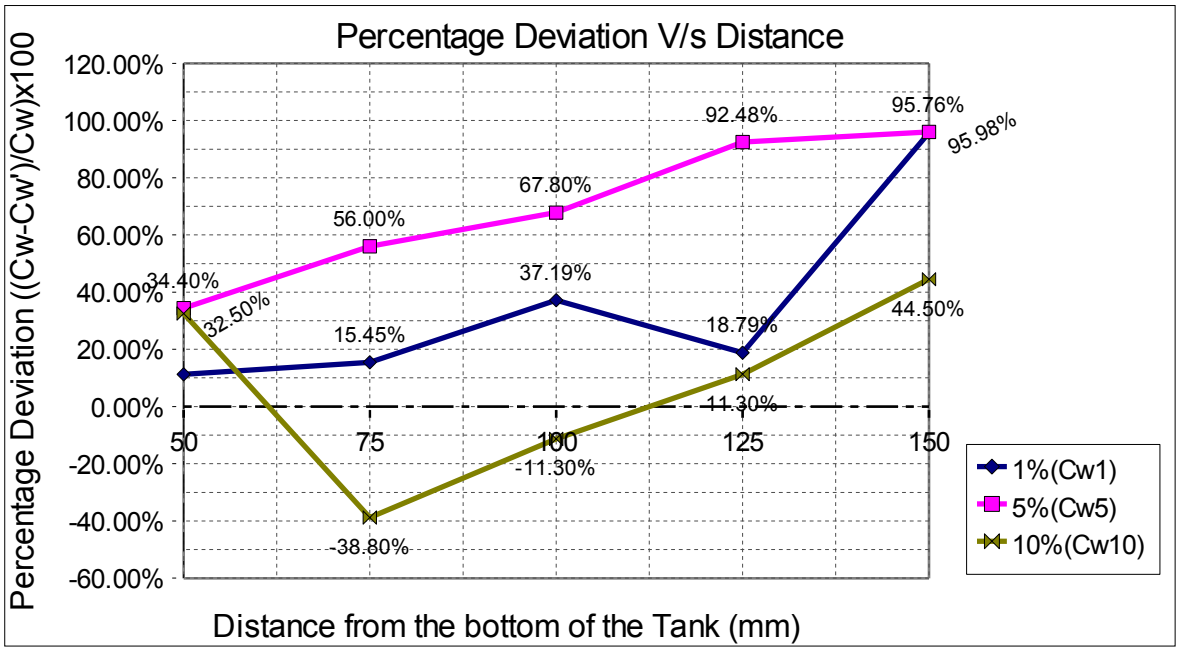

Figure 4.11: Percentage deviations from Cw, propeller-2

** Positive deviation corresponds to the lesser concentration value than the original value (Cw) whereas negative corresponds to higher than the original (Cw) one.*

With Propeller-4 :

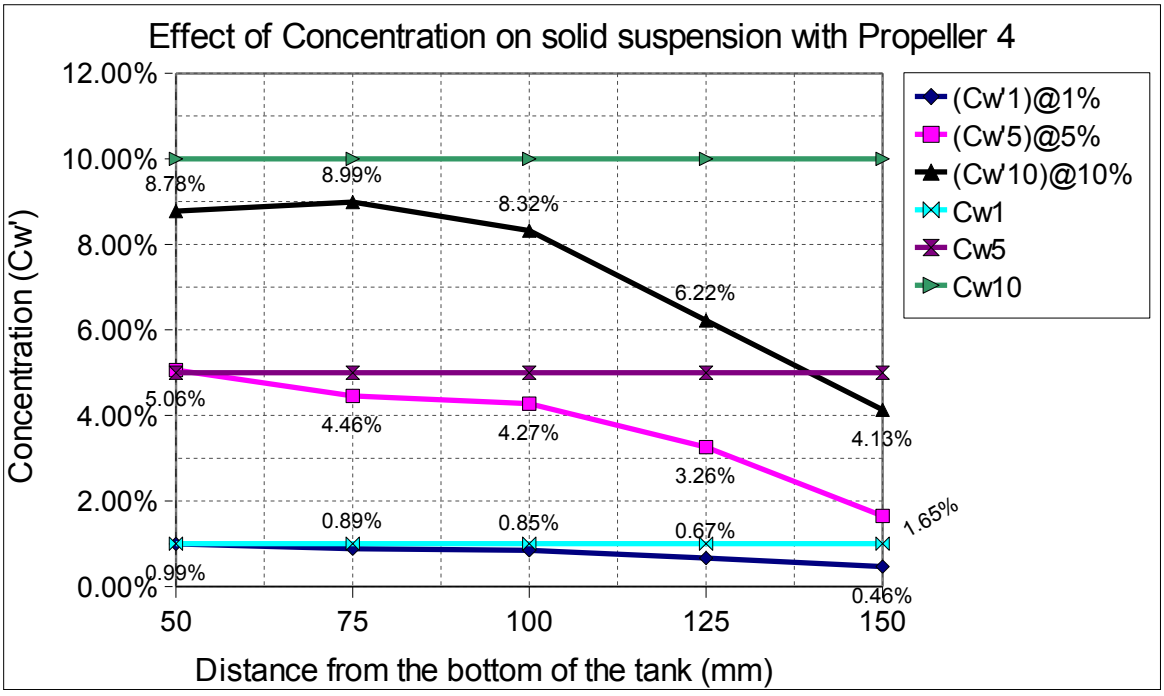

Figure 4.12: Effect of solid concentration (Cw) on propeller-4

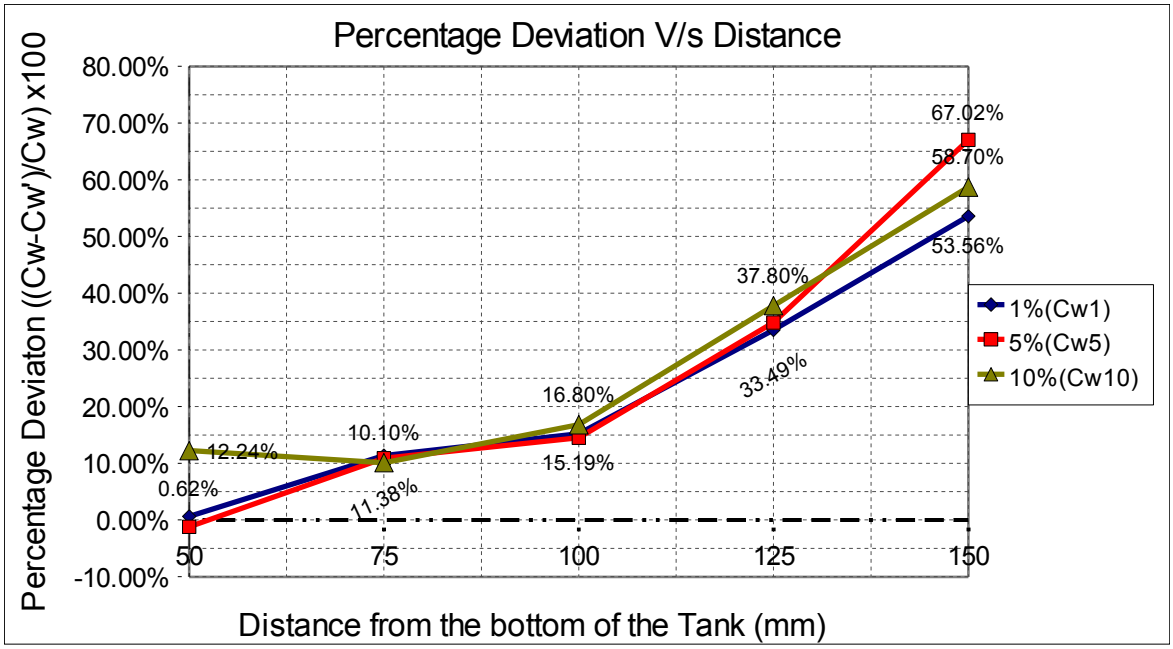

Figure 4.13: Percentage deviations from Cw, propeller-2

** Positive deviation corresponds to the lesser concentration value than the original value (Cw) whereas negative corresponds to higher than the original (Cw) one.*

4.5.2 Effect of different propellers on solid suspension in pot tester

Table 4.10 : Scheme of Experimentation (propellers)

Propeller Type	Original Concentration (Cw)	Rotational Speed (rpm)
Propeller-1	1.00%	360
Propeller-2		
Propeller-3		
Propeller-4		

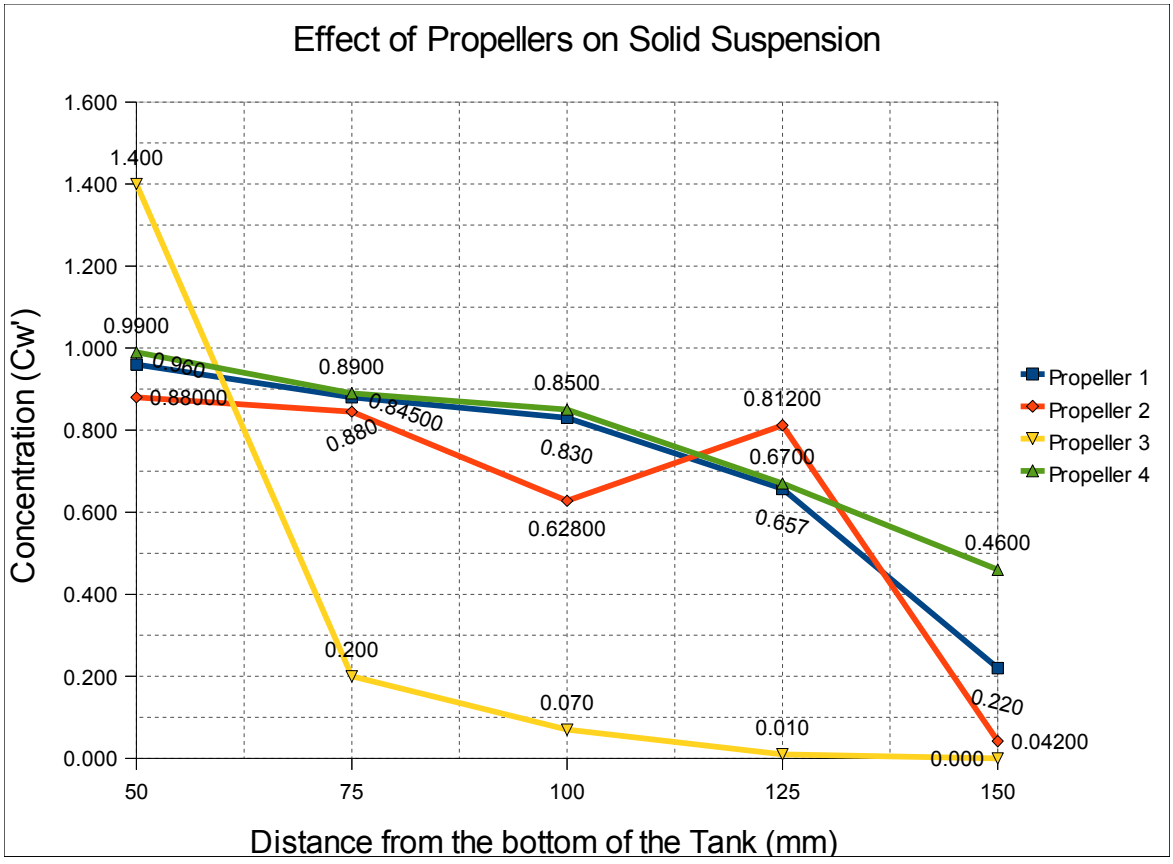

Figure 4.14: Effect of different propellers on solid suspension, Cw=1%

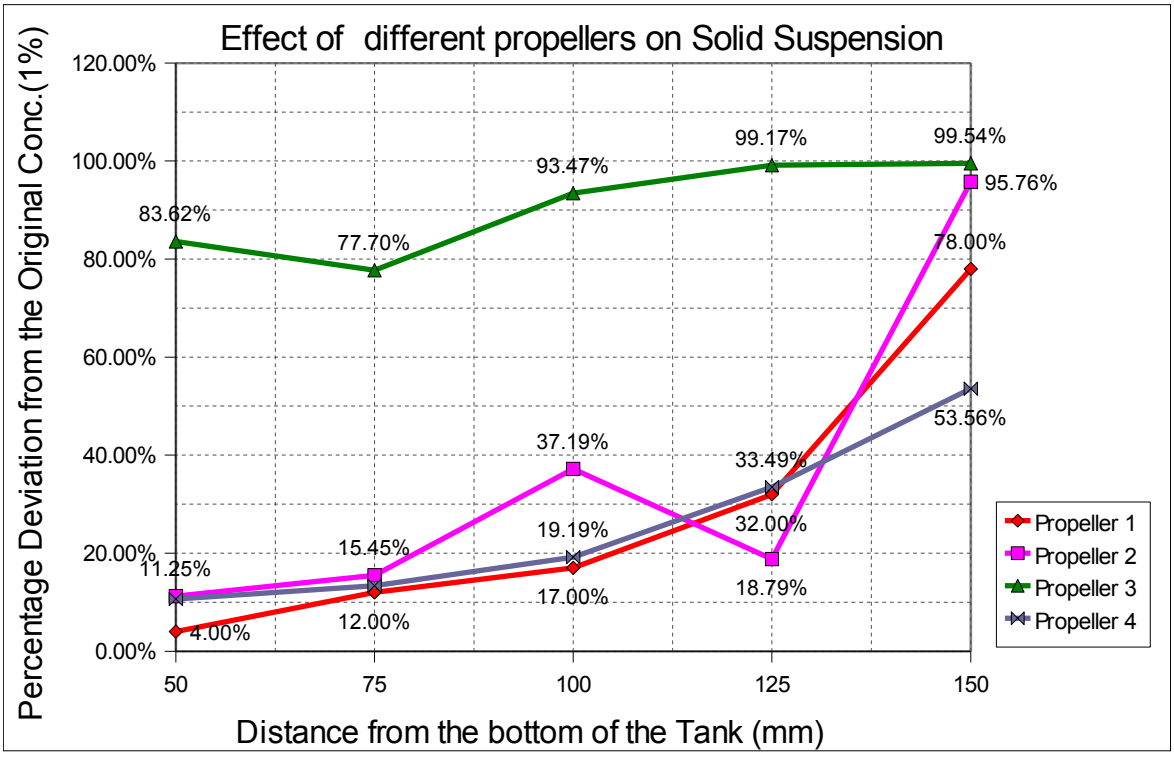

Figure 4.15: Percentage deviation from the original concentration(Cw=1%)

** Positive deviation corresponds to the lesser concentration value than the original value (Cw) whereas negative corresponds to higher than the original (Cw) one.*

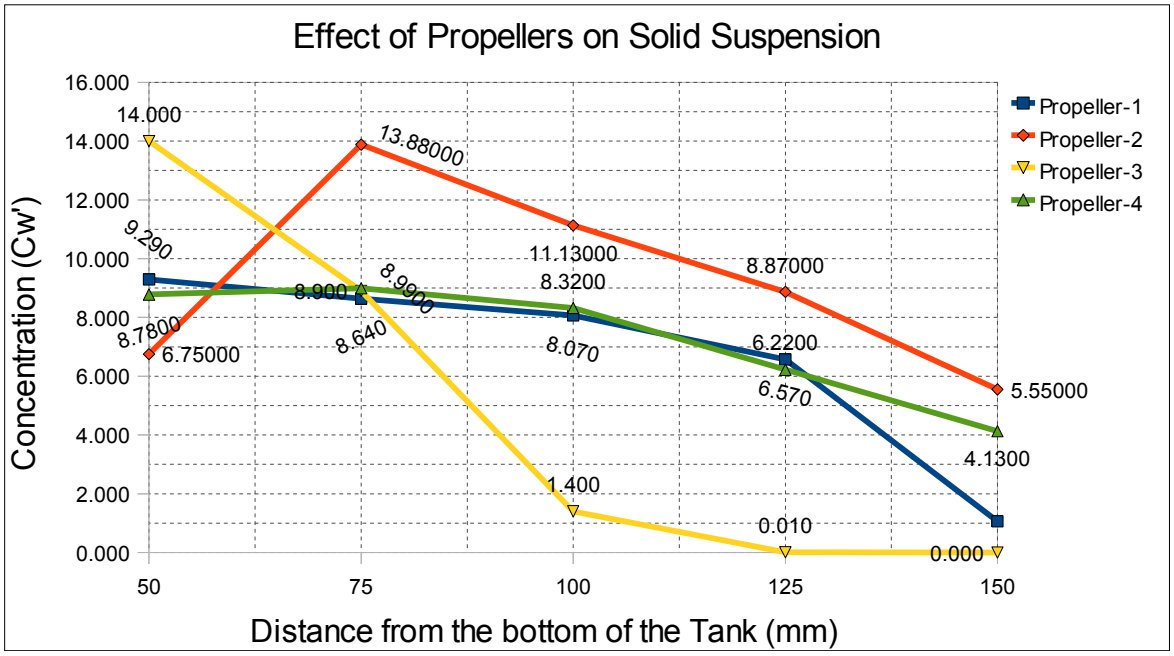

Figure 4.16: Effect of different propellers on solid suspension,Cw=10%, 360 rpm

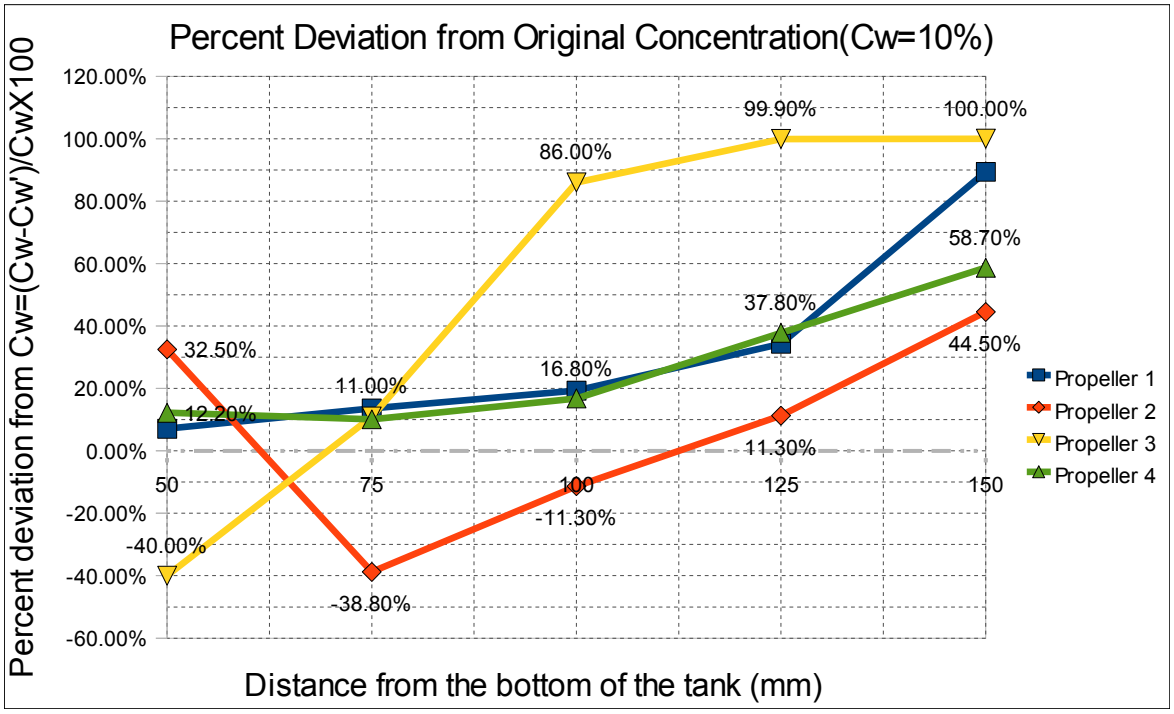

Figure 4.17: Percentage Deviation from the Original Concentration(Cw=10%)

** Positive deviation corresponds to the lesser concentration value than the original value (Cw) whereas negative corresponds to higher than the original (Cw) one.*

4.5.3 Effect of different rotational speeds on solid suspension.

With Propeller-1 :

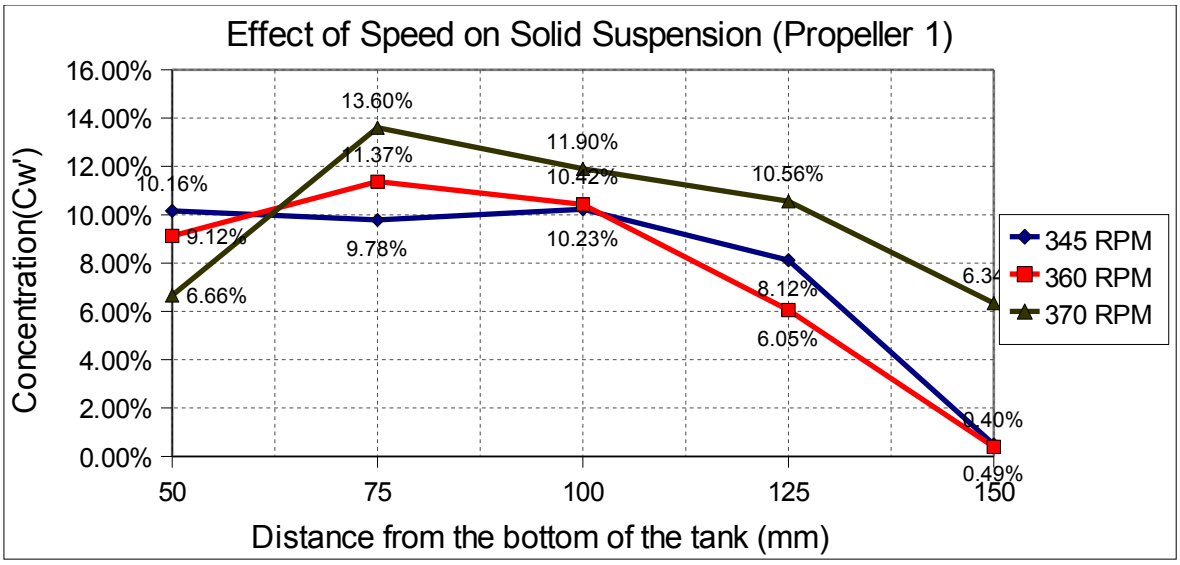

Figure 4.18: Effect of Rotational Speed on Solid Suspension, propeller-1

With Propeller-4 :

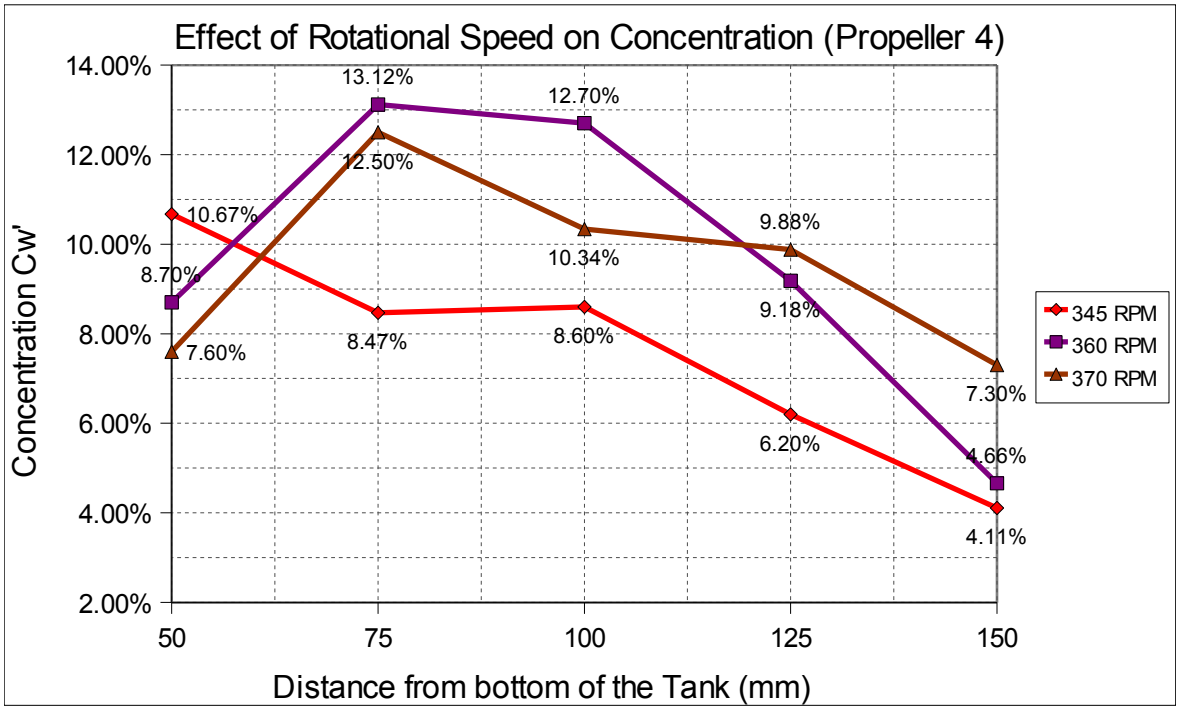

Figure 4.19: Effect of rotational speed on solid suspension, propeller-4

4.5.3 Effect of change in baffle design on solid suspension.

Solid particles in motion in the slurry pot, get obstructed by the baffles and some of them due to the loss of velocity and energy in the collision with the obstructed baffles move to the bottom part of the baffle and get settled. Some of them are carried away by vortex effect but most of them which are closer to the baffle-wall bottom remain settled. In this way solid particles get trapped at the bottom of all the four baffles.

In the changed baffles, a clearance of 50 mm is provided so that the particles, when at bottom, are not obstructed and move away with the momentum of fluid.

Baffle width taken is 25mm, with D/T ratio well within $1/9 < D/T < 1/12$. No change has been made to the other dimensions except the baffle height. Hence, the dimension of the new baffles used are (25mm X 10mm X 175mm).

The experiments conducted with the new baffles are compared with the previous results. Effect of change in baffle design has been studied at the three rotational speeds 345 rpm, 360 rpm and 370 rpm respectively. The best two propellers, Propeller-1 and Propeller-4 (chosen on the basis of results obtained from the experiments conducted on all 4 propellers for solid

suspension (shown in figure 4.14)) were used in the experiments. The original concentration (Cw) was kept constant at 10%. The results in comparison to the previous one are shown below.

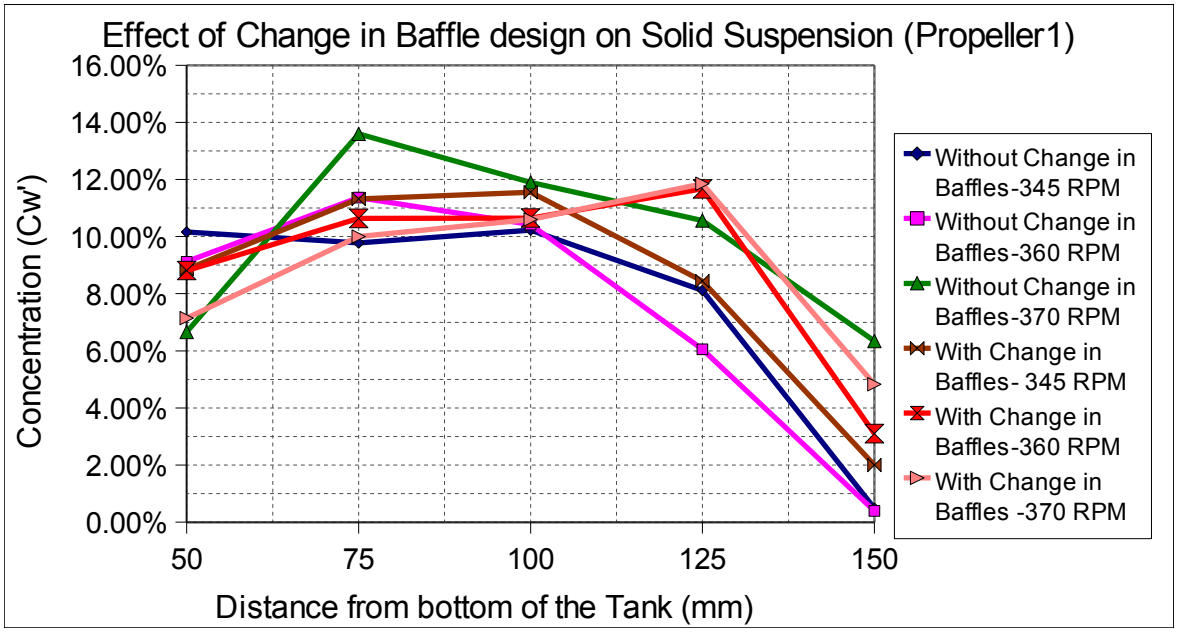

Figure 4.20: Effect of change in baffle design on solid suspension, propeller-1

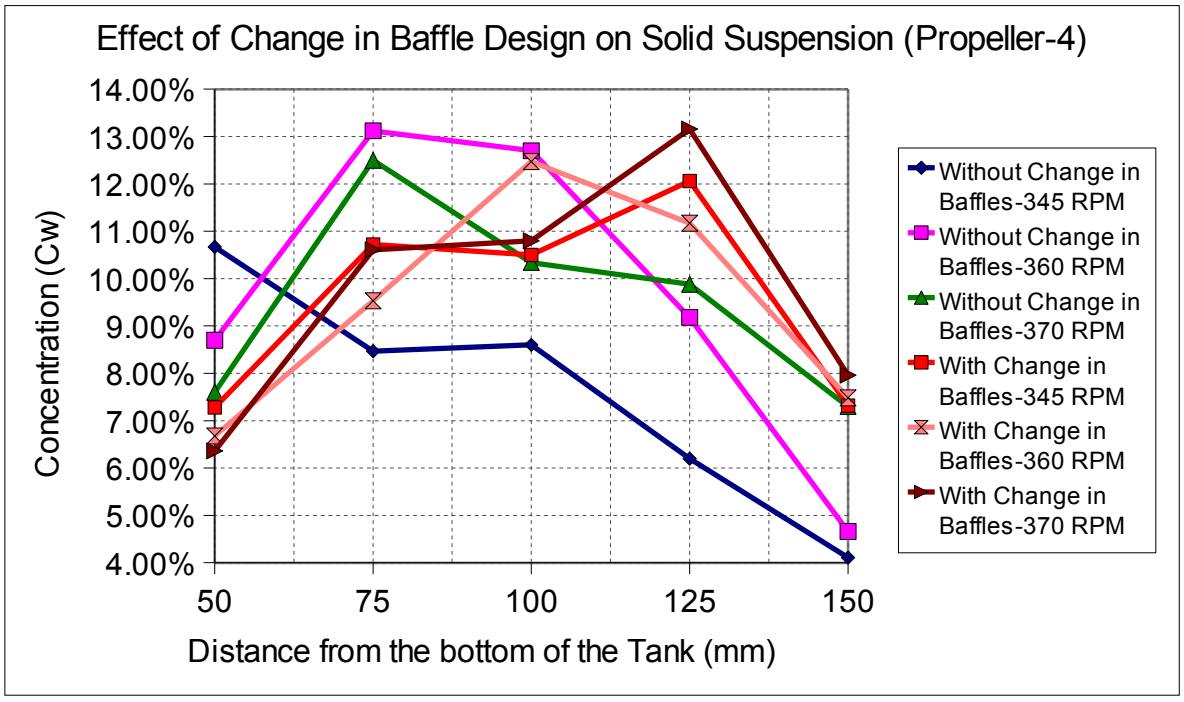

Figure 4.21: Effect of change in baffle design on solid suspension, propeller-4

CHAPTER 5

MODELING AND SIMULATION

5.1 MODELING OF THE SLURRY POT COMPONENTS

Fluid volume of the slurry pot has been modeled in GAMBIT. The basic components of Slurry Pot are cylinderical flat bottom tank, 4 Baffles, Impeller inserted through bottom and impeller Shaft. In order to do the CFD analysis on the suspension system, basic fluid domain consisting of all the components had to be modelled. The procedure followed to model the domain is follows:

5.1.1 Cylinderical tank

Fluid volume of cylinderical tank was generated by taking cylinder diameter as 240 mm and the height equal to 225 mm. Four rectangular baffles with dimensions 25mm x 10 mm x 225 mm were created and moved to the tank walls with 25mm side along the radius of the tank. All four baffles were then subtracted from the tank volume in order to obtain the desired fluid volume (as shown in figure 5.1).

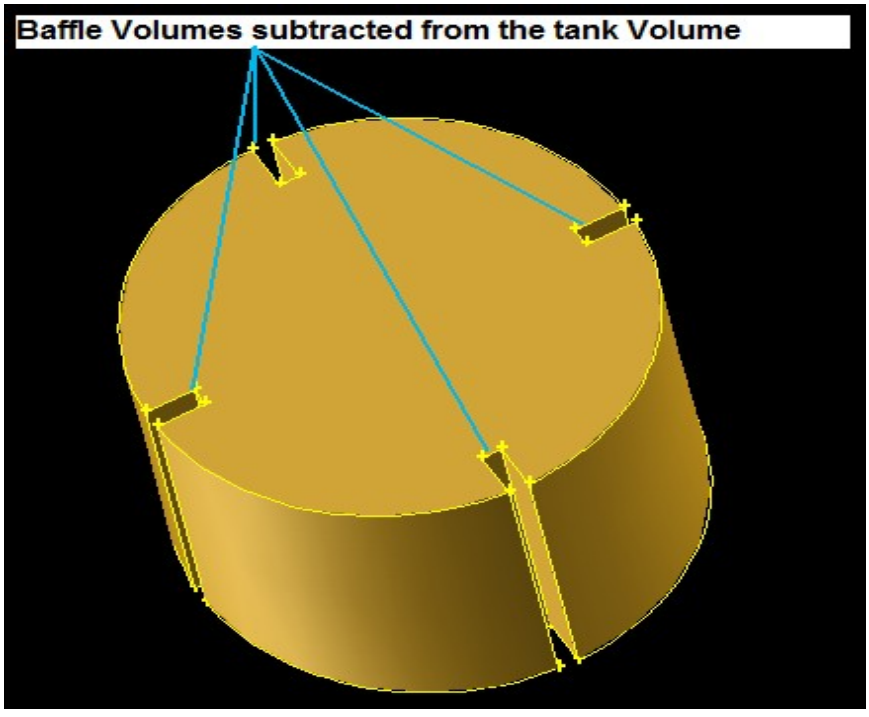

Figure : 5.1 Tank fluid volume after baffle subtraction

5.1.2 Impeller

In order to model the impeller with shaft, the first step followed was to create a shaft volume and then each impeller blades were modeled one by one.A local coordinate axis was created in order to rotate the impeller blades at 45 degrees on their respective axis. All the impellers were modeled by following the same procedure but by only changing their dimensions. All the blade volumes and shaft volumes were united to create one impeller volume which was then subtracted and retained from the cylinder tank fluid volume.

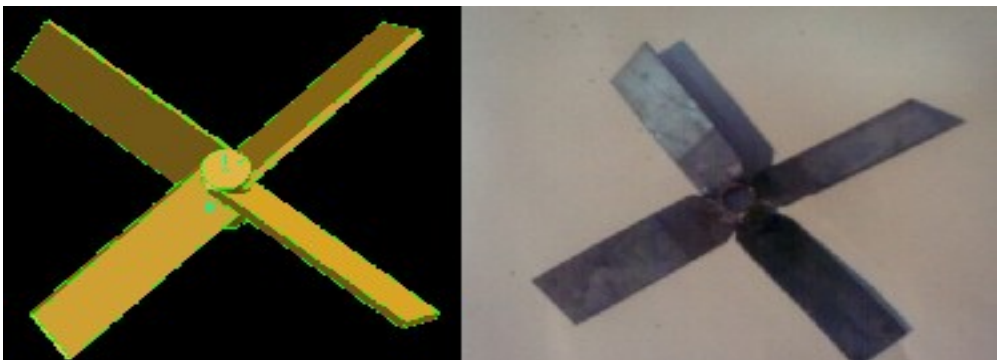

Figure 5.2 : a) CAD model of the Impeller, b) Impeller

The retention of the impeller volume after subtraction from the tank fluid volume was done because the same volume would be required for boundary conditions. Figure 5.3 below shows the CAD model and the original model after insertion of the impeller in the tank. CAD model generated is the fluid volume of the tank shown in figure 5.3.b.

Figure 5.3: a) CAD model of fluid volume with propeller b) Cylinder with propeller

5.1.3 Rotating Frame

To apply Multiple Reference Frame method, rotating cylinder is to be created which will be of size equal to the impeller diameter and will be placed on the axis of rotation of the impeller.

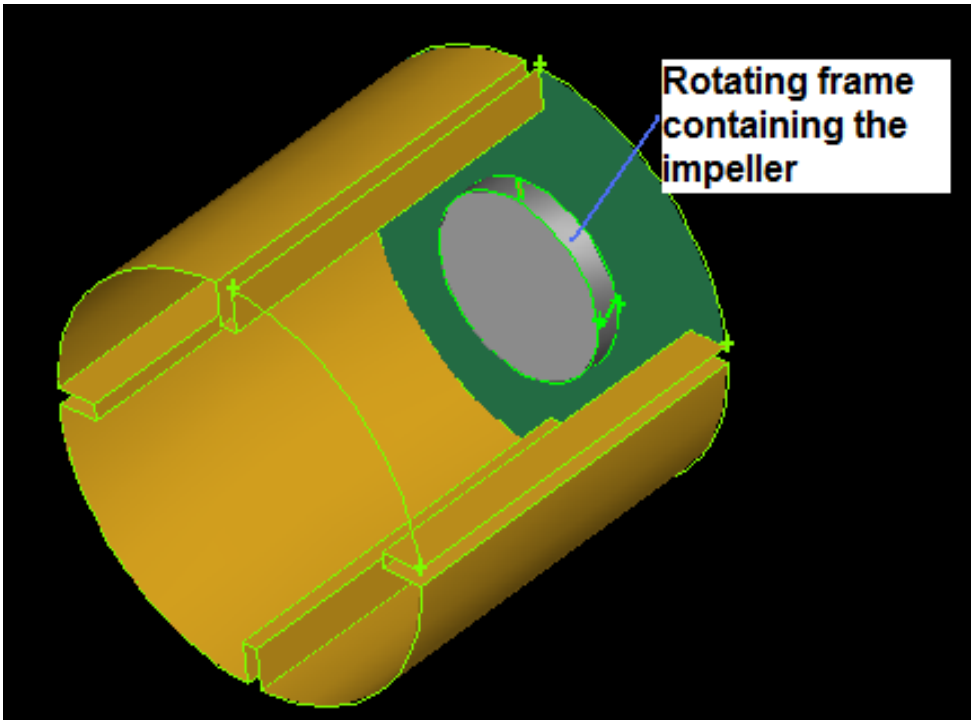

Figure 5.4 : Slurry pot model with rotating frame

5.2 MESHING

All the three Volumes; Cylinderical Tank, Rotating frame and Impeller were meshed with meshing schemes as shown in Table 5.1. Cylinderical tank (slurry pot) was meshed with interval count of six whereas, Rotating frame and Impeller were meshed with interval counts 4 and 2 respectively.This was done as these parts were small and were the main area of focus. By increasing the number of elements we can improve the accuracy of the results but, that will be at the cost of computational efficiency. The elements created in meshing (as shown in table 5.1) are nearly a best fit between solution accuracy and computational time. Figure 5.5 shows the meshes for each volume i.e, Cylinderical tank, Impeller and the Rotating frame.

Table 5.1: Meshing scheme and number of elements

Volume	Meshing Scheme	No. of Elements
Cylinderical Tank	Tet/Hybrid, Hexcore	66333
Rotating Frame	Hex/Wedge, Cooper	5475
Impeller	Tet Hybrid,T-Grid	6809

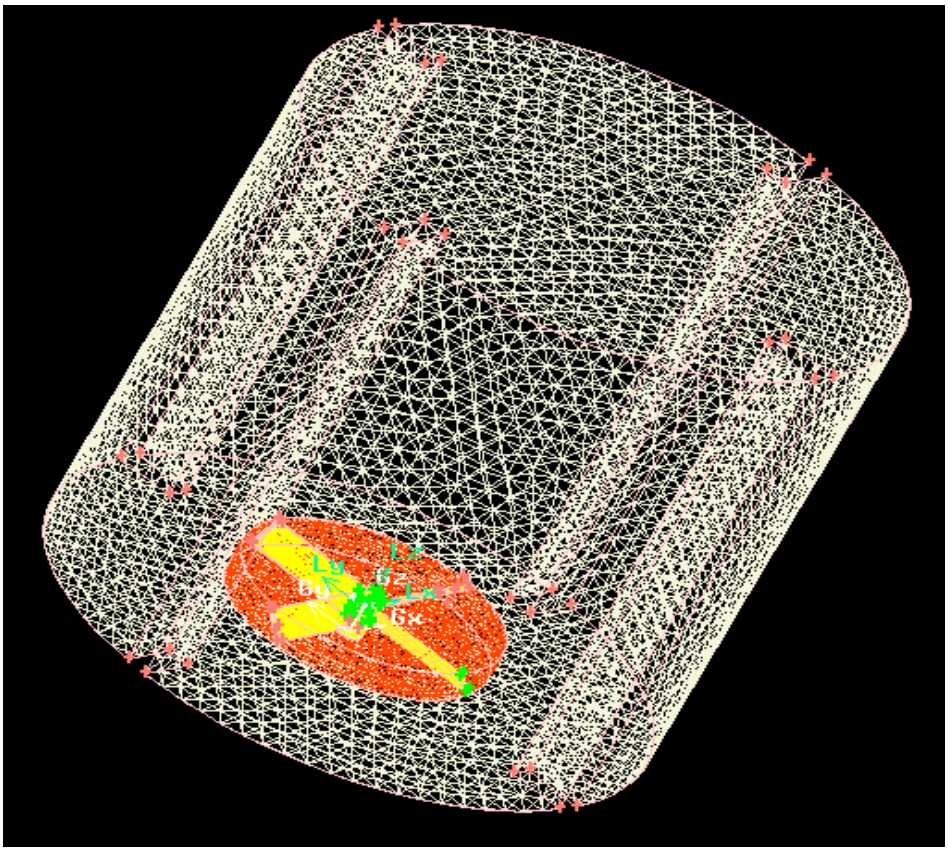

Figure 5.5 : Mesh of Tank, Impeller and Rotating Frame

5.3 BOUNDARY CONDITIONS:

As the fluid is not moving out of the tank volume, all the boundary condition would be of wall type. Under tab specific boundary types, boundary conditions for Cwall, Pwall and Mframe were declared in GAMBIT. All the outer,bottom & upper and wall faces of tank were set as wall type and named Cwall. Simalarly Pwall for impeller and Mframe for moving frame were created. Under tab specific continuum types, initial sand and water zones were defined.

5.4 SIMULATION

After meshing of the slurry pot assembly in GAMBIT, commercial CFD code FLUENT is used for simulation purpose. The boundary conditions moving wall or stationary wall are given at tank, moving frame and impeller. In the rotating frame containing an impeller, the impeller is at rest. In the stationary frame containing the tank walls and baffles, the walls and baffles are at rest. The performance results are obtained at different concentration and rotational speed for different types of propellers.

5.4.1 Assumptions

The following assumptions were taken for simulation:

1. The walls of the casing were assumed to be smooth hence any disturbances in flow due to roughness of the surface were neglected.

2. The friction co-efficient for all surfaces were set to 0, hence friction between the walls and fluid was neglected.

3. No leakage losses.

5.4.2 Solution parameters

1. 3-D solver used to solve for simulation.

2. Multiple reference frame technique used in the simulation of the suspension system.

3. Multiphase (two phases, silicon carbide sand and water) Eulerian-dispersed model was used in the simulation.

4. Standard K-Epsilon model is used for turbulence modeling.

5. Convergence criteria for the continuity, velocity and turbulence parameters was set to 10^{-3}.

6. First order scheme is used for pressure correction as well as for solving momentum, turbulent kinetic energy and turbulence dissipation rate.

7. Symlal-Obrien correction was used for drag coefficient.

8. Packing limit for sand was set at 0.60

5.4.3 Simulation Results

54.3.1 Contours :

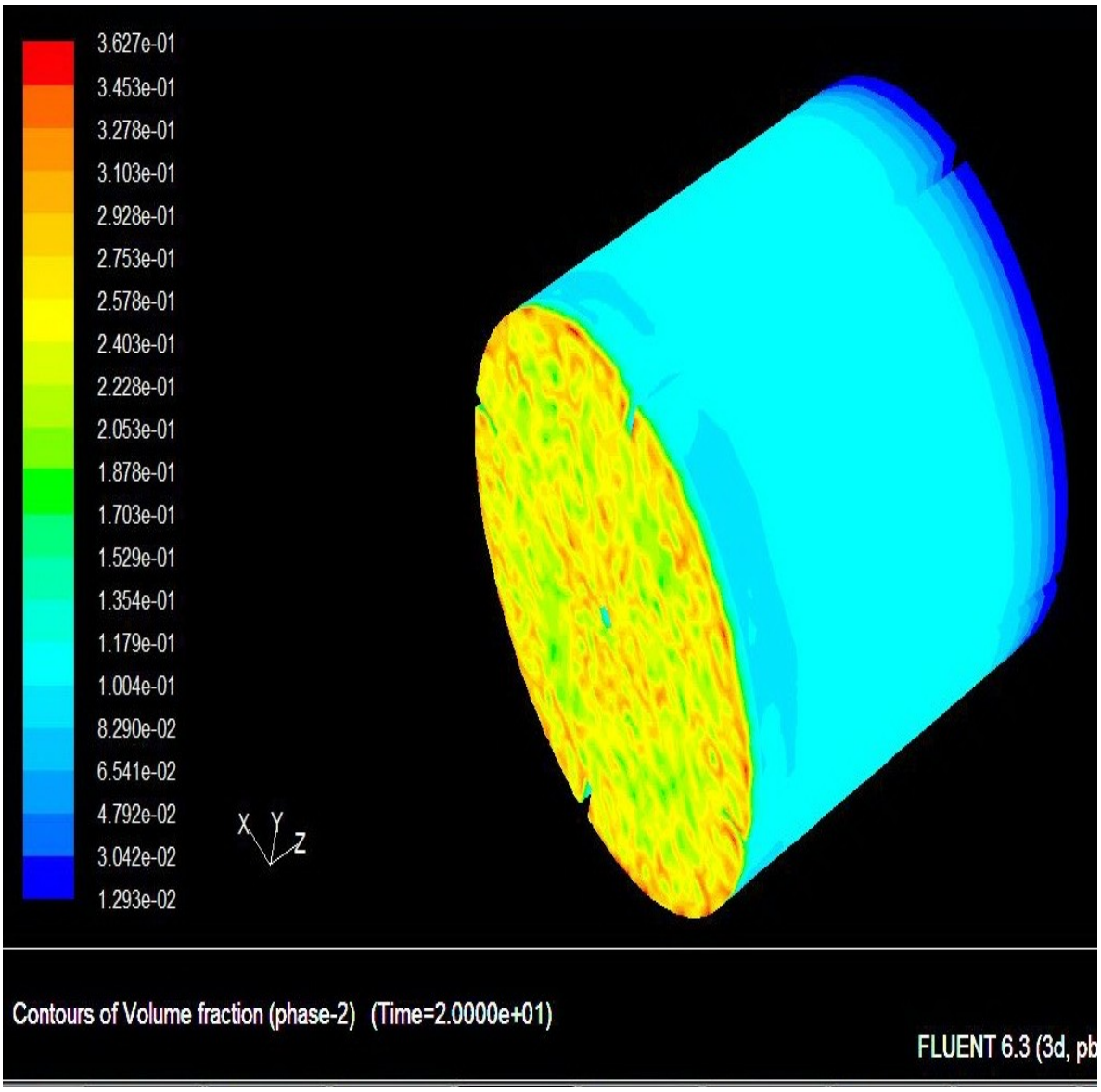

Figure 5.6: Sand Concentration contours at 10% Cw, 360 RPM ,Propeller 1

The contour in figure 5.6 shows that the Volume Fraction of solids is maximum at the bottom of the tank. It is minimum at the top portion, coloured blue, and uniform in the central part of the tank.

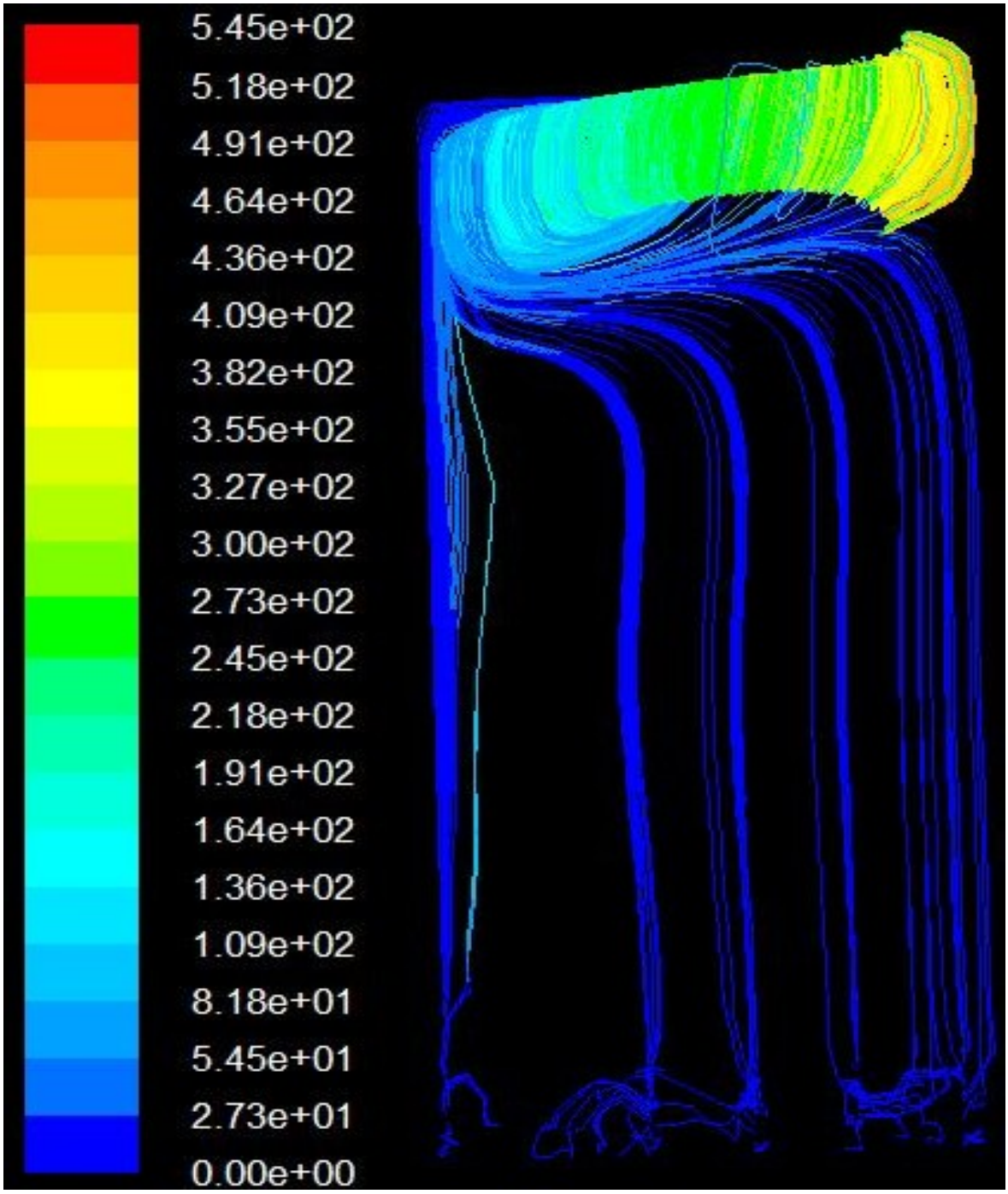

Figure 5.7 :Pathlines of fluid inside slurry pot, shown in the left portion of the Y-Z plane

Figure 5.7 show the path followed by the water particles in the tank. Water, as shown in the pathlines, move up towards the top periphery of the tank and then get diverted to the center of the tank.

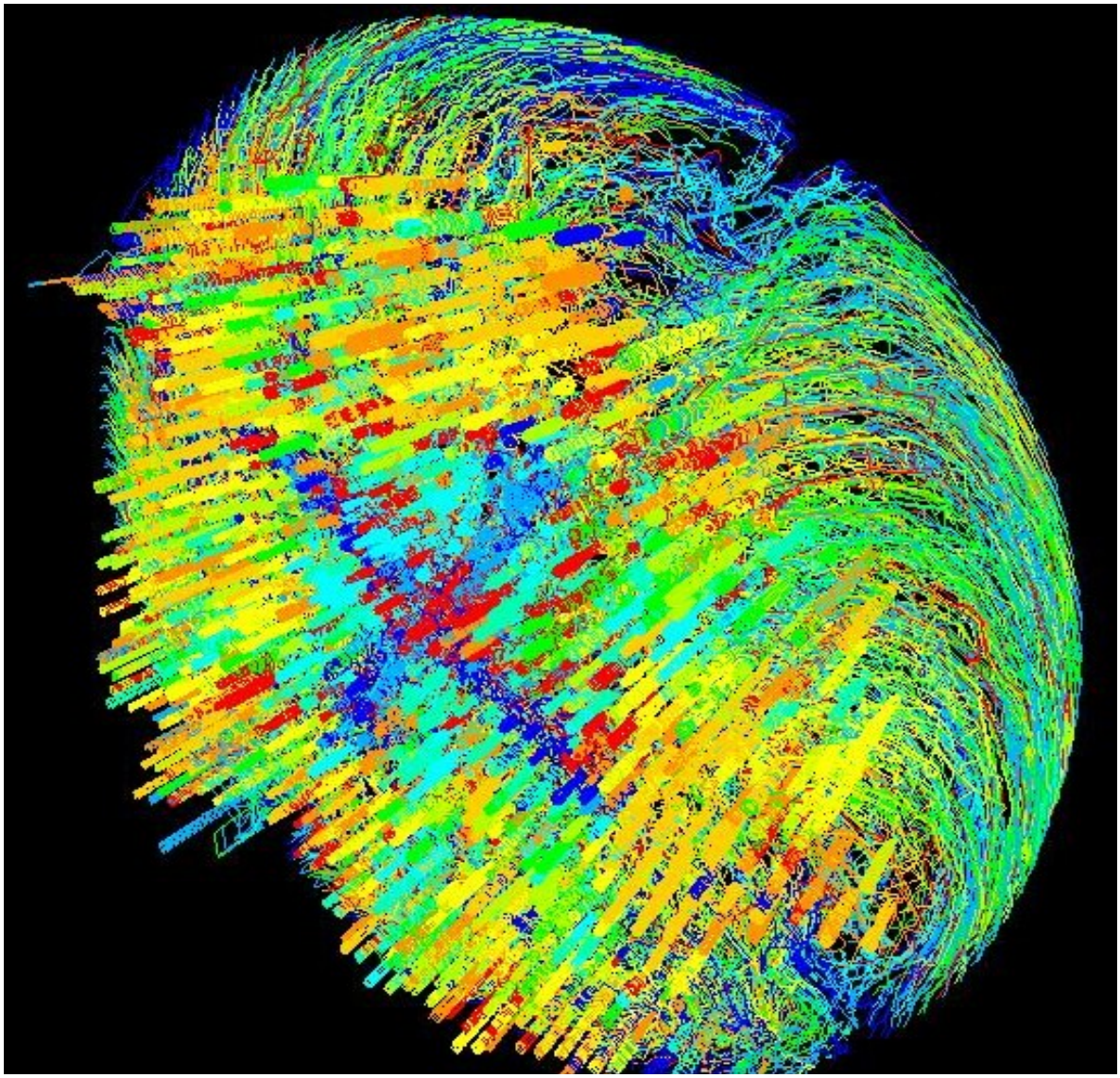

Figure 5.8: Pathlines of sand particles at the bottom of the tank

A pathline is the path traced by an individual particle in a given time interval. The pathlines shown above are of sand particles in the bottom part of the slurry tank. The particles, as shown in the figure above, move up after being swept by the impeller at the bottom of the tank. Figure 5.9 and Figure 5.10 below show the pathlines at the bottom face and the top face of the slurry tank.

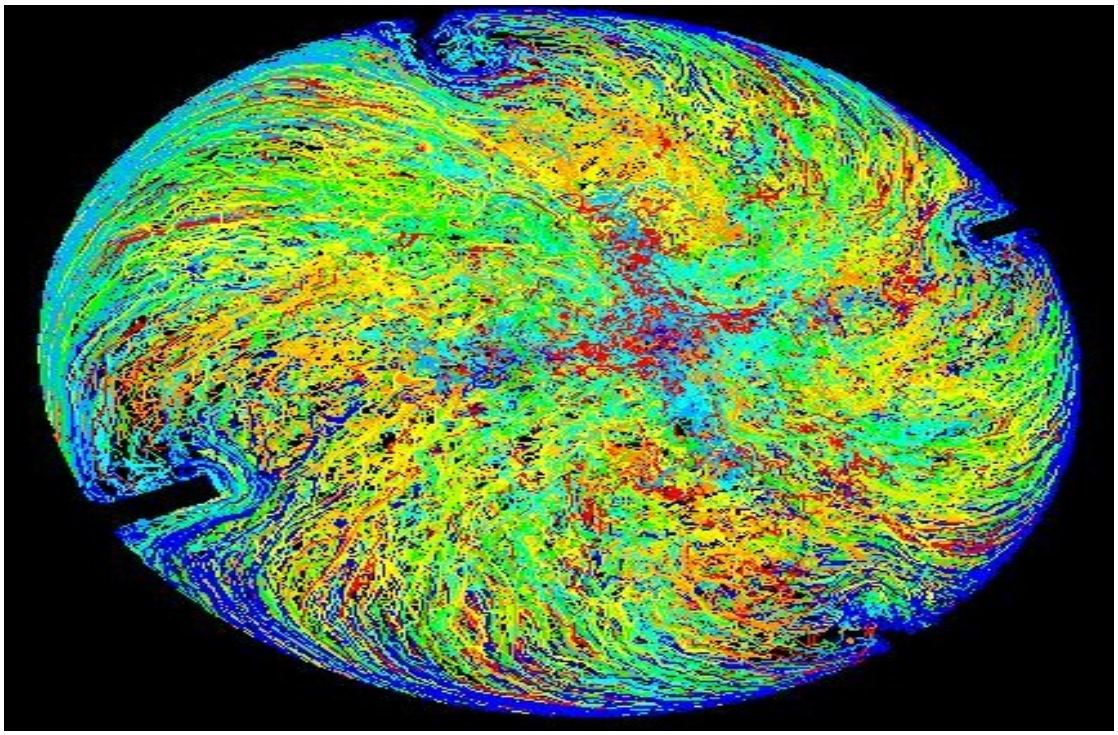

Figure 5.9 : Pathlines at the bottom face of the slurry tank

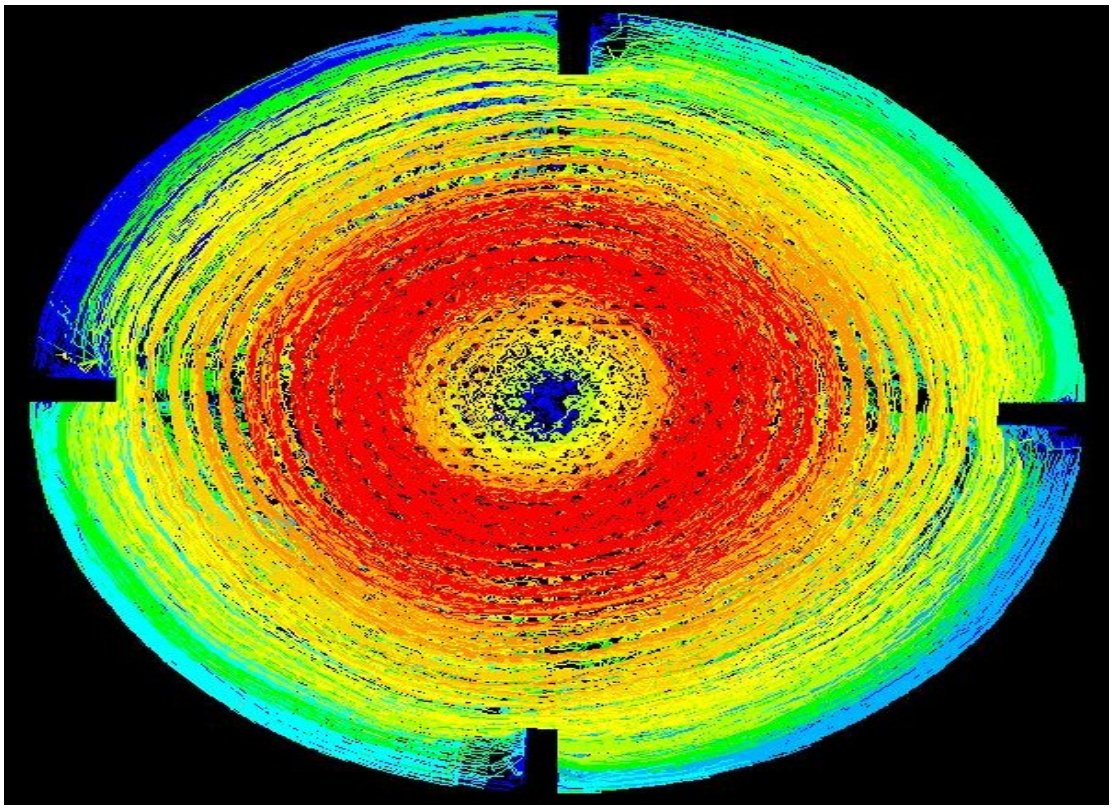

Figure 5.10 : Pathlines at the top face of the slurry tank

5.4.3.2 Effect of propeller geometry

Volume Fraction line taken at (X=119 mm, Y=10 mm)

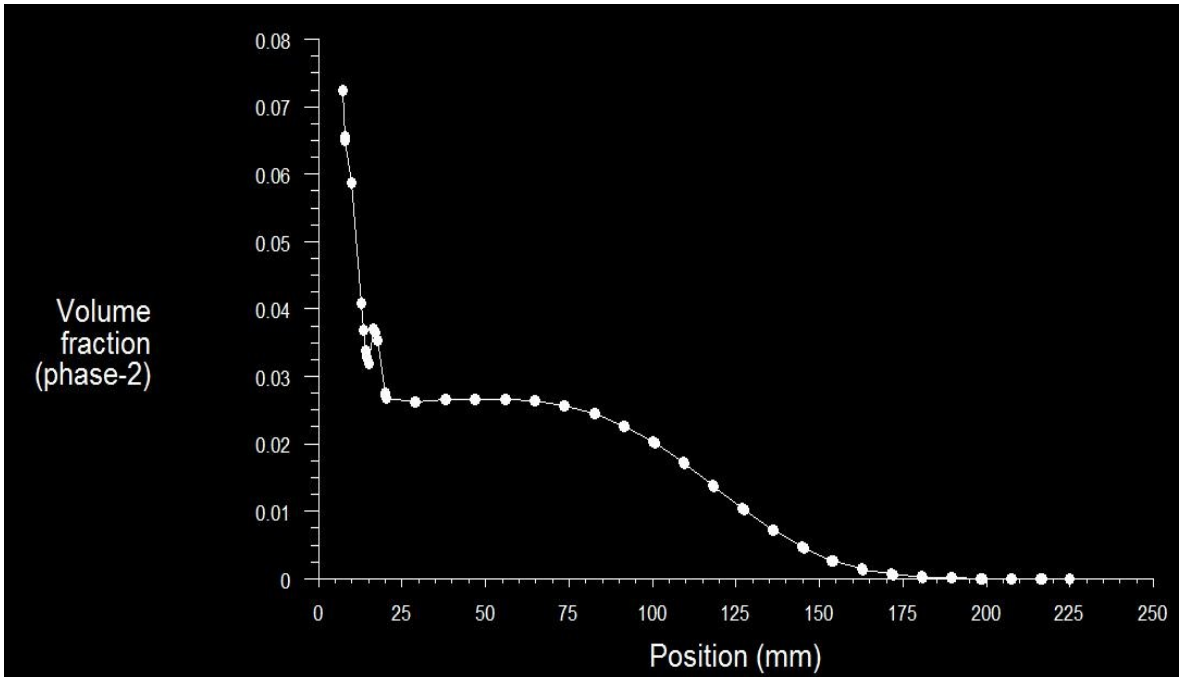

Figure 5.11: Sand Concentration X-Y plot at 10% Cw, 360 rpm, propeller-1

Volume Fraction line taken at (X=119 mm, Y=10 mm)

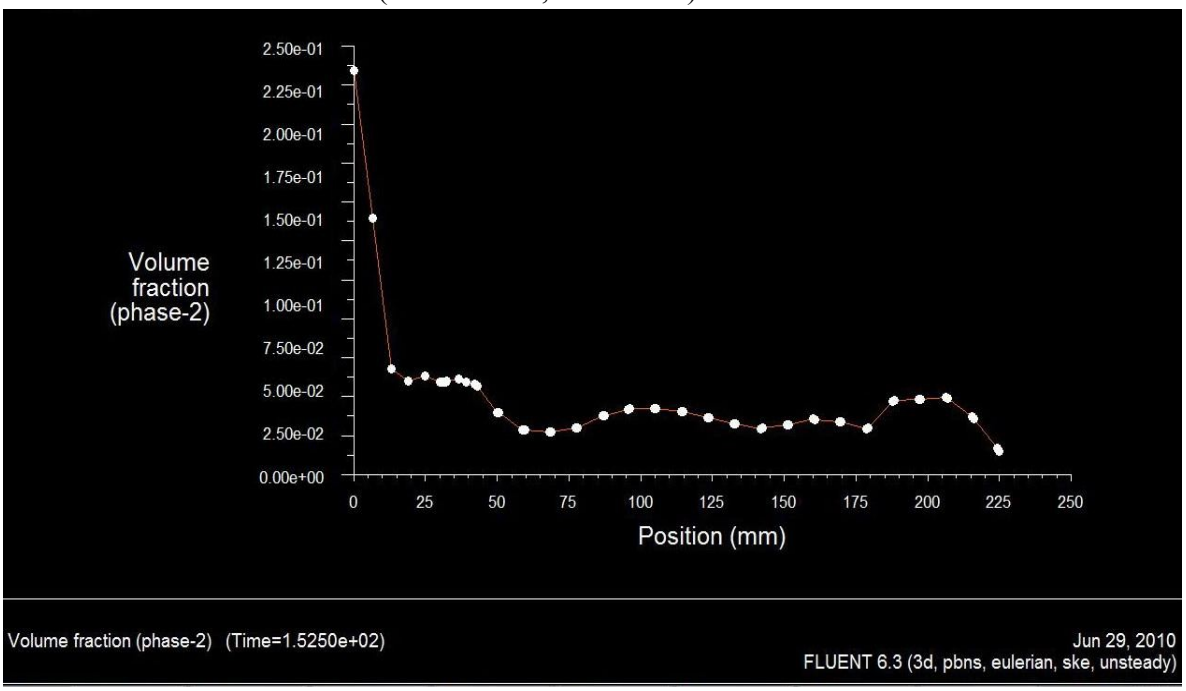

Figure 5.12: Sand concentration X-Y plot at 10% Cw, 360 rpm, propeller-2

Volume Fraction line taken at (X=119 mm, Y=10 mm)

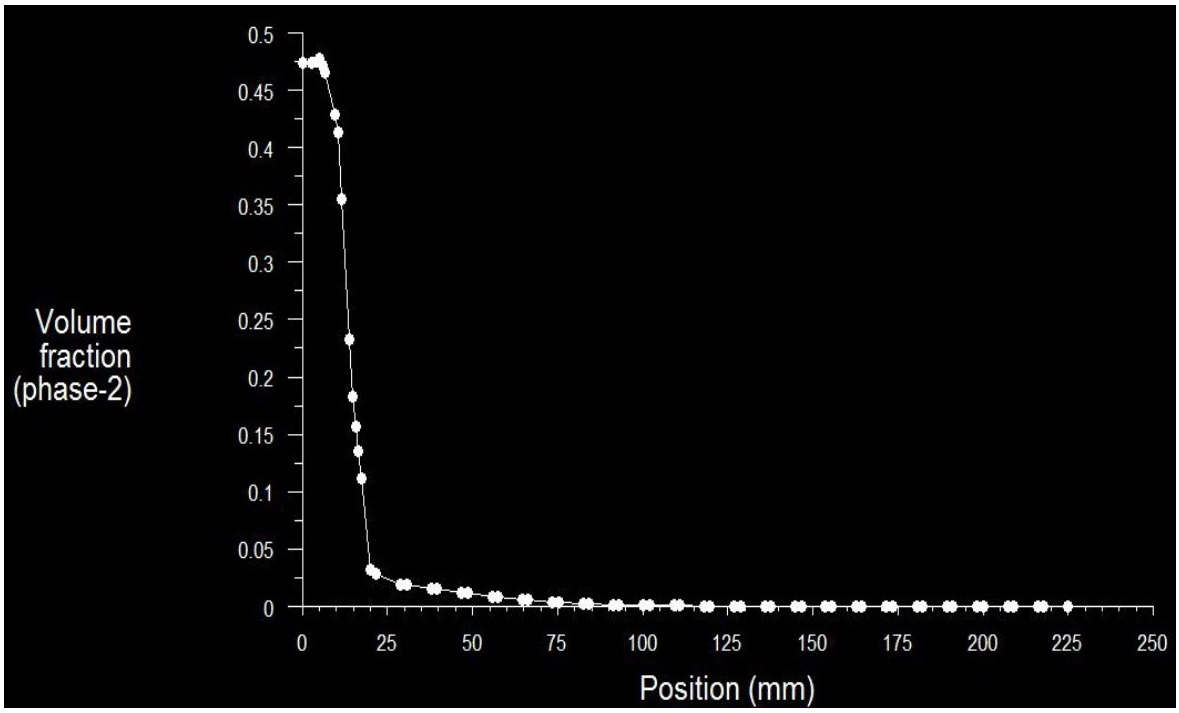

Figure 5.13: Sand concentration X-Y plot at 10% Cw, 360rpm, propeller-3

Volume Fraction line taken at (X=119 mm, Y=10mm)

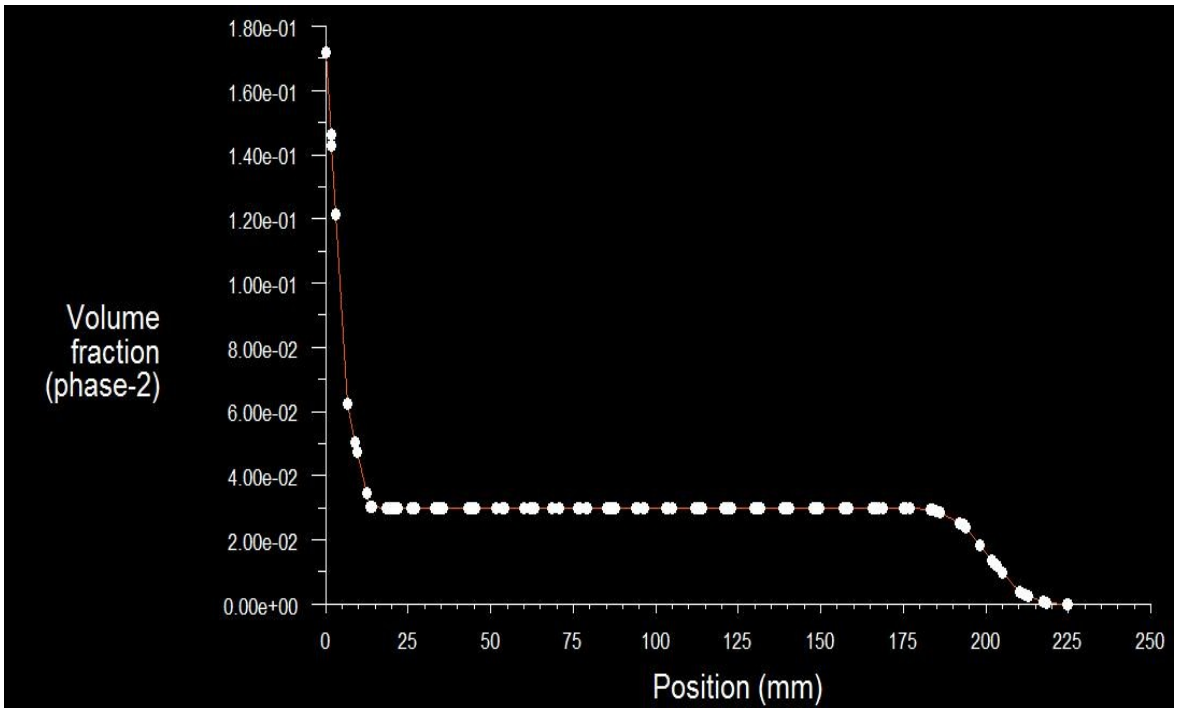

Figure 5.14: Sand concentration X-Y plot at 10% Cw, 360 rpm, propeller-4

Volume Fraction line taken at (X=119 mm, Y=10mm)

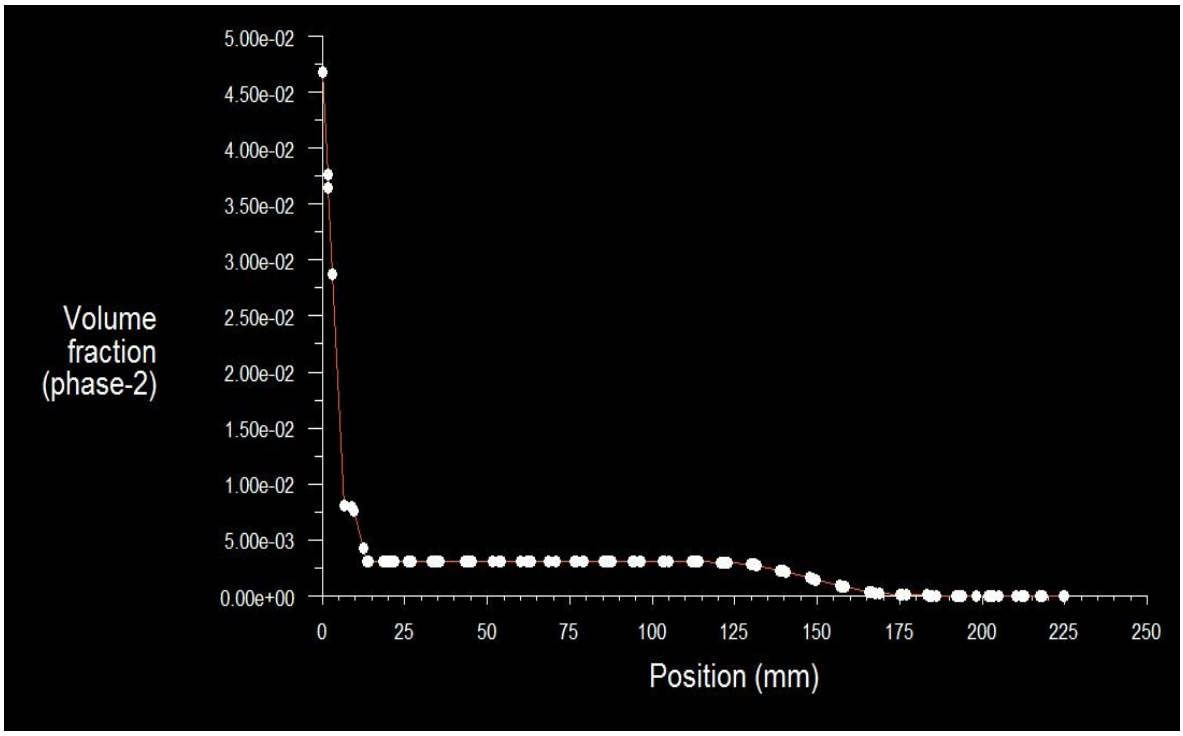

Figure 5.15: Sand concentration X-Y plot at 1% Cw, 345 rpm, propeller-1

Volume Fraction line taken at (X=119 mm, Y=10mm)

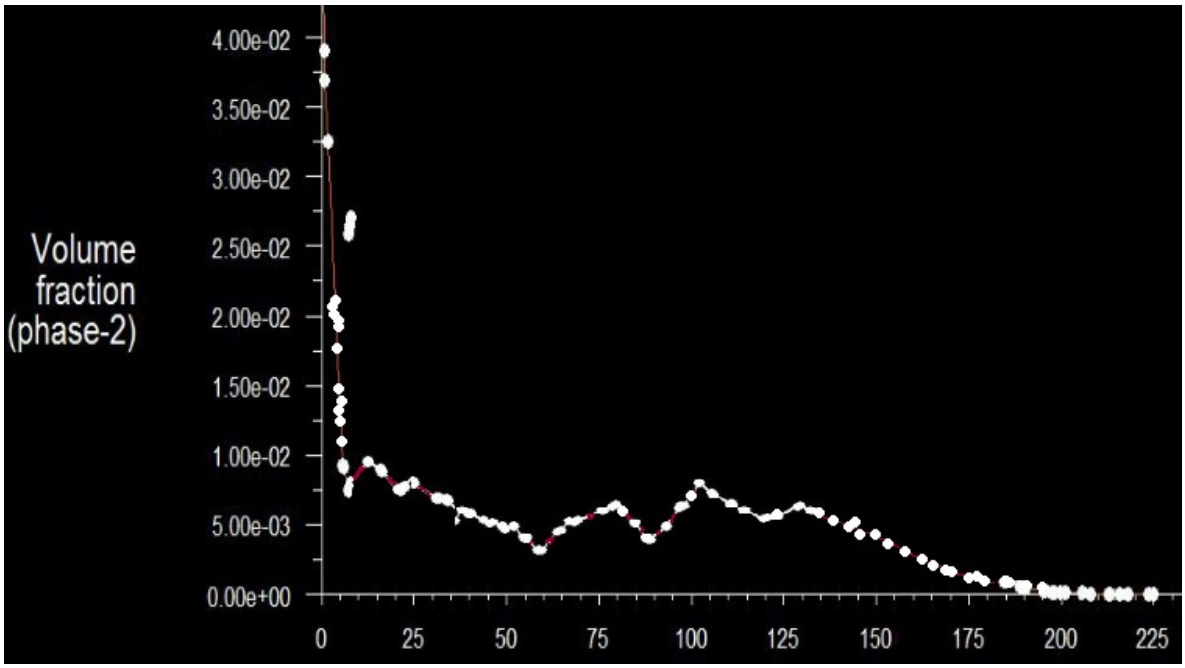

Figure 5.16: Sand concentration X-Y plot at 1% Cw, 345 rpm, propeller-2

Volume Fraction line taken at (X=119 mm, Y=10mm)

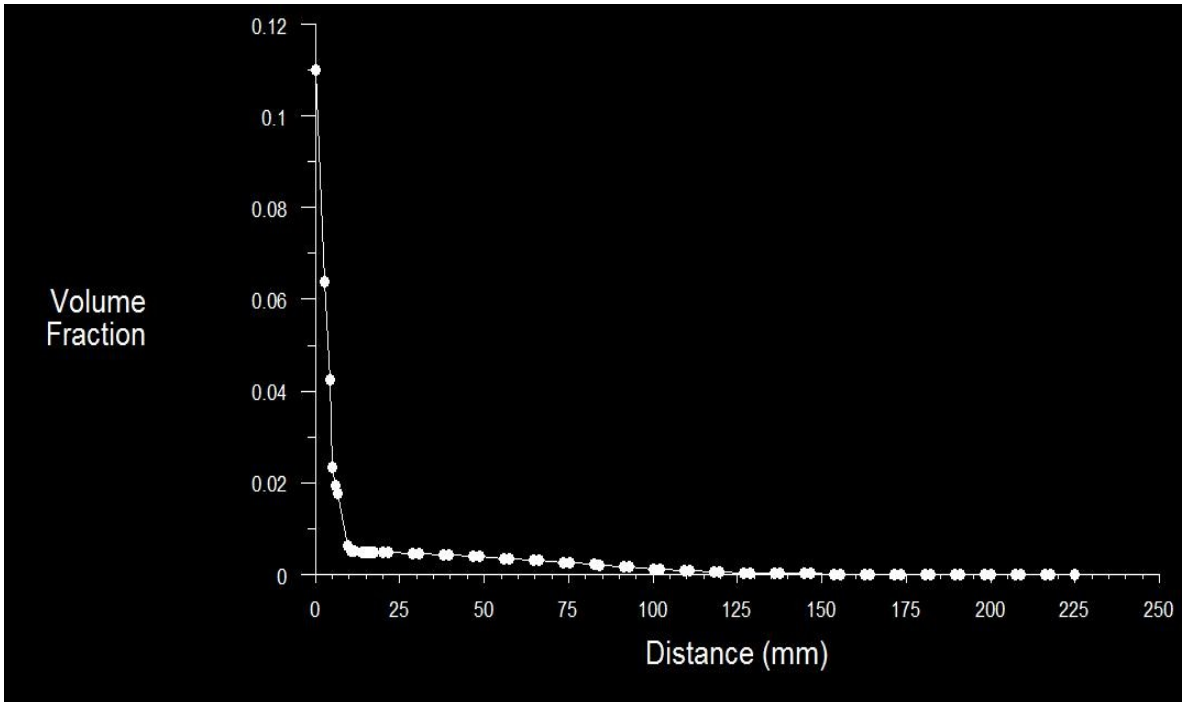

Figure 5.17: Sand concentration X-Y plot at 1% Cw, 345 rpm, propeller-3

Volume Fraction line taken at (X=119 mm, Y=10mm)

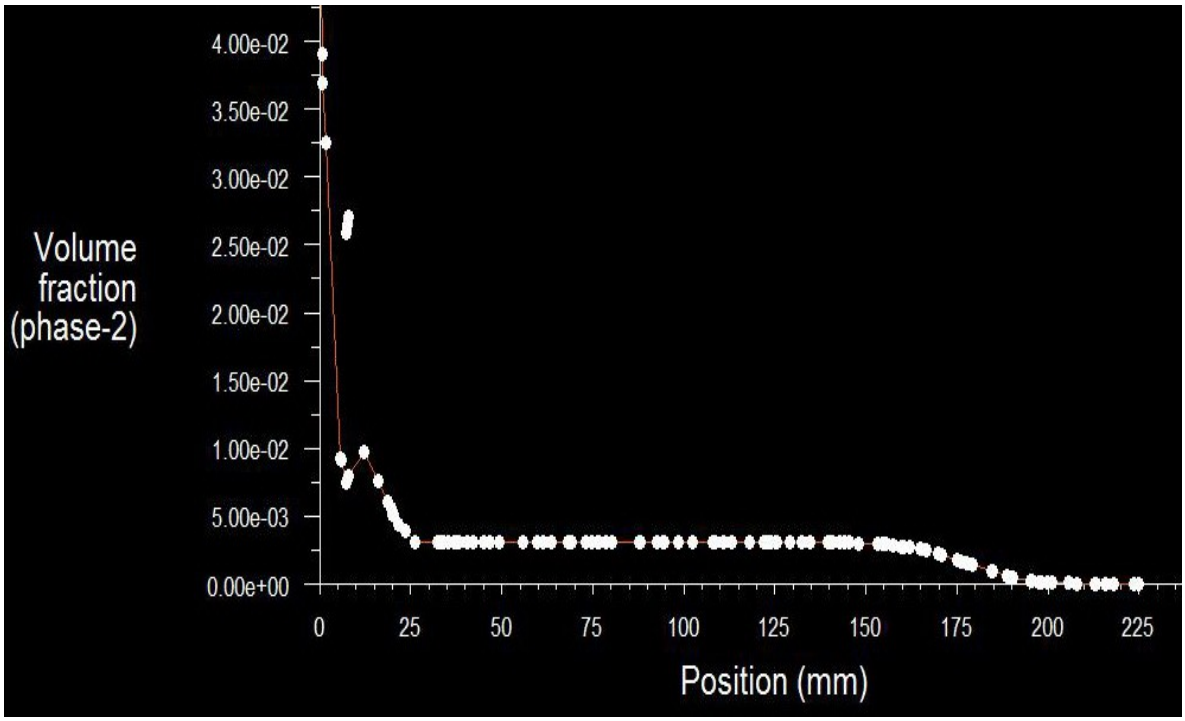

Figure 5.18: Sand concentration X-Y plot at 1% Cw, 345 rpm, propeller-4

5.4.3.3 Effect of change in original concentration on suspension

Volume Fraction line taken at (X=119 mm, Y= 10mm) along Z axis.

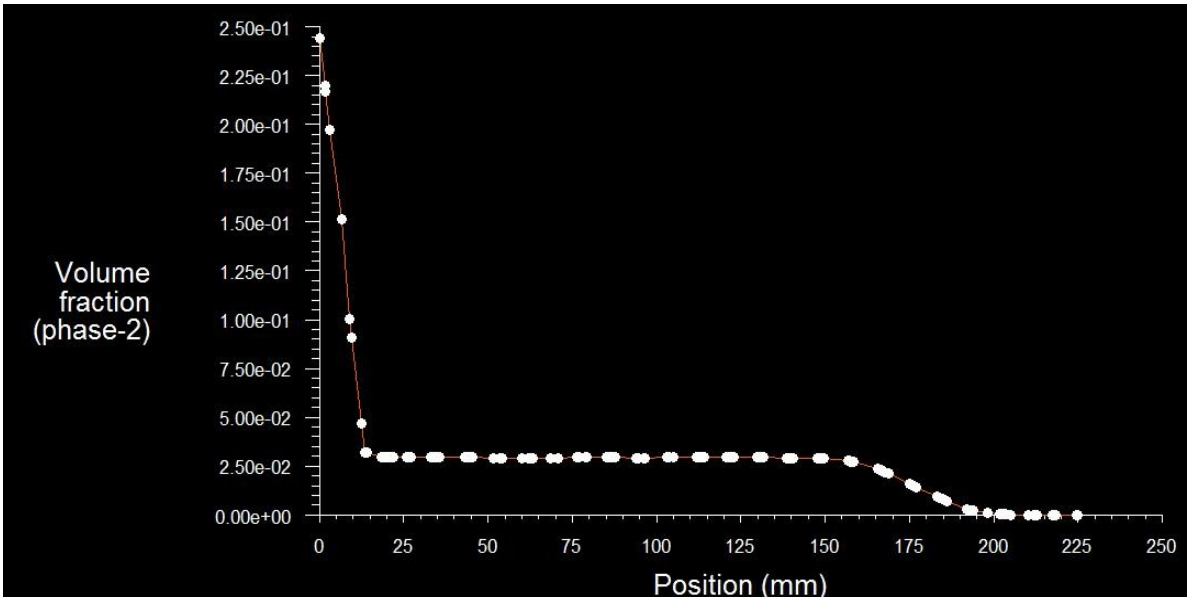

Figure 5.19: Sand supension X-Y plot at 10% Cw, 360 rpm, propeller-4

Volume Fraction line taken at (X=119 mm, Y= 10 mm) along Z axis.

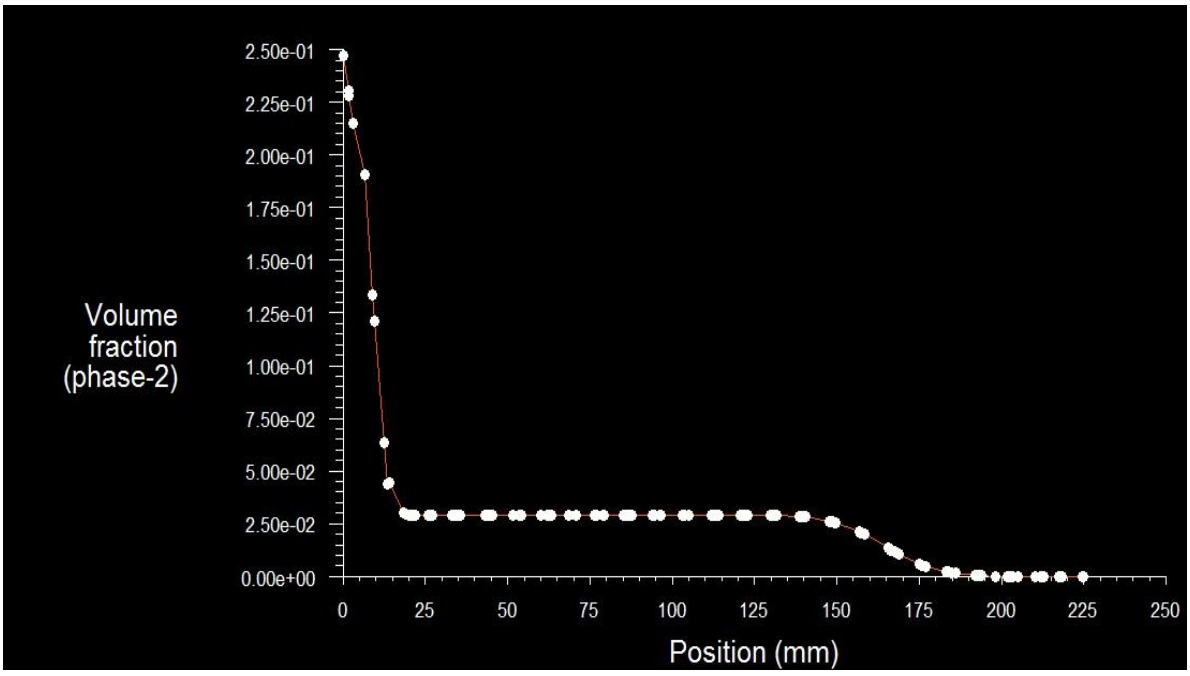

Figure 5.20: Sand Concentration X-Y plot at 5% Cw, 360 rpm, propeller-4

Volume Fraction line taken at (X=119 mm, Y=10mm)

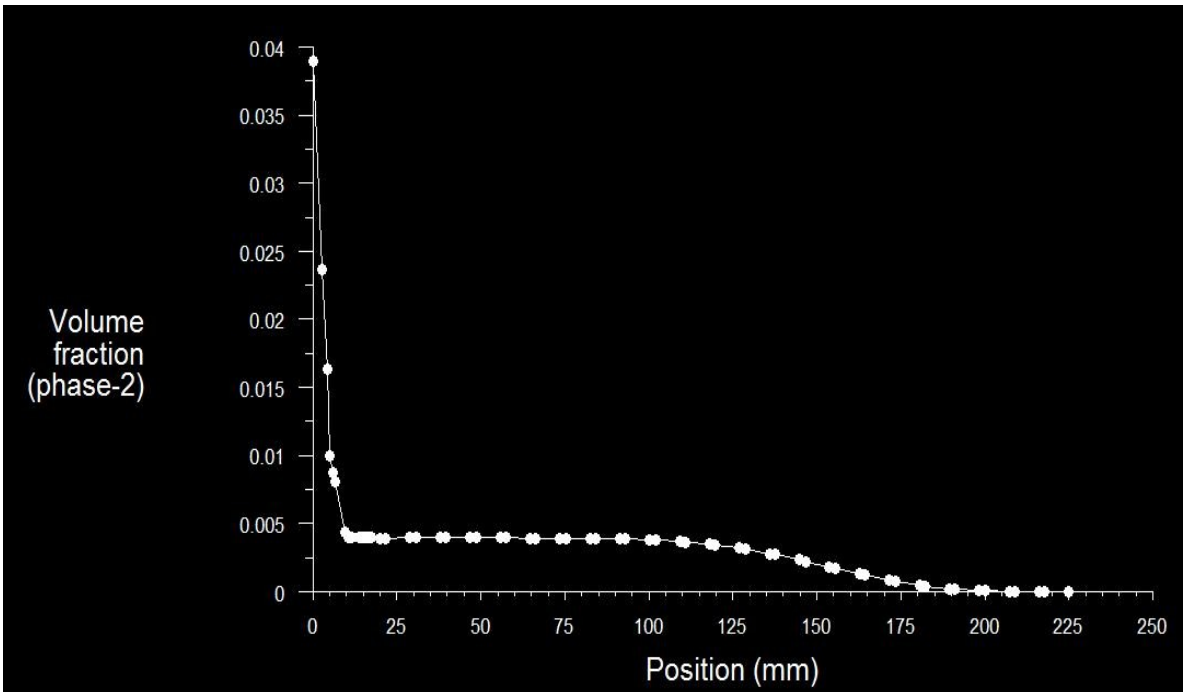

Figure 5.21: Sand Concentration X-Y plot at 1% Cw, 360 rpm, propeller-4

5.4.3.4 Effect of Change in speed on suspension

Volume Fraction line taken at (X=119 mm, Y=10mm)

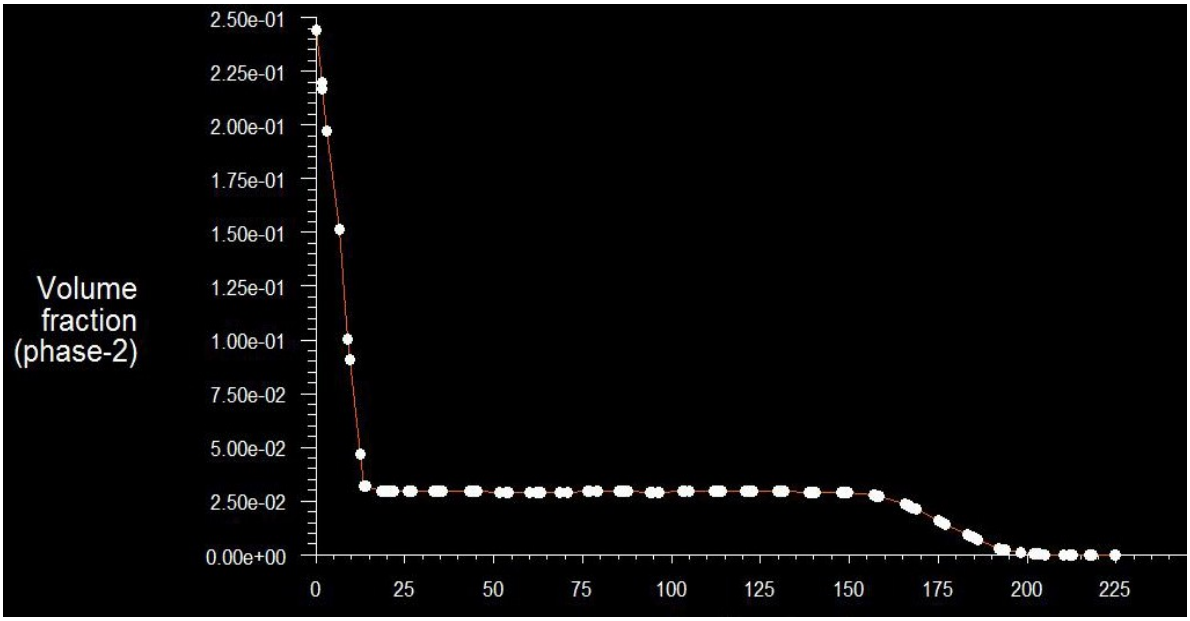

Figure 5.22: Sand Concentration X-Y plot at 10% Cw, 345rpm, propeller-4

Volume Fraction line taken at (X=119 mm, Y=10mm)

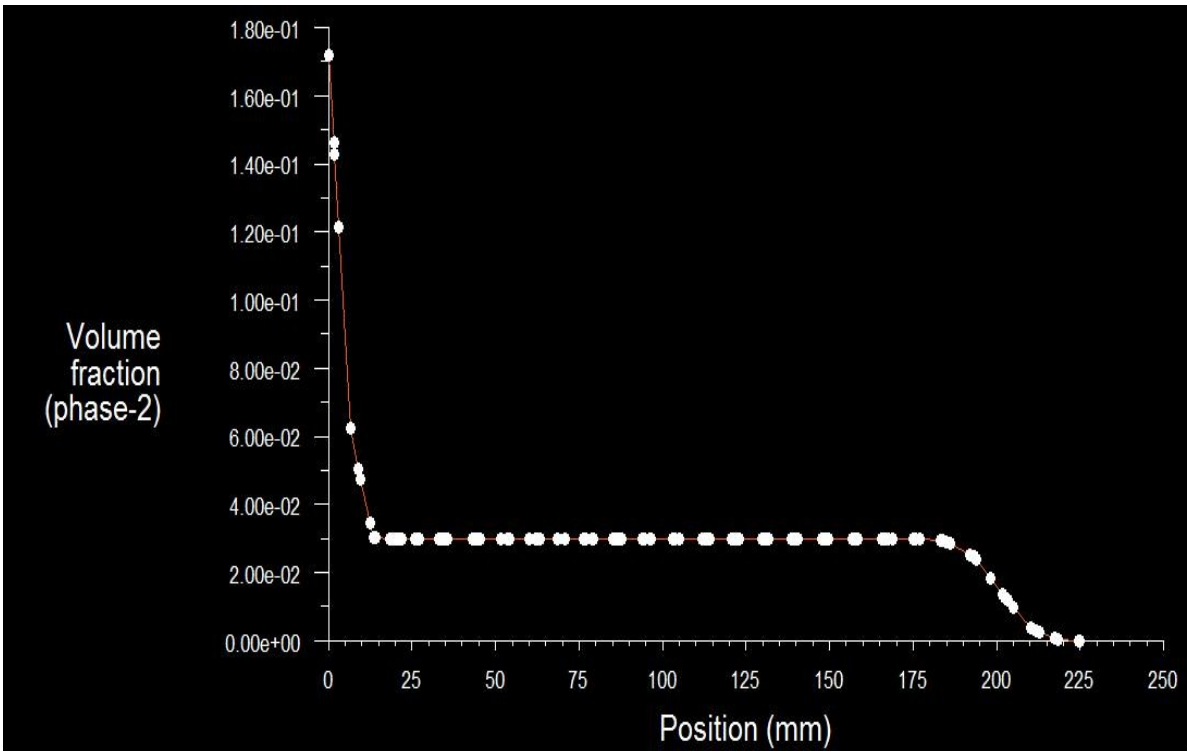

Figure 5.23: Sand Concentration X-Y plot at 10% Cw, 360 rpm, propeller-4

Volume Fraction line taken at (X=119 mm, Y=10mm)

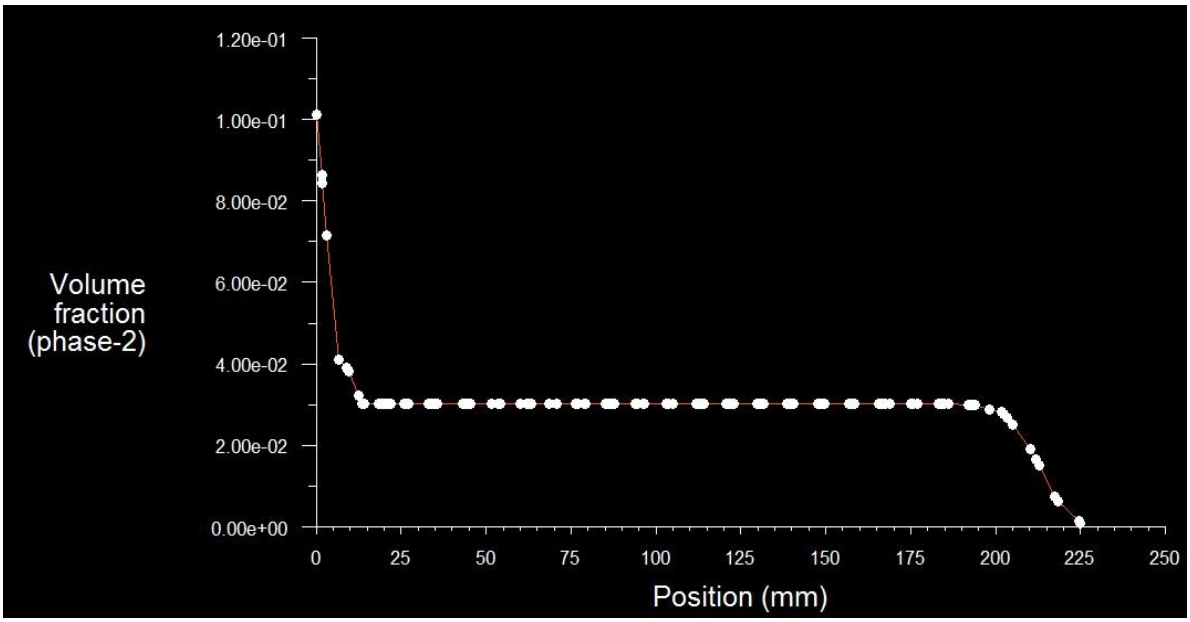

Figure 5.24: Sand Concentration X-Y plot at 10%Cw, 370rpm, propeller-4

5.4.3.5 Effect of baffle clearance on suspension

Volume Fraction line taken at (X=119 mm, Y= 10mm)

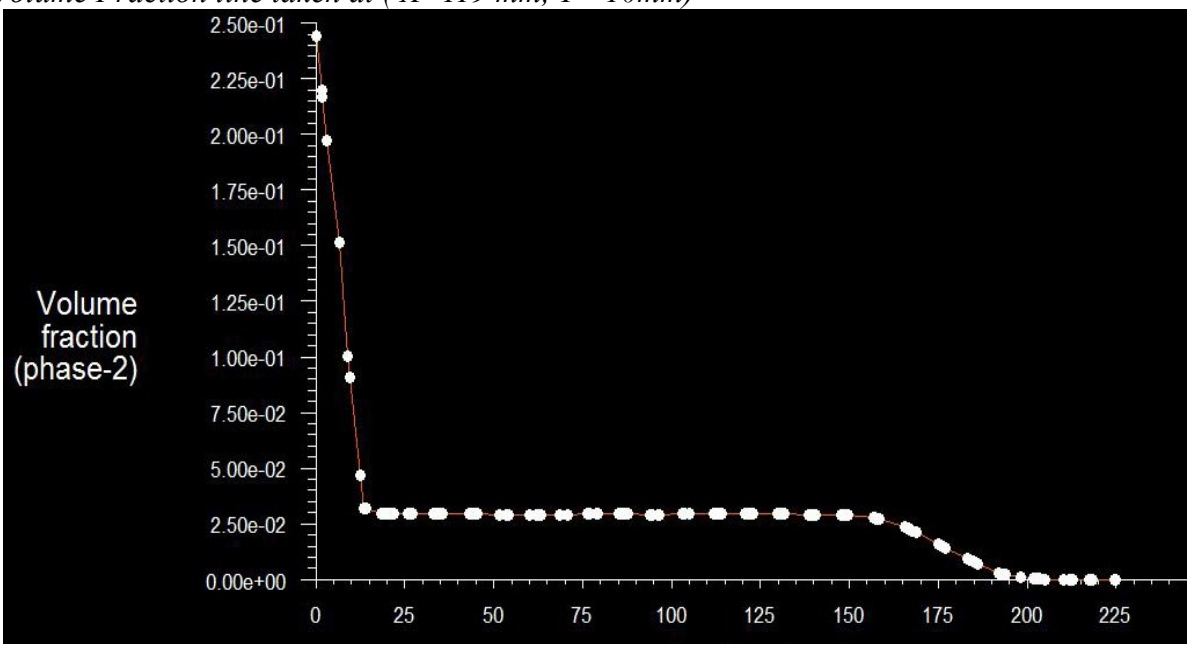

Figure 5.25: X-Y plot at 10% Cw, 345rpm,propeller-4, original baffles

Volume Fraction line taken at (X=119 mm, Y= 10mm)

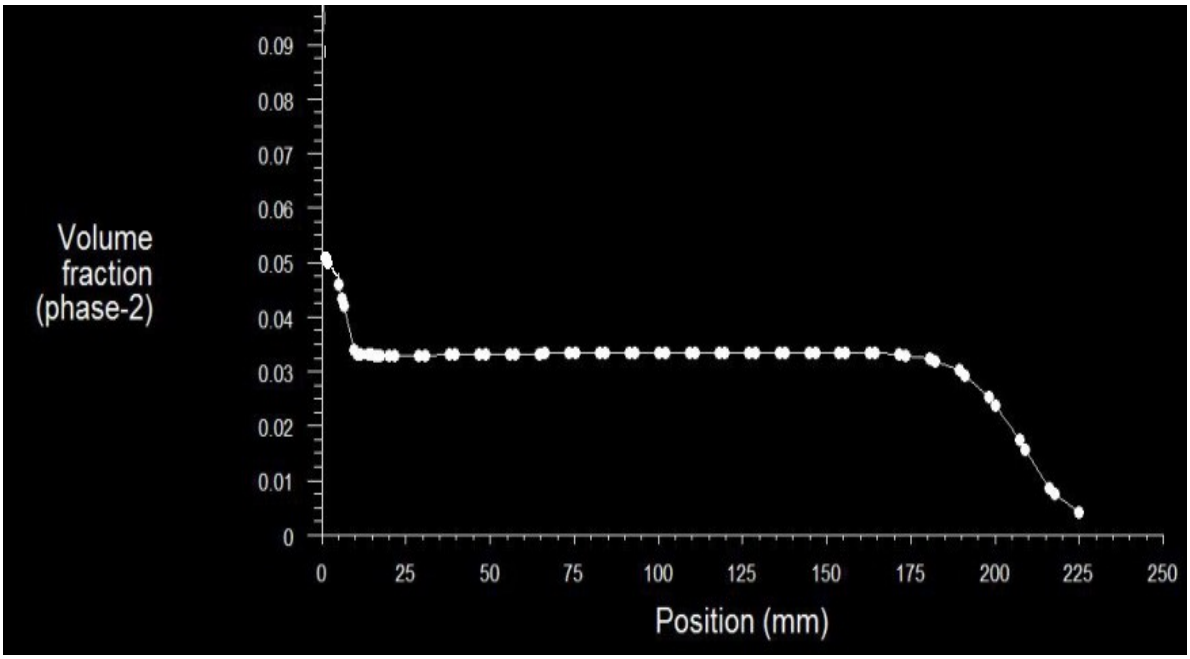

Figure 5.26: X-Y plot at 10% Cw, 345rpm, propeller-4, changed baffles

Volume Fraction line taken at (X=119 mm, Y= 10mm)

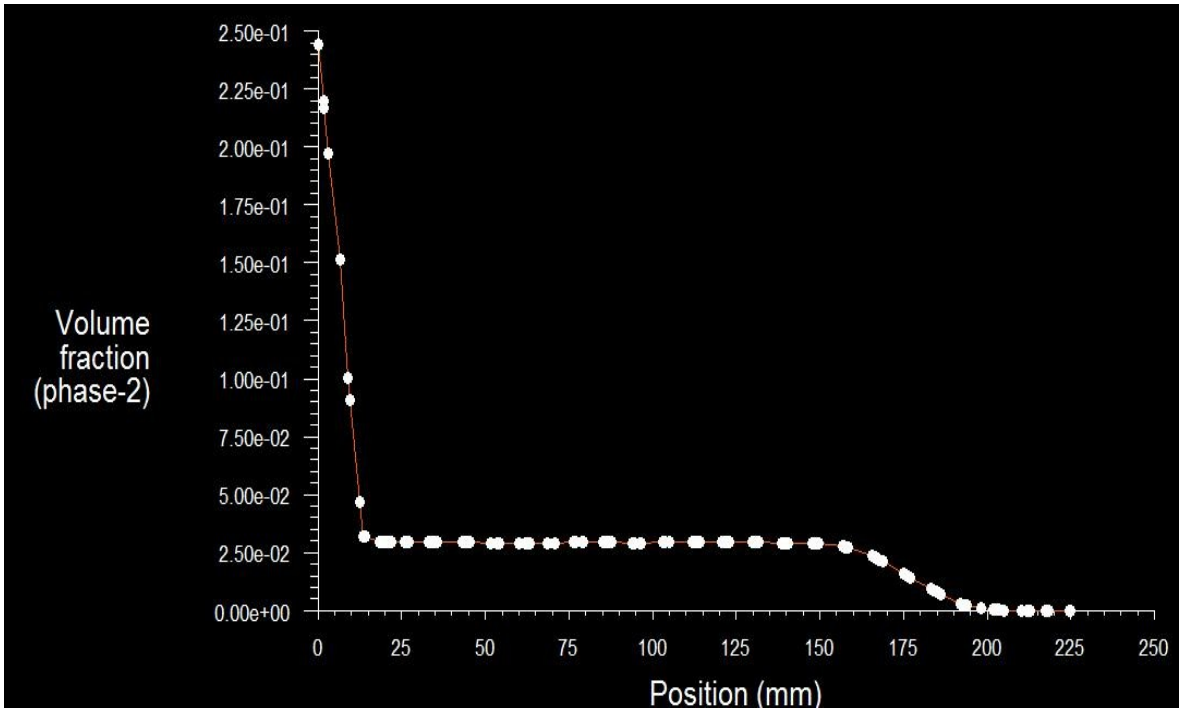

Figure 5.27: X-Y plot at 10% Cw, 360rpm, propeller-4, original baffles

Volume Fraction line taken at (X=119 mm, Y= 10mm)

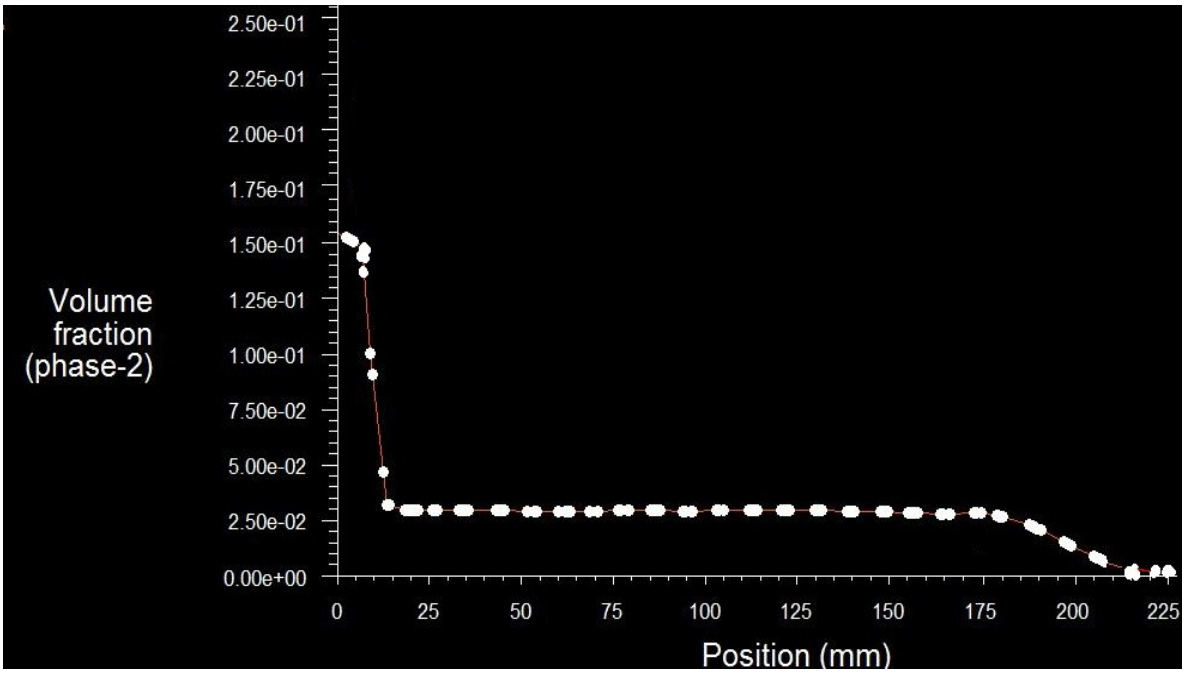

Figure 5.28: X-Y plot at 10%Cw, 360rpm, propeller-4, changed baffles

Volume Fraction line taken at (X=119 mm, Y= 10mm)

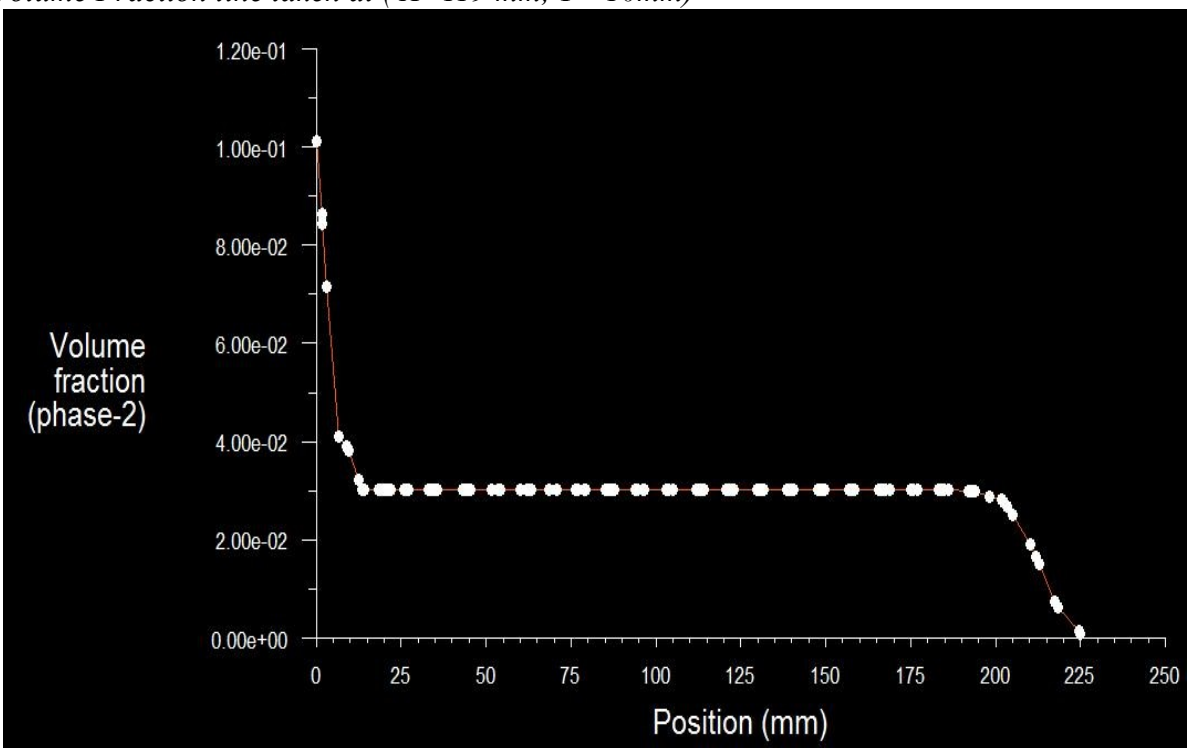

Figure 5.29: X-Y plot at 10% Cw, 370rpm, propeller-4, original baffles

Volume Fraction line taken at (X=119 mm, Y= 10mm)

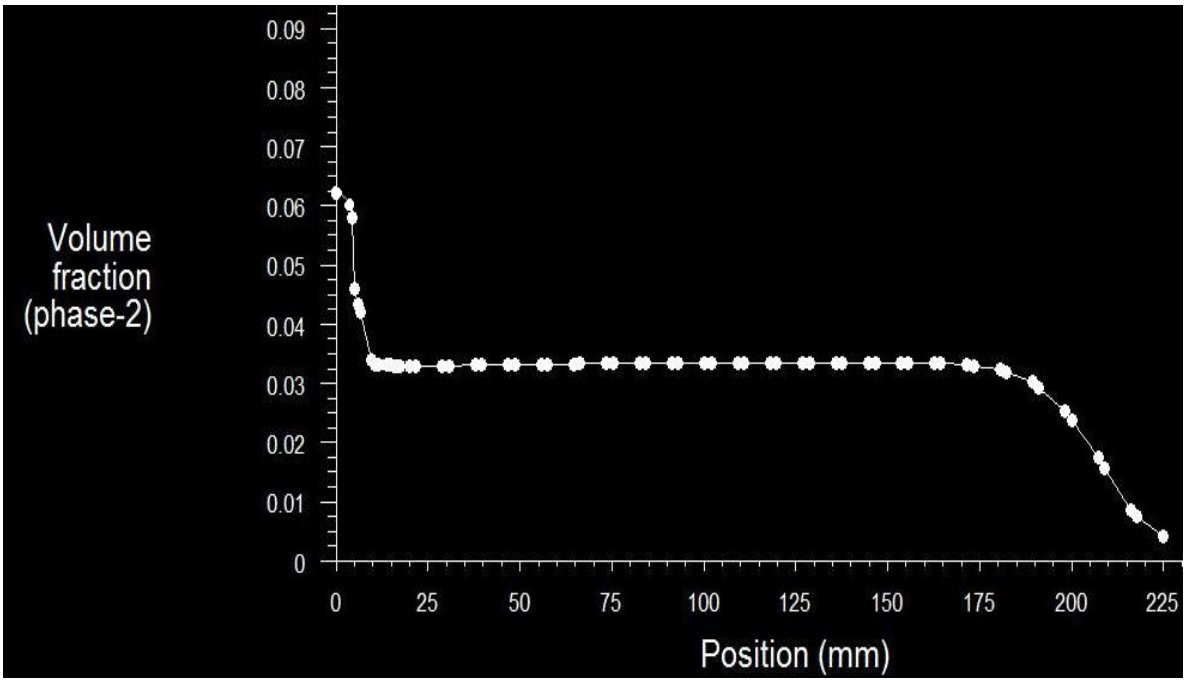

Figure 5.30: X-Y plot at 10%Cw, 370rpm, propeller-4, changed baffles

CHAPTER 6

RESULTS AND DISCUSSIONS

The results obtained through experimental investigation and simulation of the erosion wear suspension sytem are studied and compared in the following sections. Effect of change in concentration, design of propeller, change in rotational speed and change in design of baffles were investigated both through experimentation and simulation. The effect of each parameter on the quality of suspension has been studied through the results obtained in the experiments and simulation.

6.1 EFFECT OF CHANGE IN PROPELLER GEOMETRY

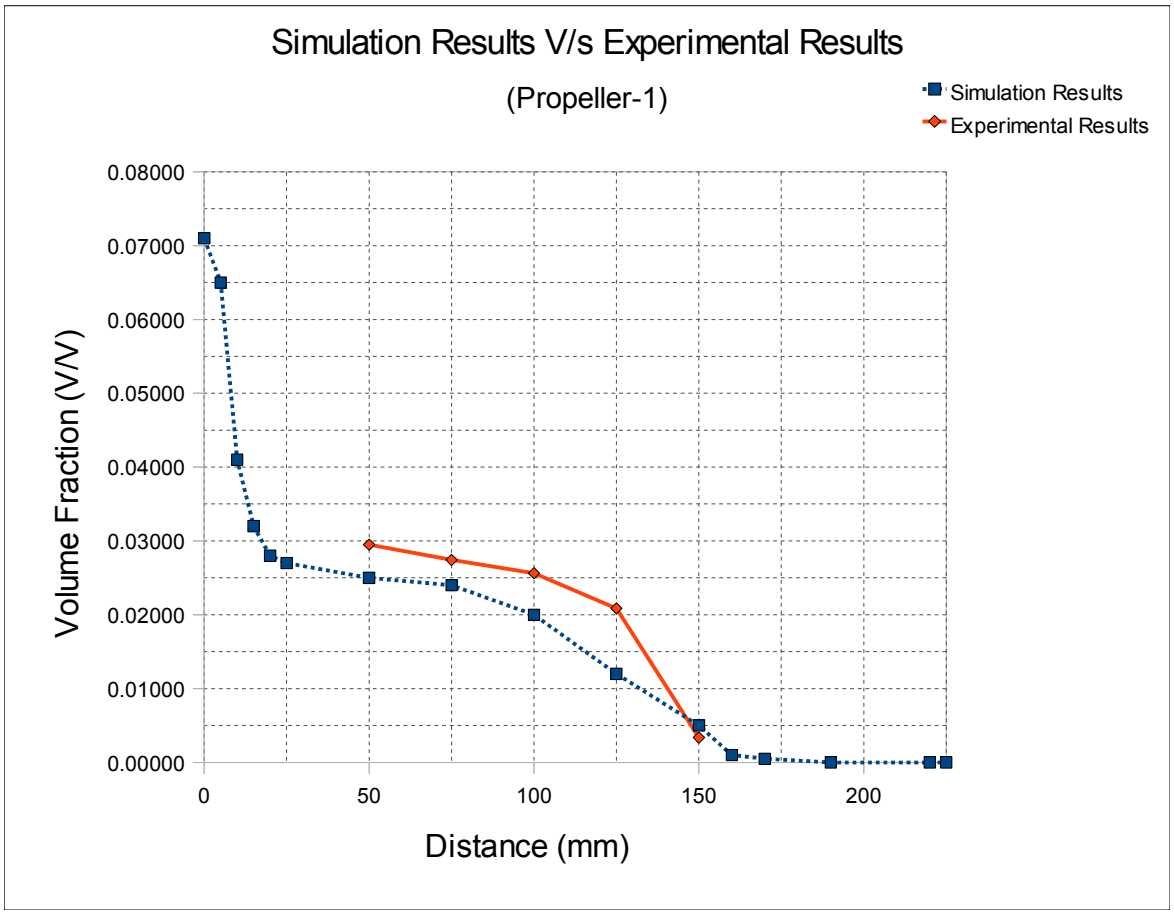

Figure 6.1: Sand Concentration X-Y plot at 10% Cw, 360 rpm, Propeller-1

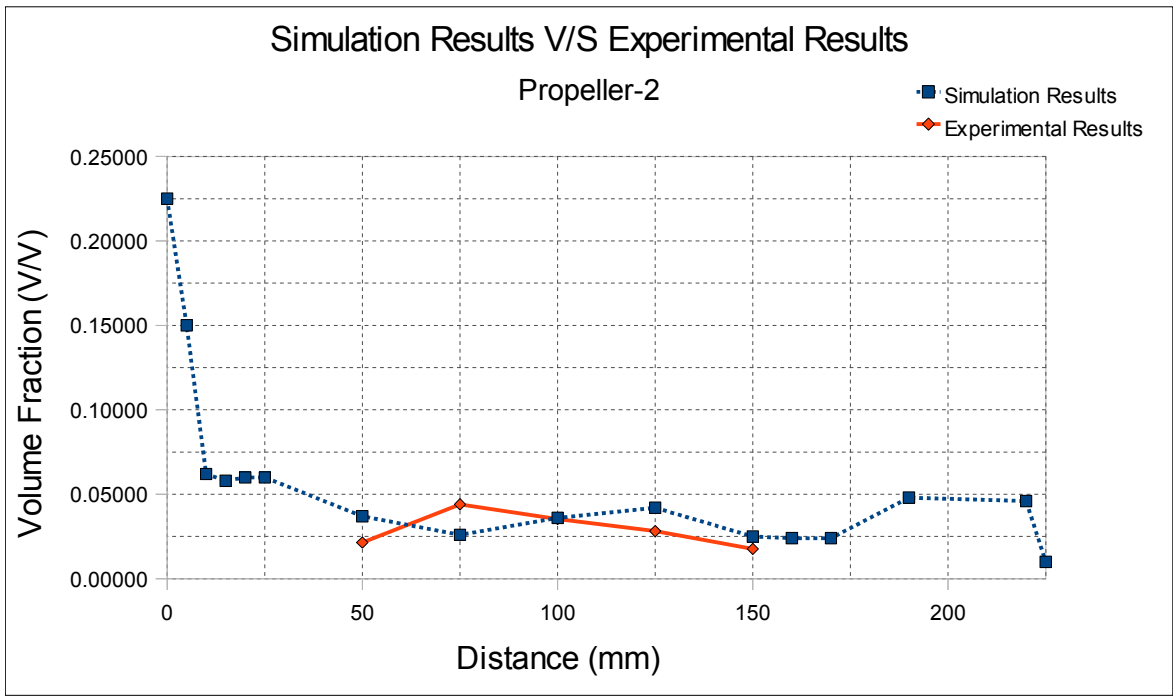

Figure 6.2: Sand concentration X-Y plot at 10% Cw, 360 rpm, Propeller-2

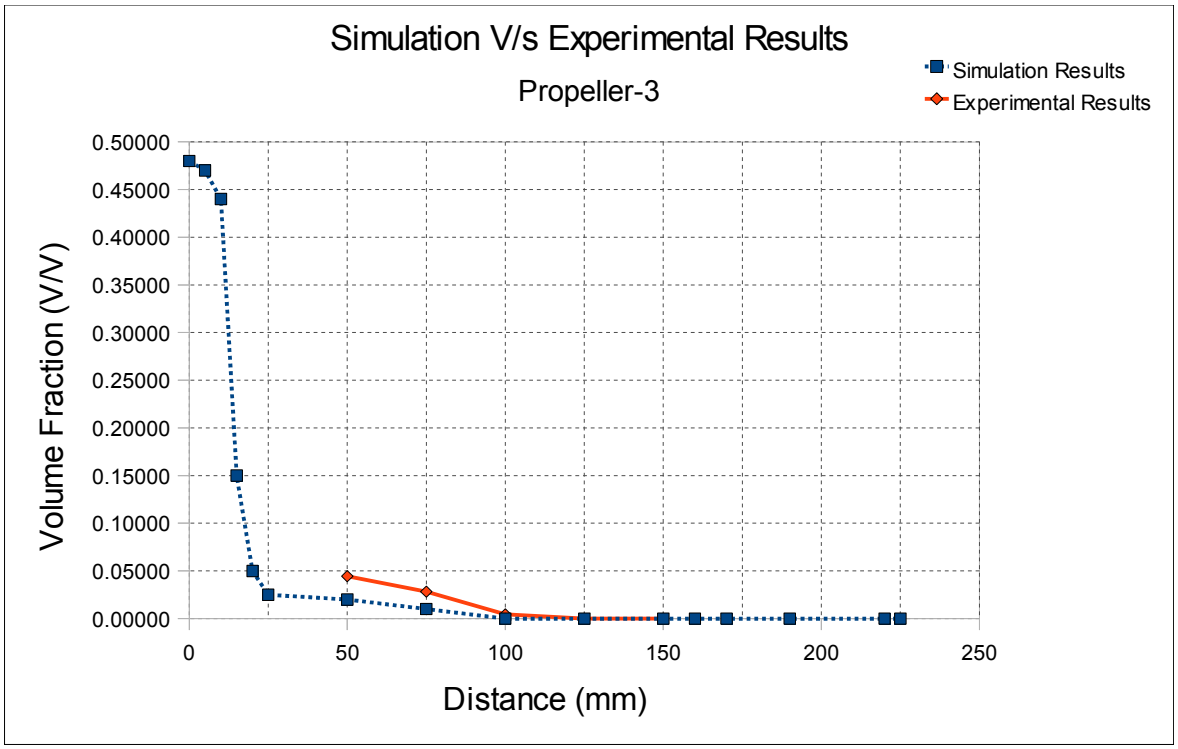

Figure 6.3: Sand concentration X-Y plot at 10% Cw, 360 rpm, propeller-3

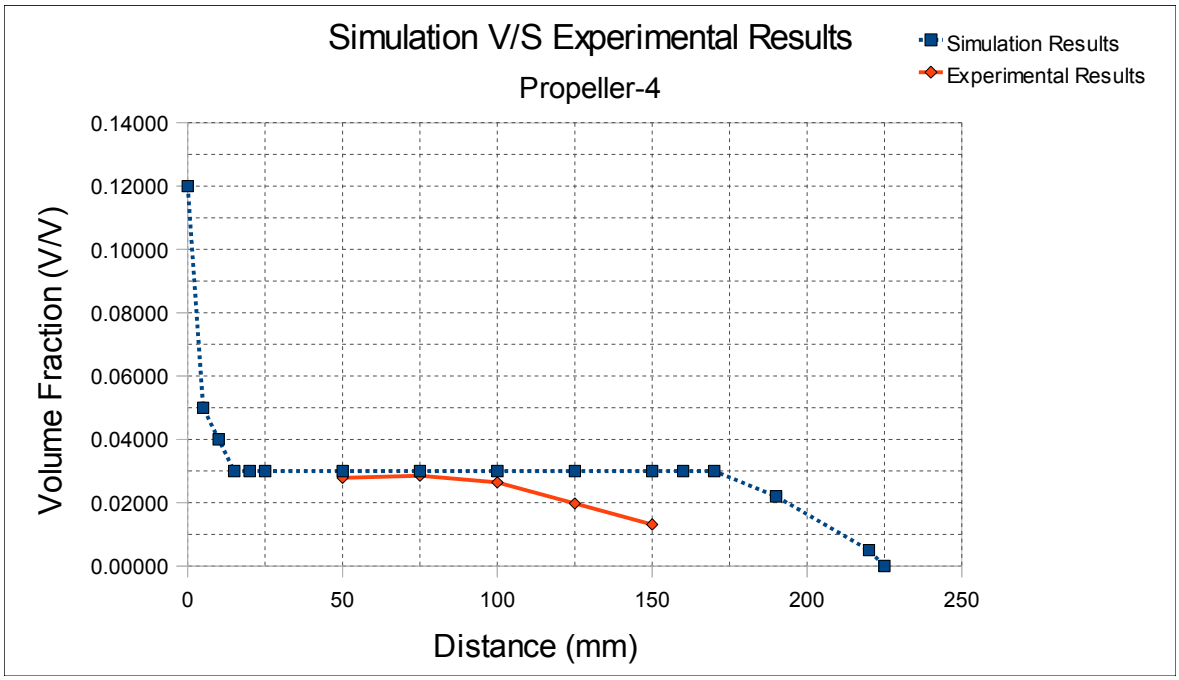

Figure 6.4: Sand concentration X-Y plot at 10% Cw, 360 rpm, propeller-4

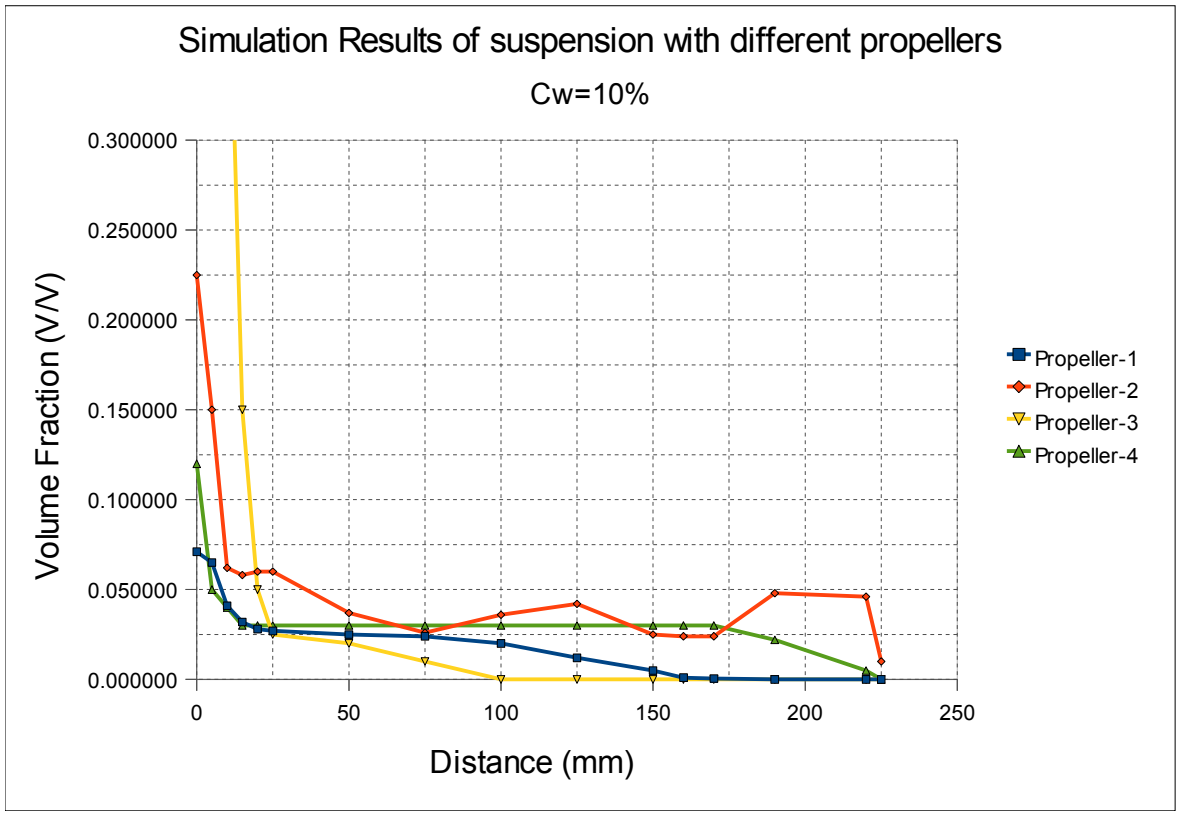

Figure 6.5: Effect of different propellers on solid suspension,Cw=10%, 360 rpm.

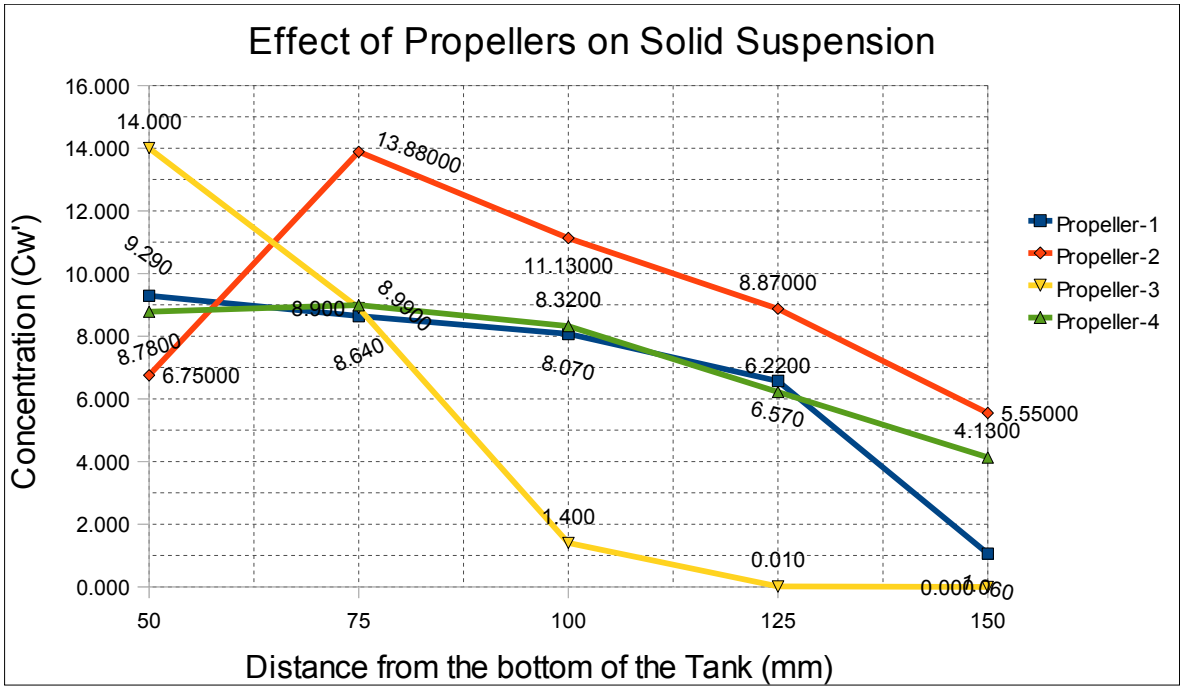

Figure 6.6: Effect of different propellers on solid suspension, Cw=10%, 360 rpm(Experimental)

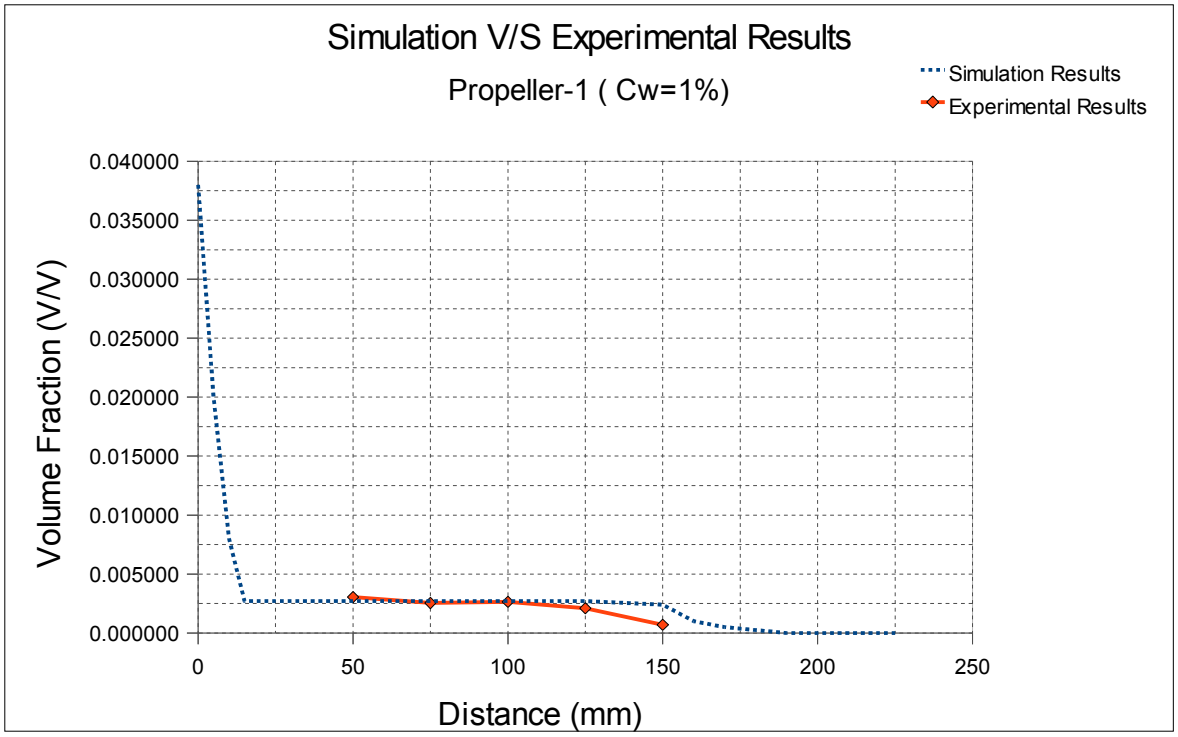

Figure 6.7: Sand concentration X-Y plot at 1% Cw, 360 rpm, propeller-1

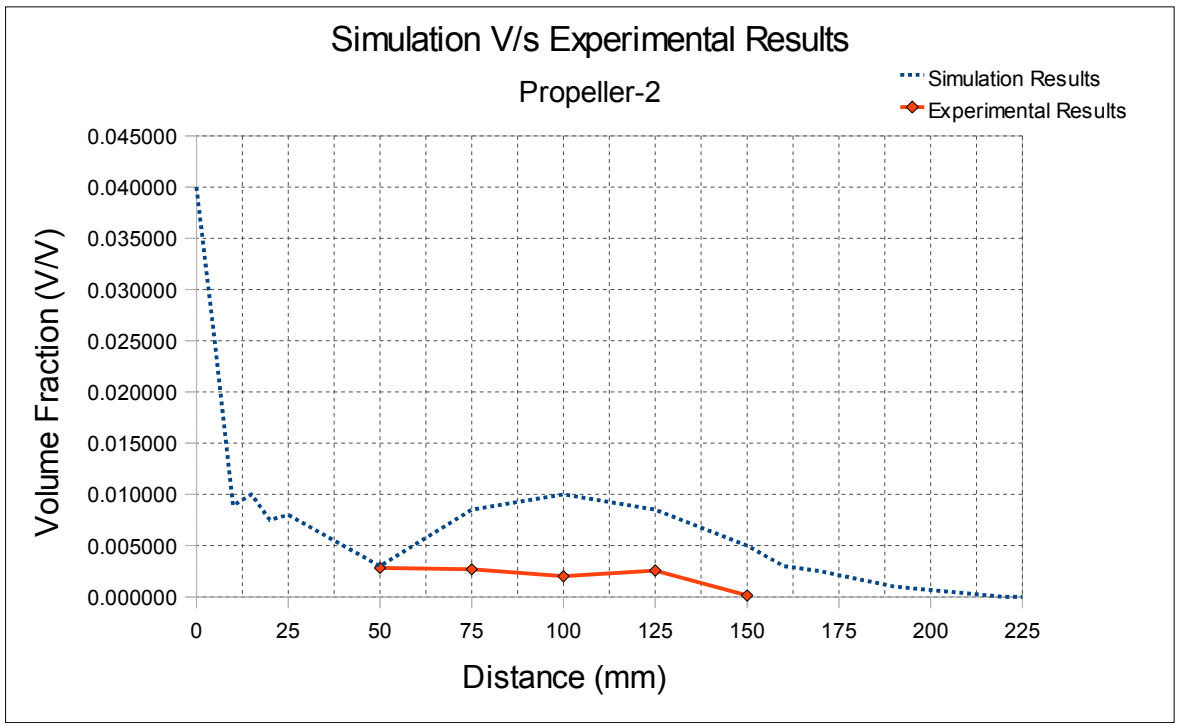

Figure 6.8: Sand concentration X-Y plot at 1% Cw, 360 rpm, propeller-2

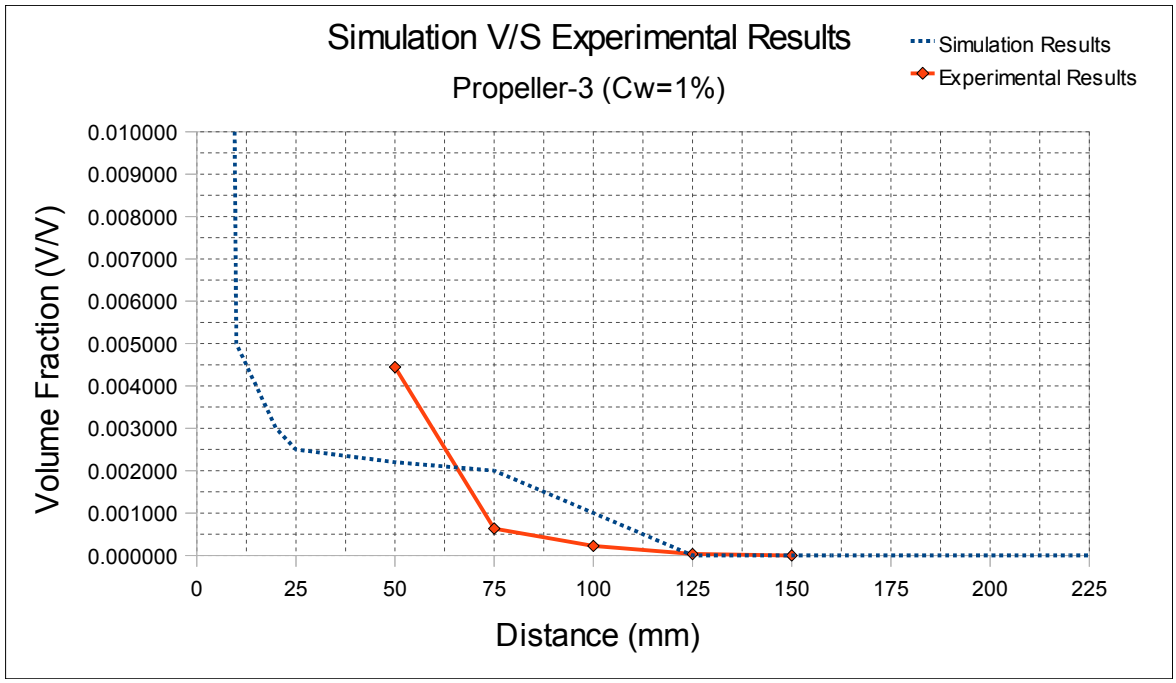

Figure 6.9: Sand concentration X-Y plot at 1% Cw, 360 rpm, propeller-3

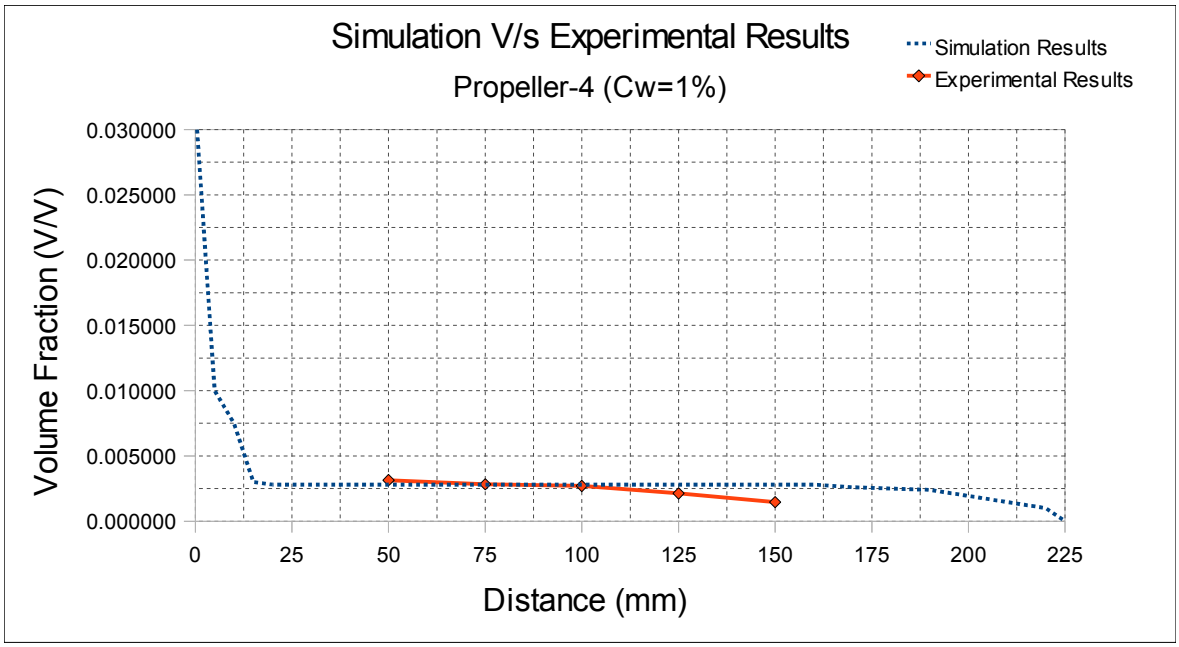

Figure 6.10: Sand concentration X-Y plot at 1% Cw, 360 rpm, propeller-4

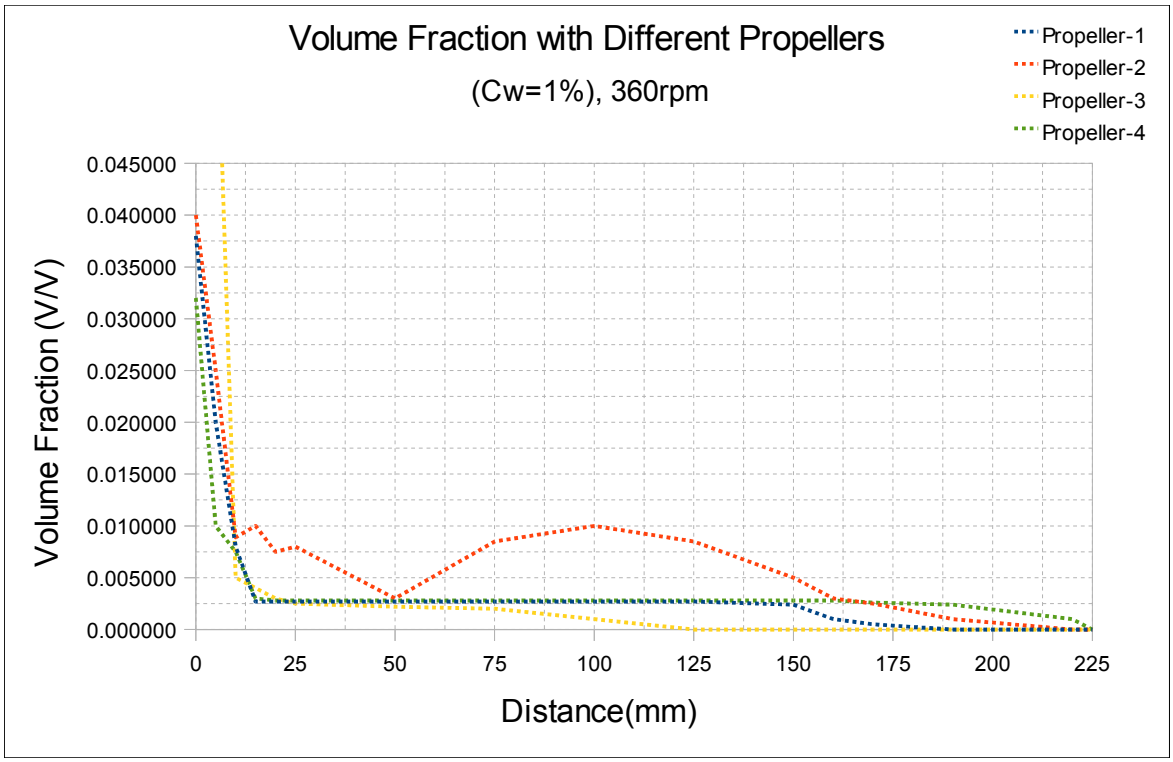

Figure 6.11: Effect of different propellers on solid suspension, Cw=10%, 360 rpm(Simulation)

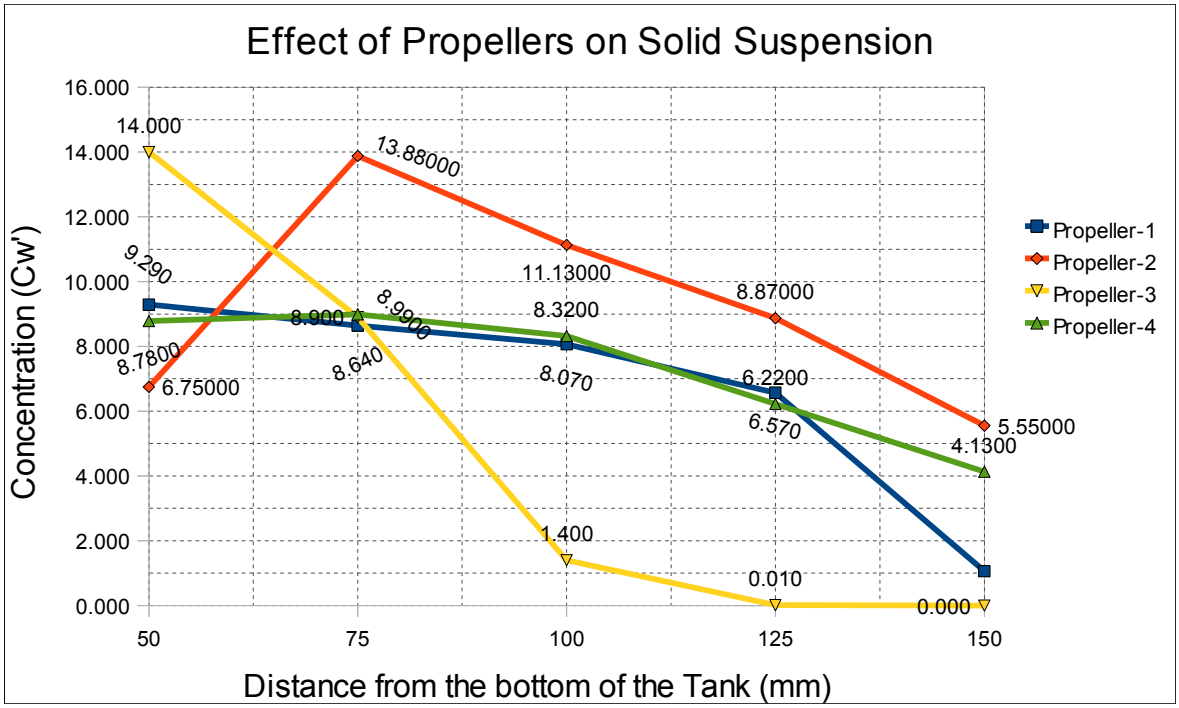

Figure 6.12: Effect of different propellers on solid suspension, Cw=1%, 360 rpm(Experimental)

The experimental as well as simulation results show that the propellers with D/T ratio more than 0.6 have (Propeller-2 and Propeller-3) failed miserably. Propeller-2 and propeller-3 both have D/T ratio of 0.75.

The graphs (figures 6.7, 6.9 and 6.10) show that propeller-3 has failed to suspend particles axially. Most of the concentration has been shown suspended only in the bottom part of the tank (upto 75mm). Very little concentration is obtained from the upper part of the tank, both by experimental and simulation methods. The results supports the literature published in papers which state that, if the D/T ratio of a PBT propeller is more than 0.6, the propeller will be more of a radial type than that of the mixed flow type.

Also, more the blade thickness, more will be the shearing thrust imparted to the particles. Propeller-3 has blade thicknes equal to 5 mm which is less than that of propeller-2 (w=15). Therefore, propeller-2 has been able to provide more shear thrust to the particles than propeller-3, which is the reason behind comparably fair performance of propeller-2 than propeller-3.

The quality of suspension [14] both with experimenal and simulation results are given in table 6.2 and 6.3, respectively. For uniform suspension: $\sigma < 0.2$, For just suspended condition: $0.2 < \sigma > 0.8$, and for incomplete suspension: $\sigma > 0.8$.

Table 6.1: Relative standard deviations at Cw = 1% and 10% (Experimental).

Relative standard deviation (σ) (Experimental)	Propeller-1	Propeller-2	Propeller-3	Propeller-4
σ at 1% orginal concentration	0.39	0.47	0.91	0.30
σ at 10% original concentration	0.44	0.31	0.76	0.33

Table 6.2: Relative standard deviations at Cw = 1% and 10% (Simulation).

Relative standard deviation (σ)	Propeller-1	Propeller-2	Propeller-3	Propeller-4
σ at 1% orginal concentration	0.13	1.59	0.72	0.07
σ at 10% original concentration	0.49	0.25	0.85	0.0

Table 6.1 and Table 6.2 show that the standard deviation of propeller-3 is near 0.8 in simulation as well as experimental results, clearly signifying that the suspension is incomplete. Therefore, the use of propeller-3 was not suitable for uniform suspension and was rejected on the grounds of results obtained. Propeller-4 has shown σ value consistently lesser or closer to 0.2, signifying the good quality of suspension. Fur further experiments related to the effect of change in concentration, speed and baffle design, experimental results were obtained using propeller-4.

6.2 EFFECT OF CHANGE IN ORIGINAL CONCENTRATION

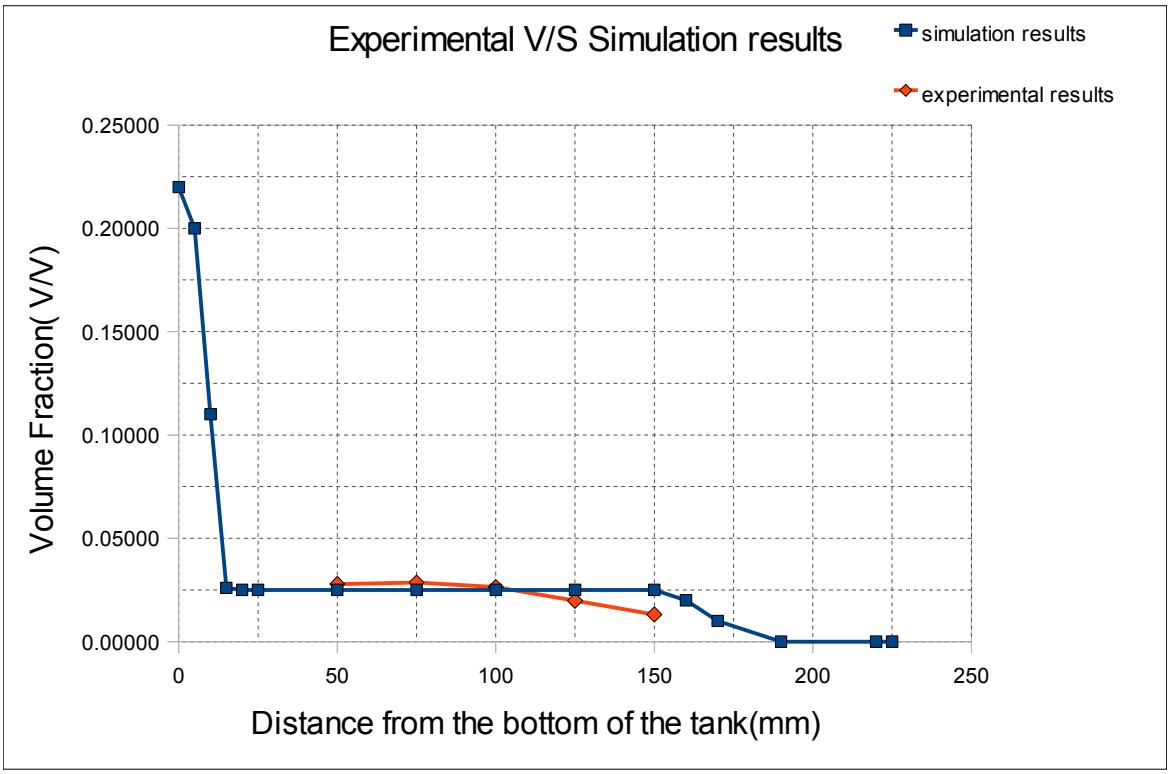

Figure 6.13: Sand supension X-Y plot at 10% (Cw),V/V=0.03, 360 rpm, propeller-4

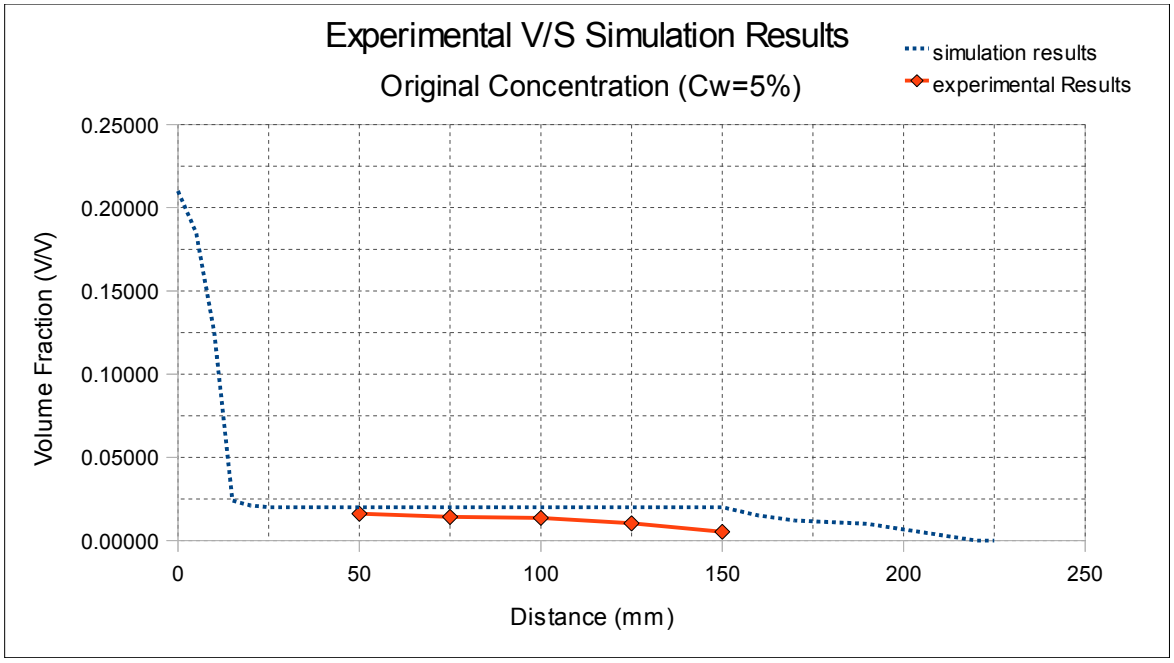

Figure 6.14: Sand supension X-Y plot at 5% Cw, V/V=0.02, 360 rpm, propeller-4

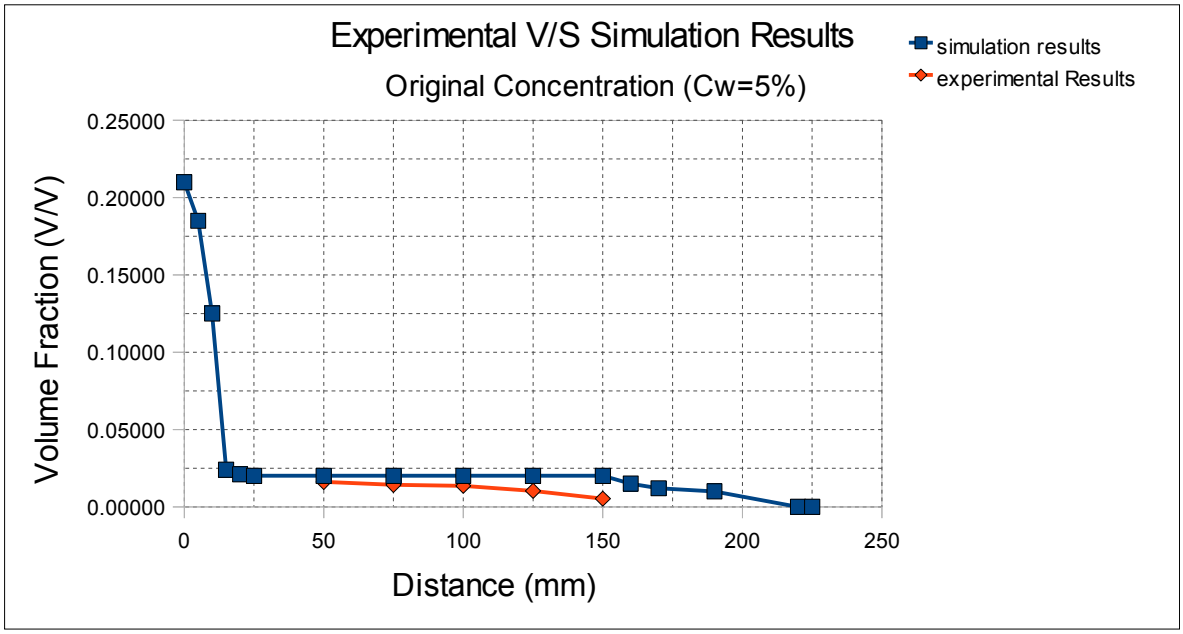

Figure 6.15: Sand supension X-Y plot at 1% Cw, 360 rpm, propeller-4

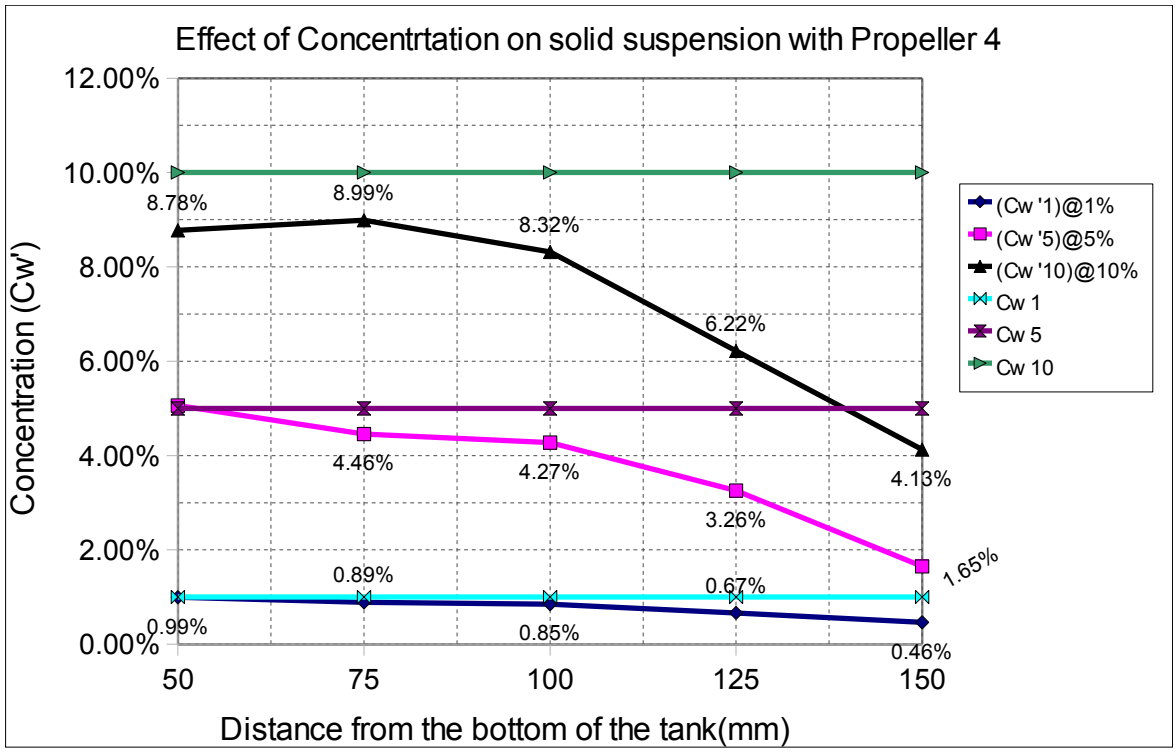

Figure 6.16: Sand supension X-Y plot at Cw=10%, 5%, 1% , propeller-4, Experimental

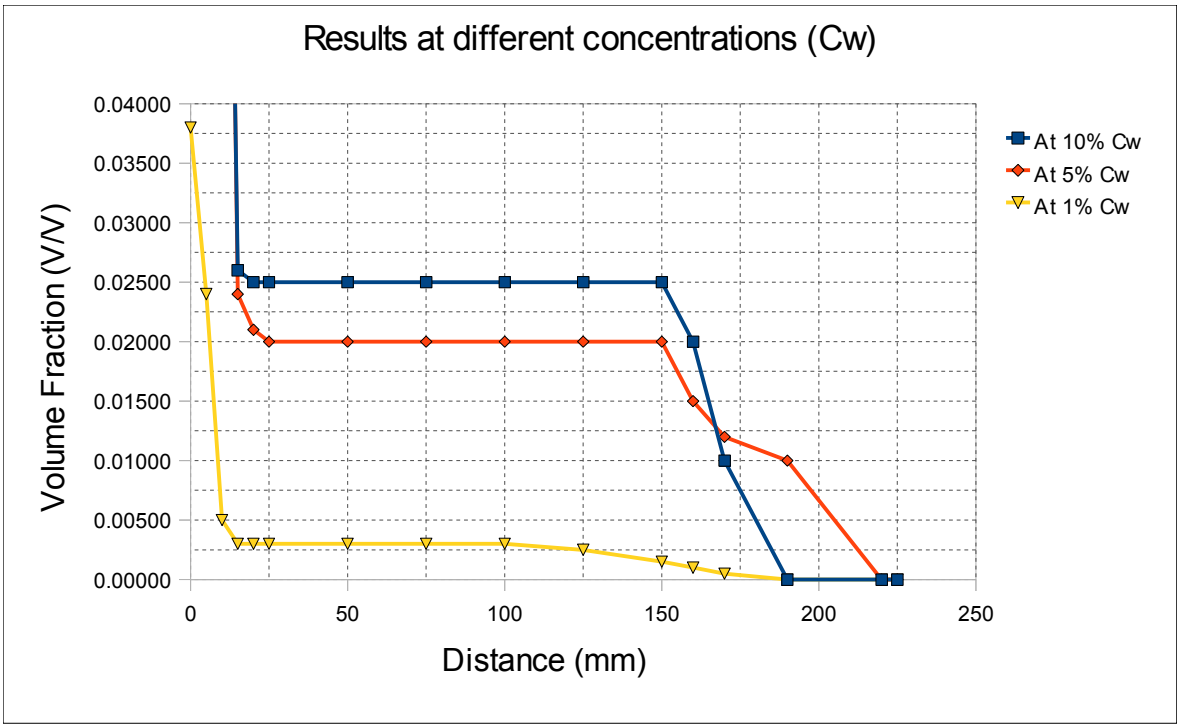

Figure 6.17 : Sand supension X-Y plot at Cw=10%, 5%, 1% , propeller-1(Simulation)

The above results show that the concentration of the SiC particles is more at the bottom and least at the top of the tank volume. Experimental results (Figure-4) explain that the concentration collected (Cw') at the lowest port (L1,50mm) is maximum than those collected at the other ports R1, L2, R2 and L3 respectively, Whereas, Simulation results show that the Volume fraction profile is constant between 50 mm 125 mm for all the propellers and show maximum deviations only in the region of 0 -25mm and 175 mm-225 mm from the bottom of the tank, respectively.

The experimental graph shows that the results obtained with 1% original concentration have minimum percentage deviation from the orginal concentration, whereas, those obtained with 10% original concentration show maximum. The increase in original concentration by keeping rotational speed constant, has resulted in poor solid suspension (as shown in figure 6.4). The inter-particle collision increases with an increase in original concentration, taking away the kinetic energy possessed by them. This validates that the suspension is going to be poorer if the rotational speed is kept constant and the original concentration increased. Minimum suspension speed is a function of original concentration and an increase in original

concentration would also increase the minimum suspension speed.

Simulation results validate the experimental results as the former show similar pattern of volume fraction distribution along the walls of the tank.

Oshinowo et al [14] has mentioned a method to measure the solid concentration quantitatively. The relative standard deviation (σ) has been used to measure the quality of suspension. The relative standard deviation is the square root of the sum of squares of percentage deviations from the original concentration(Cw).

For uniform suspension: $\sigma < 0.2$, For just suspended condition: $0.2 < \sigma > 0.8$, and for incomplete suspension: $\sigma > 0.8$ [14].

The relative standard deviations at various concentrations for propeller-4 are tabulated below.

Table 6.3: Comparison of quality of suspension at different concentrations

Propeller-4	Experimental Results			Simulation Results		
	At 10% Cw	At 5% Cw	At 1% Cw	At 10% Cw	At 5% Cw	At 1% Cw
σ	0.3	0.45	0.27	0.27	0	0.14

6.3 EFFECT OF CHANGE IN ROTATIONAL SPEED

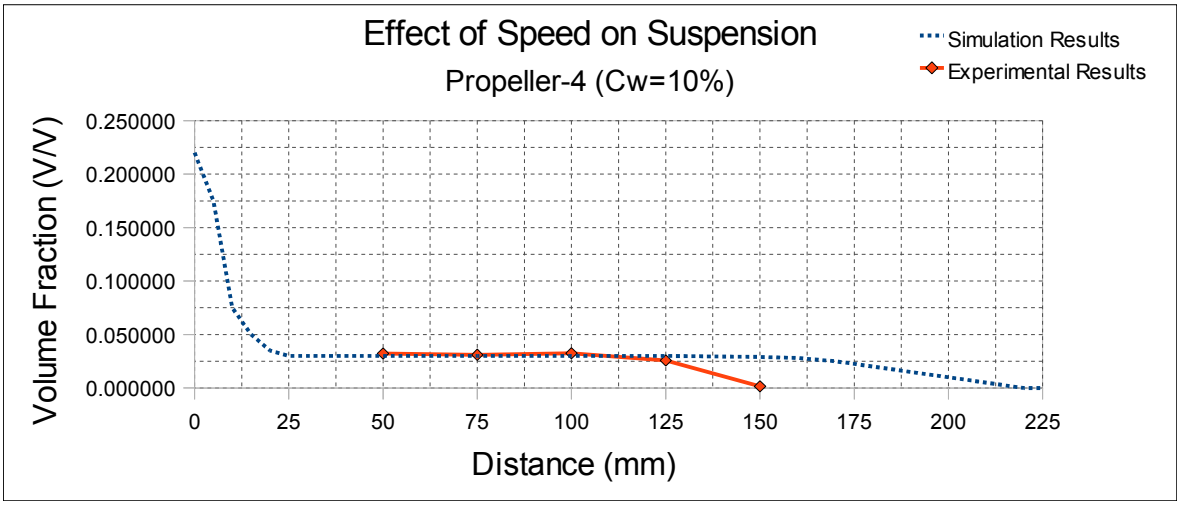

Figure 6.18 : Effect of rotational speed (345 rpm) on solid suspension, propeller-4

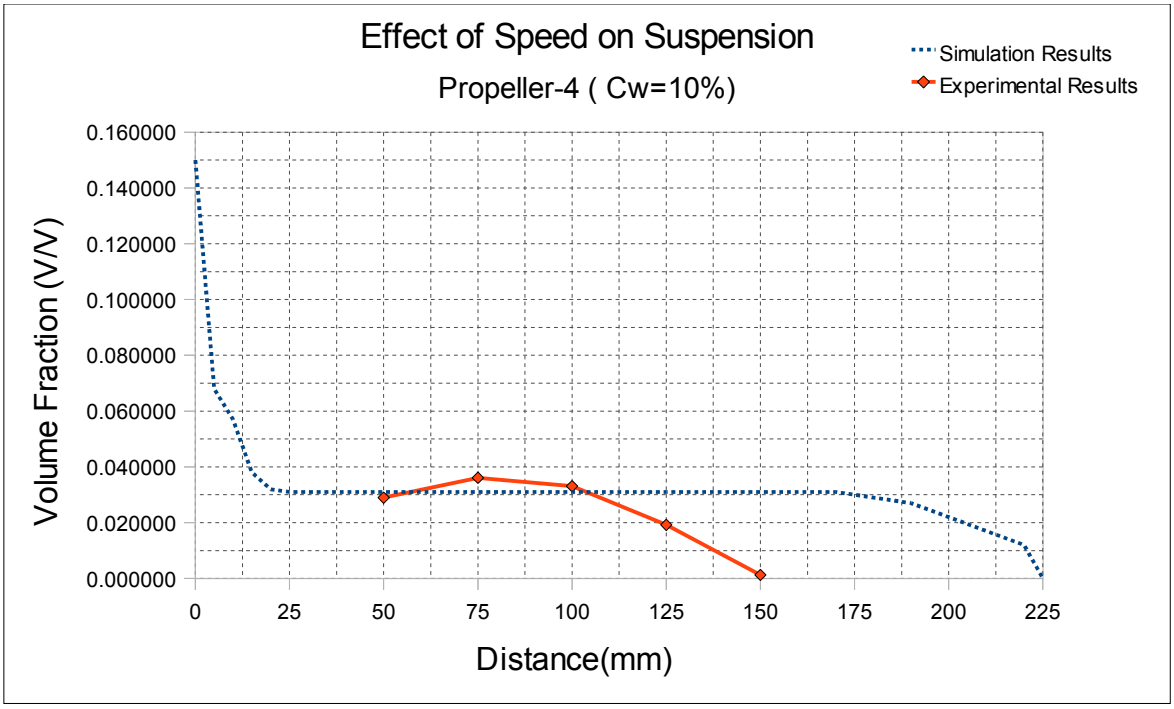

Figure 6.19 : Effect of rotational speed (360 rpm) on solid suspension, propeller-4

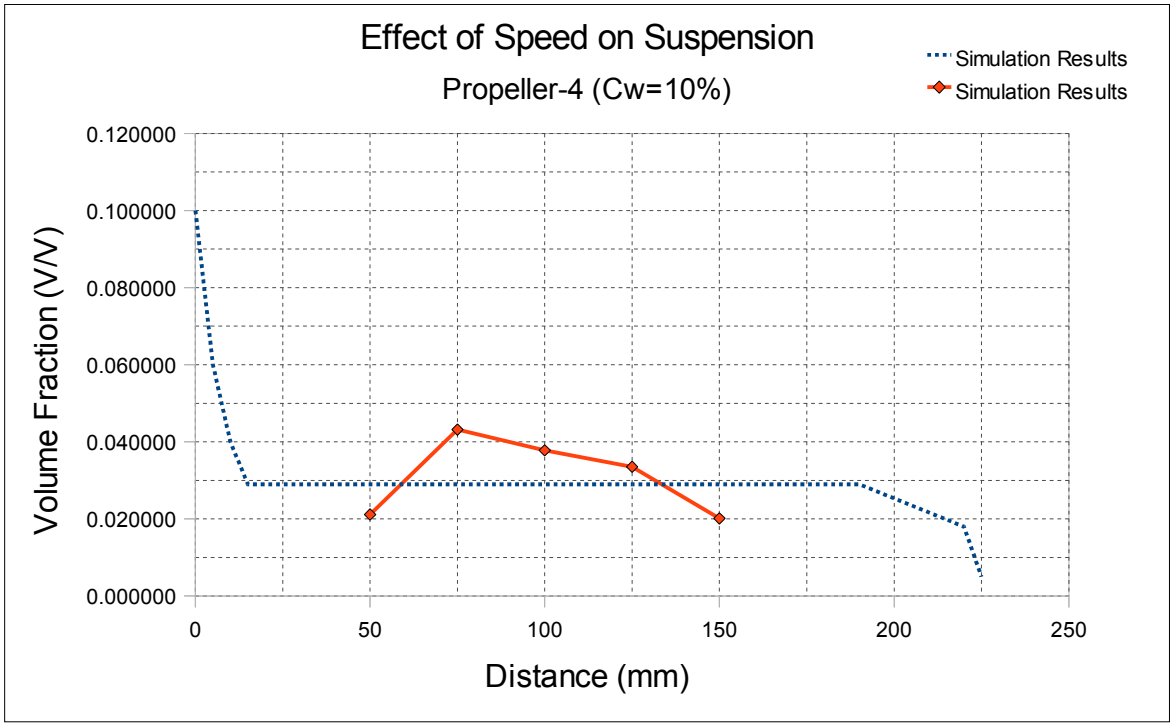

Figure 6.20 : Effect of rotational speed (370) on solid suspension, propeller-4

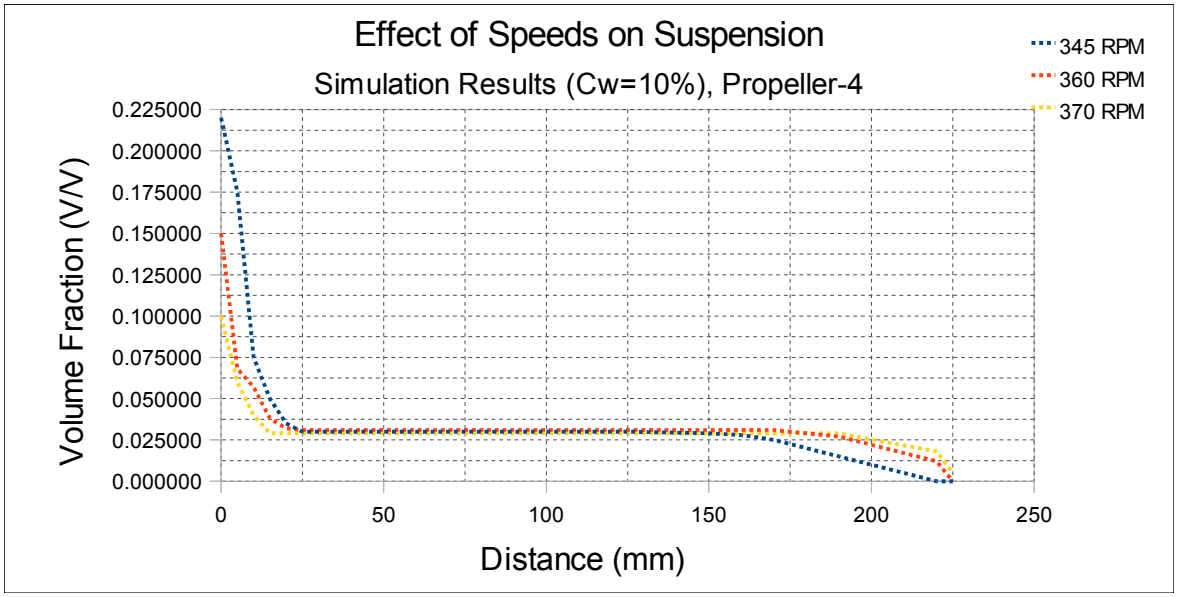

Figure 6.21 : Effect of rotational speeds on suspension, propeller-4(Simulation results)

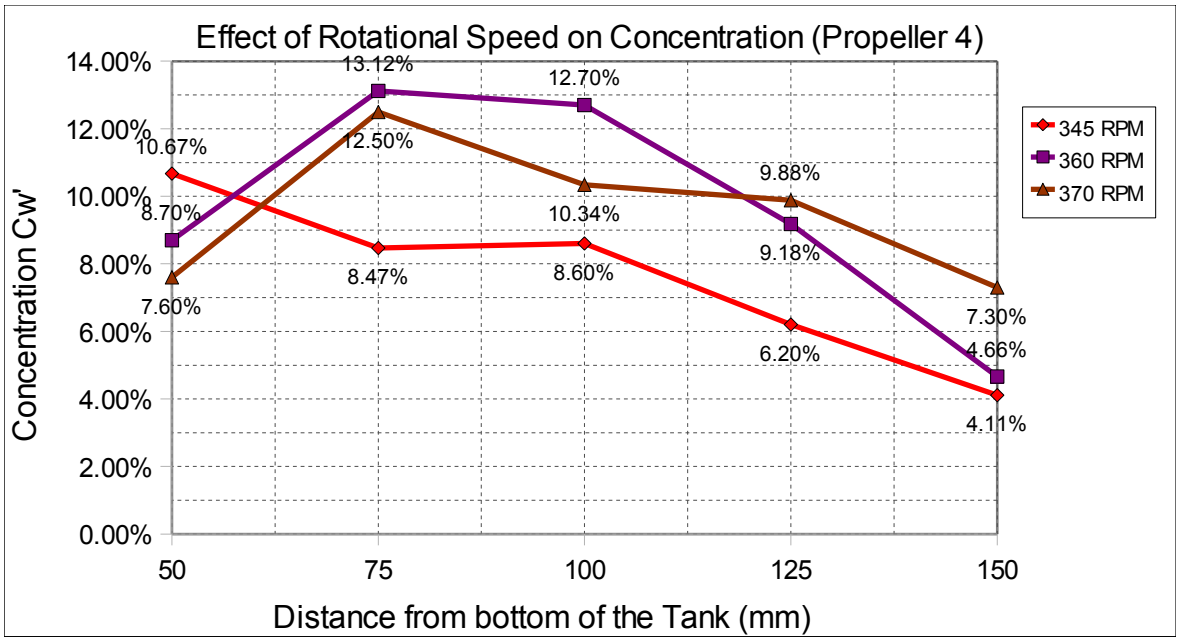

Figure 6.22: Effect of rotational speed on suspension, propeller-4 (Experimental)

The experimentals results show(figure 6.18-6.22) that the solid concentration at the bottom of the tank decreases as rpm is increased. The same is validated by the simulation results taken at 10% concentration, rotational speed at 345,360 and 370 rpm with propeller-4. Solid concentration at the top portion of the slurry pot increases with increase in rpm. This is due to

the greater lift force imparted on the particles by the motion of the impeller.

The relative standard deviations at 345, 360 and 370 rpm with propeller-4 are tabulated below.

Table 6.3: Relative standard deviations at different rpm, Cw=10%

Relative standard deviation (σ)	345 RPM	360 RPM	370 RPM
σ (Experimental)	0.33	0.31	0.20
σ (Simulation)	0.46	0.33	0.26

The relative standard deviation (σ) decreases when the impeller rotational speed is increased. For propeller-4: $\sigma_{370} < \sigma_{360} < \sigma_{345}$. This shows that propeller-4 has reached the stage of uniform suspension. However, previous studies on solid suspension explains that the suspension will not get better at speeds appreciably higher (more than 10% of N_{js}) than that required for minimum suspension at a given concentration.

6.4 EFFECT OF BAFFLE CLEARANCE

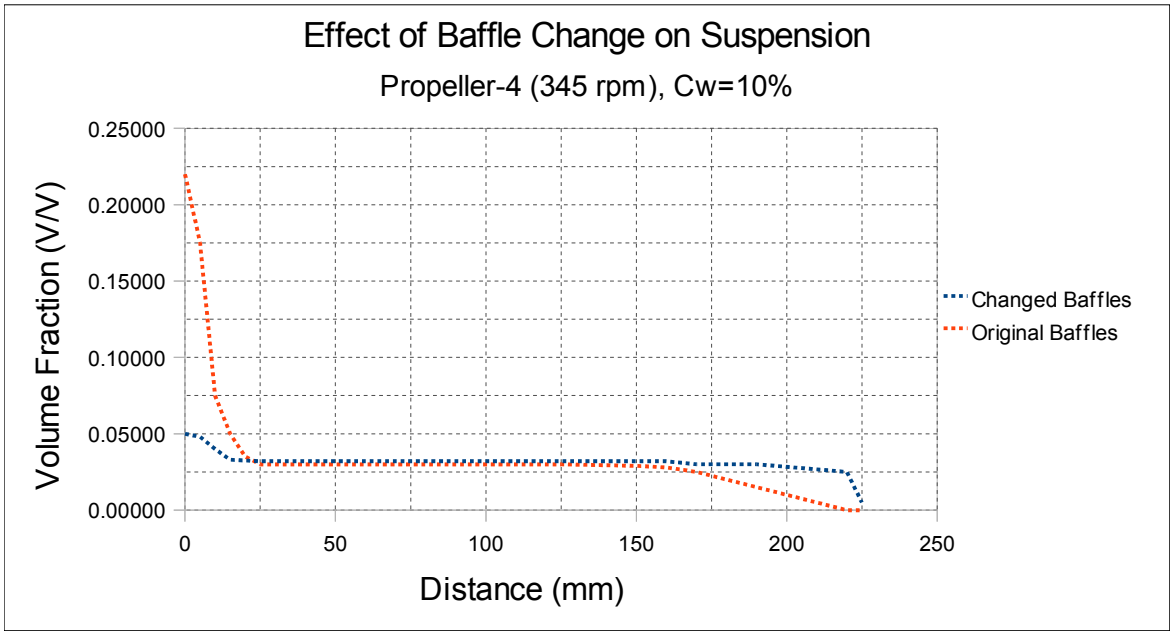

Figure 6.23: Effect of change in baffle design on solid suspension, simulation results

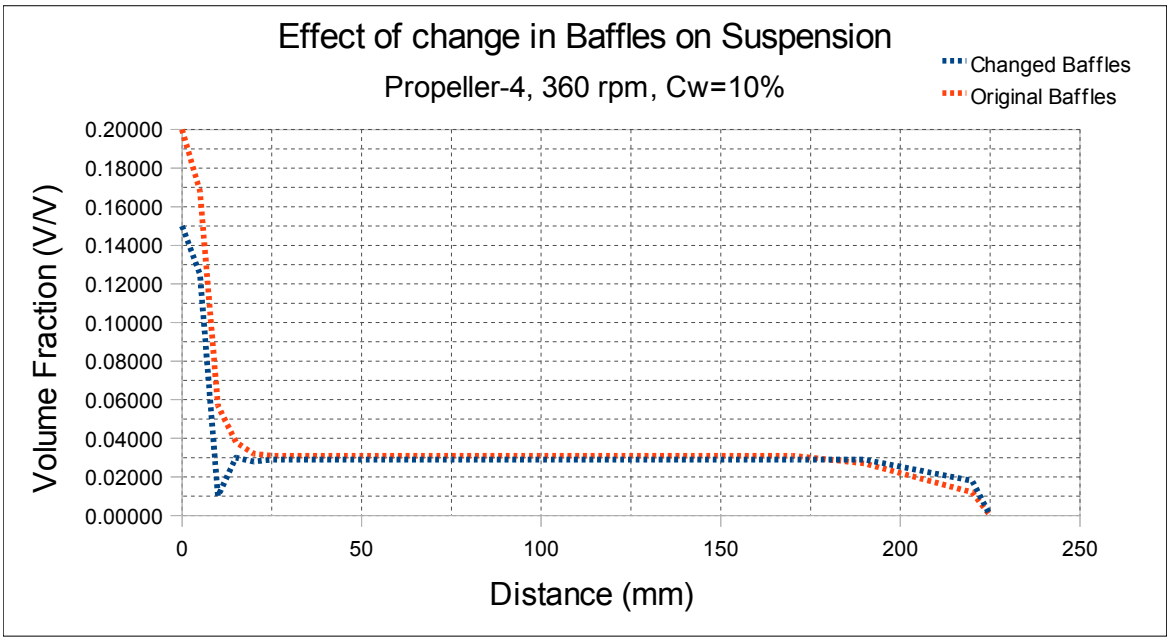

Figure 6.24: Effect of change in baffle design on solid suspension, propeller-4, 360 rpm

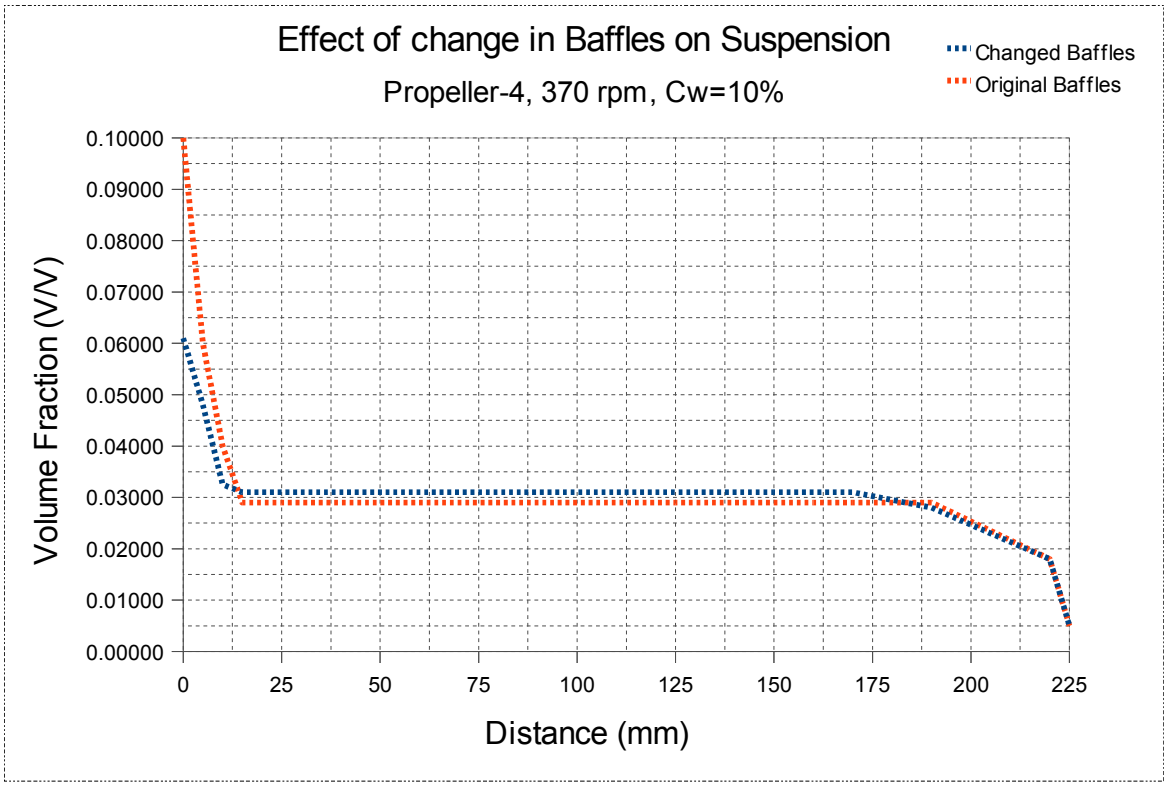

Figure 6.25: Effect of change in baffle design on solid suspension, propeller-4, 370 rpm

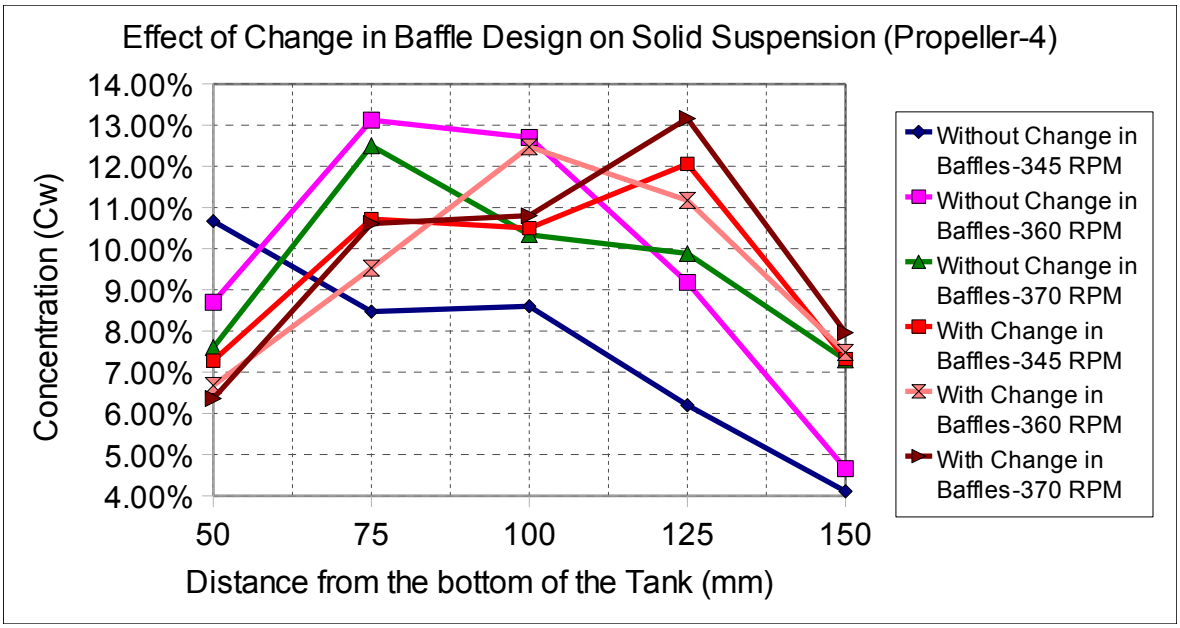

Figure 6.26: Effect of change in baffle design on solid suspension, propeller-4

Table 6.3: Relative standard deviations at different rpm, Cw=10%

Relative standard deviation (σ)	Experimental Results					
	Without change in baffles			With change in baffles		
	345 RPM	360 RPM	370 RPM	345 RPM	360 RPM	370 RPM
σ with propeller-4	0.33	0.31	0.20	0.2	0.22	0.24

Table 6.3: Relative standard deviations at different rpm, Cw=10%

Relative standard deviation (σ)	Simulation Results					
	Without change in baffles			With change in baffles		
	345 RPM	360 RPM	370 RPM	345 RPM	360 RPM	370 RPM
σ with propeller-4	0.46	0.33	0.25	0.24	0.30	0.25

The experimental and simulation results with the provision of 50 mm clearance in baffle length from the bottom show that the quality of suspension has improved with the use of both the propellers. The relative standard deviation has reduced from 0.33 at 345 rpm to 0.20, signifying the improvement in the quality of suspension.

CHAPTER 7

CONCLUSION AND FUTURE SCOPE

Conclusion

Quality of solid-liquid suspension in a slurry pot has been studied both by the experimental and simulation method. Effect of change in propeller geometry, rotational speed, original concentration and change in design of baffles on the quality of suspension were investigated. Silicon-carbide in granular form (550 microns) was used in the experiments. Both the experimental as well as simulation results show that the propeller-4 with D/T ratio equal to 0.60, has better quality of suspension than the other three propellers used in the investigation. Increase in rpm has improved the quality of suspension of solids but, at further higher speeds, the quality of suspension may decrease. Increase in original concentration (Cw) at constant speed has decreased the quality of solid-liquid suspension. The provision of baffle clearance at the bottom of the tank has given better quality of solid-liquid suspension.

Future Scope

1. The wear tests in the slurry pot tester can be performed by using propeller-4 (D=145mm, w=27mm) and by the provision of baffle clearance at the bottom of the tank.
2. The simulation results of Eulerian model can be compared with the mixture model.
3. The computational approach can be used to simulate propeller and stir tank in the stir casting processes to study the quality of suspension.
4. The Energy dissipation rates and the vorticity in the stir tank can also be studied using computational fluid dynamics codes.

REFERENCES

1. M.A.Rayan, M.Shawky, (1989), “Evaluation of wear in a centrifugal slurry pump”, Alexandria University Proceedings of ISME.
2. Desai P. V ,Pagalthivarthi V, Addie G. R. (1990), “Particular motion and concentration fields in centrifugal slurry pumps”, Particulate Science and Technology,Vol. 8:1, pp 77 – 96.
3. Clark H. McI., (1991), “The influence of flow field in slurry erosion”, Tribology International.
4. N.R.Steward, A.J.S. Spearing(1992), “Combating pipeline wear-an advanced technology” journal of South African Institute of Mining.
5. J. Postelhwaite, S.Neseic(1993), “ Erosion in disturbed liquid pipe flow-Effect of flow geometry and surface roughness” Corrosion Engineering,Volume49, No.10.
6. Rajat Gupta, S.N. Singh,V.Seshadri(1994), “Prediction of uneven wear in a slurry pipeline on the basis of pot tester”.
7. Yuan Zhong, Kiyoshi Minemura (1995), “ Numerical prediction of erosion wear in pump casing under solid water two phase flow.” Elsvier Science Journal.
8. Yuan Zhong,Kiyoshi Minemura (1996), “ Measurement of erosion due to particle impingement and numerical prediction of wear in pump casing.” Elsvier Science Journal.
9. Nick Stokes and Zili Zhu (1997), " Simulation of two phase flows in a stirred mixing tank", International conference on CFD in Mineral and Metal Processing and Power Generation.
10. Gary Brown (1999), “Prediction of erosion in a slurry pipeline tee”.
11. Lee S. Y., Dimenna R. A., and Duignan M. R. 2001, “Designing a scaled erosion test with CFD methods”, U.S. Department of EnergyWSRC-MS-2001-00500.
12. Hawthorne H.M. 2002, “Some Coriolis slurry erosion test developments”, Tribology International, Vol. 35 ,pp 625–630.
13. Gandhi B.K, Singh S. N., Seshadri V. 2001, “Performance characteristics of centrifugal slurry pumps”, Journal of Fluids Engineering ,Vol. 123, pp 271-280.

14. Larne M. Oshinowo, Andre Bakker, (2002) "CFD modeling of solids suspension in stirred tanks", Symposium on Computational Modeling of Metals, Minerals and Materials, TMS Annual Meeting, February 17-21, 2002, Seattle, WA.

15. D. Chapple, S.M. Kresta, A. Wall, A. Afacan, (2002) " The effect of impeller and tank geometry on power number for a pitched blade turbine". Institution of Chemical Engineers, Vol 80, Part A.

16. G. Zhou, S. Litian, P. Yu (2003), " CFD study of the mixing process in rushton turbine stir tanks ", Third International conference on CFD in the Minerals and Process Industries, 10-12 December, 2003.

17. Feng Wang, W. Wang, Y. Wang, Z. Mao (2003), "CFD simulation of solid-liquid two-phase flow in a baffled stirred vessels with Rushton Impellers", Third International Conference on CFD in the Minerals and Process Industries CSIRO,Melbourne, Australia, 10-12 December, 2003.

18. J.J. Derksen, " Numerical simulation of the soli suspension in the stirred tank " AIChE Journal, November 2003, Volume 49, No. 11.

19. Gandhi B K., Borse Satish V. 2004, “Nominal particle size of multi-sized particulate slurries for evaluation of erosion wear and effect of fine particles”, Journal of Wear, Vol. 257 , pp 73-79.

20. R.J.K.Wood,T.F.Jones (2004), “Investigations of sand-water induced erosive wear of AISI 304L stainless steel pipes by pilot-scale and laboratory-scale testing”.

21. G. Montante, F. Magelli (2005), "Modelling of solid distribution in stirred tanks: analysis of simulation strategies and comparison with the experimental data". International Journal of Computational Fluid Dynamics, Volume-19, No. 3, 2005, 253-262.

22. R. Thorpe, P. Stevensen (2005), " Suspension of particles from the bottom of pipes and stirred tanks by gassed and ungassed flows". IchME, Volume 46, Page 6605-6611.

23. R.J. Llewellyn, S.K. Yick, K.F. Dolman (2005), “Scouring erosion resistance of metallic materials used in slurry pump service” Elsevier, Wear256(2005).

24. A. Sellgren, G. Addie, R. Visintainer and K. Pagalthivarthi (2005), “Prediction of

slurry pump component wear and cost".

25. T. Kumaresan, Nandkishore K. Nere, J. Joshi (2005), " Effect of internals on the flow pattern and mixing in stirred tanks". Ind. Eng. Chem. Res. 2005, 44, 9951.

26. Tian Harry H., Graeme R. Addie 2005, "Experimental study on erosive wear of some metallic materials using Coriolis wear testing approach", Journal of Wear vol. 258 , pp 458–469.

27. G. Desale, B. Gandhi, S.C. Jain (2005), " Improvement in the design of pot tester to simulate erosion wear due to solid-liquid mixture". 15th International Conference on Wear of Materials, Volume 259, Issues 1-6, Pages 196-202.

28. Feng Jianjun, Karl Friedrich, and Dohmen Hans Josef, (2007), "Numerical investigation on pressure fluctuations for different configurations of vaned diffuser pumps", International Journal of Rotating Machinery ,Vol 2007, Article ID 34752, 10 pages.

29. Desale Girish R., Gandhi B.K., Jain S.C.,(2007), "Slurry erosion of ductile materials under normal impact condition", Journal of Wear, Vol. 264, pp 322–330.

30. William A. John, (2007), " Wear and wear particles-some fundamentals",Tribology international, 38 (2005), Elsevier Science Journal.

31. N. Ridgway, C.B.Colby, B.K.O'Neill (2009), "Slurry pump gland seal wear",Tribology International.

32. Wang Yao, Ming J. Zhong, Xian Feng Fan (2009), " Design of an experimental system for wear assessment of slurry pumps".

33. Yulin Wu, Huijing Yuan, Jie Shao and Shuhong Liu (2009), "Experimental Study on Internal Flow of a Mini Centrifugal Pump by PIV Measurement", International Journal of fluid machinery and systems,Vol 2,No2.

34. Masaya Suzuki, Kazuaki Inaba (2009) , " Numerical simulation of sand erosion in a square section 90 degrees bend", journal of science and technology,Vol3,No7.

35. J. Wu, Y. Jhu and L. Pullum (2009), " Impeller geometry effect on velocity and solid suspension ". Thermals and fluids engineering, CSIRO, Victoria, Australia

36. Joseph I. Achebo (2009), "Computational Analysis of Erosion Wear Rate in a Pipeline Using the Drift Flux Models based on Eulerian Continuum Equations",

Proceedings of the World Congress on Engineering 2009 Vol I WCE 2009, July 1 - 3, 2009, London, U.K.

37. S. Haavisto, J. Syrjanen, A. Koponen, M. Manninen (2009)," Particle velocity and concentration profiles of sand-water slurry in stirred tank-measurement and modelling ". Seventh Inernational conference on CFD in the Minerals and Processing Industries, CSIRO, Melbourne, 9-11 December.

38. K. Mohanrangam, D. Stephens (2009), "CFD modeling of floating and settling phases in settling tanks", Seventh International conference on CFD in the Minerals and Processing Industries, CSIRO, Melbourne, 9-11 December.

39. O. Khazam, S.M. Kresta (2009), " Drawdown of floating solids in stirred tanks". Thirteenth European Conference on Mixing.

BIBLIOGRAPHY

40. Fluent user's guide, volume 6.1, Feb 2009.

41. www.haywardgordon.com

42. www.lawrencepumps.com, volume 4, issue-1.

43. WEIR Minerals Division, technical bulletin Vol. 18.

44. Labanoff Val S, (1992), "Centrifugal pumps design and applications", 2nd edition Gulf Publishing Company.

45. Technical Bulletin LaBour Pump Company-901, Ravenwood Drive Alabama.

46. S.M. Kresta, V. Obeng, E. Paul (2004), "Handbook of industrial mixing: science and practice" , volume-1.

47. J. Ulbrecht, G. Patterson (2002), " Mixing of liquids by mechanical agitation "

48. M.F. Edwards , A. Nienow (1985), "Mixing in the process industries ".

APPENDIX

ANNEXURE-I: Tables of the experimental results

Table 4.3: Effect of change in Cw with propeller-1

Distance	(Cw'1)@1%	(Cw'5)@5%	(Cw'10)@10%	Cw1	Cw5	Cw10
50	0.96%	4.53%	9.29%	1.00%	5.00%	10.00%
75	0.88%	2.29%	8.64%	1.00%	5.00%	10.00%
100	0.83%	4.27%	8.07%	1.00%	5.00%	10.00%
125	0.68%	3.26%	6.57%	1.00%	5.00%	10.00%
150	0.22%	0.25%	1.06%	1.00%	5.00%	10.00%

Table 4.4: Percentage deviation from the original concentration, propeller-1

Distance (mm)	Percentage Deviation from Original Concentration		
	1%(Cw1)	5%(Cw5)	10%(Cw10)
50	4.00%	9.40%	7.10%
75	12.00%	54.20%	13.60%
100	17.00%	14.60%	19.30%
125	32.00%	34.80%	34.30%
150	78.00%	95.00%	89.40%

Table 4.5: Effect of change in Cw with Propeller-2

Distance	(Cw'1)@1%	(Cw'5)@5%	(Cw'10)@10%	Cw1	Cw5	Cw10
50	0.49%	3.28%	6.75%	1.00%	5.00%	10.00%
75	0.85%	2.20%	13.88%	1.00%	5.00%	10.00%
100	0.53%	1.61%	11.13%	1.00%	5.00%	10.00%
125	0.81%	0.38%	8.87%	1.00%	5.00%	10.00%
150	0.04%	0.20%	5.55%	1.00%	5.00%	10.00%

Table 4.6 : Percentage Deviation from the original concentration, propeller-2

Distance (mm)	Percentage Deviation from Original Concentration		
	1%(Cw1)	5%(Cw5)	10%(Cw10)
50	11.25%	34.40%	32.50%
75	15.45%	56.00%	-38.80%
100	37.19%	67.80%	-11.30%
125	18.79%	92.48%	11.30%
150	95.76%	95.98%	44.50%

Table 4.7 : Effect of change in Cw with propeller-4

Distance	(Cw'1)@1%	(Cw'5)@5%	(Cw'10)@10%	Cw1	Cw5	Cw10
50.00%	0.99%	5.06%	8.78%	1.00%	5.00%	10.00%
75.00%	0.89%	4.46%	8.99%	1.00%	5.00%	10.00%
100.00%	0.85%	4.27%	8.32%	1.00%	5.00%	10.00%
125.00%	0.67%	3.26%	6.22%	1.00%	5.00%	10.00%
150.00%	0.46%	1.65%	4.13%	1.00%	5.00%	10.00%

Table 4.8: Percentage deviation from the original concentration, propeller-4

Distance (mm)	Percentage Deviation from Original Concentration		
	1%(Cw1)	5%(Cw5)	10%(Cw10)
50	10.62%	-1.20%	12.24%
75	13.38%	10.88%	10.10%
100	19.19%	14.50%	10.80%
125	33.49%	34.82%	7.80%
150	53.56%	67.02%	48.70%

Table 4.9: Effect of different propellers on solid suspension, Cw=1%

Distance (mm)	At 1 % Original concentration			
	Propeller-1	Propeller-2	Propeller-3	Propeller-4
50	0.96%	0.89%	1.40%	0.99%
75	0.80%	0.85%	0.20%	0.89%
100	0.83%	0.63%	0.07%	0.85%
125	0.66%	0.81%	0.01%	0.67%
150	0.22%	0.04%	0.00%	0.46%

Table 4.9: Percentage deviation from the original concentration(Cw=1%)

Distance(mm)	At 1% Concentration			
	Propeller 1	Propeller 2	Propeller 3	Propeller 4
50	4.00%	11.25%	83.62%	10.62%
75	12.00%	15.45%	77.70%	13.38%
100	17.00%	37.19%	93.47%	19.19%
125	32.00%	18.79%	99.17%	33.49%
150	78.00%	95.76%	99.54%	53.56%

Table 4.10: Effect of different propellers on solid suspension, Cw=10%.

Distance (mm)	At 10% Original Concentration (Cw=10%)			
	Propeller-1	Propeller-2	Propeller-3	Propeller-4
50	9.29%	6.75%	14.00%	8.78%
75	8.64%	13.88%	8.90%	8.99%
100	8.07%	11.13%	1.40%	8.32%
125	6.57%	8.87%	0.01%	6.22%
150	1.06%	5.55%	0.00%	4.13%

Table 4.11: Percent deviations with different propellers, Cw=10%

Distance (mm)	At 10% Original Concentration			
	Propeller-1	Propeller-2	Propeller-3	Propeller-4
50	7.10%	32.50%	-40.00%	12.20%
75	13.60%	-38.80%	11.00%	10.10%
100	19.30%	-11.30%	86.00%	16.80%
125	34.30%	11.30%	99.90%	37.80%
150	89.40%	44.50%	100.00%	58.70%

Table 4.12: Effect of different rotational speeds on concentration (Cw') with Propeller-1

Distance From Bottom (mm)	Concentration (Cw') @ 10% Cw		
	345 RPM	**360 RPM**	**370 RPM**
50	10.16%	9.12%	6.66%
75	9.78%	11.37%	13.60%
100	10.23%	10.42%	11.90%
125	8.12%	6.05%	10.56%
150	0.49%	0.40%	6.34%

Table 4.13: Effect of different rotational speeds on concentration(Cw') with propeller-4

Distance From Bottom(mm)	Concentration (Cw') @ 10% Cw		
	345 RPM	360 RPM	370 RPM
50	10.67%	8.70%	7.60%
75	8.47%	13.12%	12.50%
100	8.60%	12.70%	10.34%
125	6.20%	9.18%	9.88%
150	4.11%	4.66%	7.30%

Table 4.14: Effect of change in baffle design on concentration(Cw') with propeller-1

Distance From Bottom (mm)	**Concentration (Cw') @ 10% Cw**					
	Without Change in Baffles			**With Change in Baffles**		
	345 RPM	360 RPM	370 RPM	345 RPM	360 RPM	370 RPM
50	10.16%	9.12%	6.66%	8.86%	8.81%	7.15%
75	9.78%	11.37%	13.60%	11.32%	10.64%	10.00%
100	10.23%	10.42%	11.90%	11.55%	10.65%	10.60%
125	8.12%	6.05%	10.56%	8.44%	11.67%	11.85%
150	0.49%	0.40%	6.34%	2.00%	3.10%	4.83%

Table 4.15: Effect of change in baffle design on solid suspension with propeller-4

Propeller 4	**Concentration (Cw') @ 10% Cw**					
Distance From Bottom(mm)	**Without Change in Baffles**			**With Change in Baffles**		
	345 RPM	360 RPM	370 RPM	345 RPM	360 RPM	370 RPM
50	10.67%	8.70%	7.60%	7.28%	6.68%	6.36%
75	8.47%	13.12%	12.50%	10.72%	9.53%	10.61%
100	8.60%	12.70%	10.34%	10.50%	12.47%	10.80%
125	6.20%	9.18%	9.88%	12.06%	11.17%	13.16%
150	4.11%	4.66%	7.30%	7.32%	7.48%	7.96%